AFRL-IF-RS-TR-2005-290
Final Technical Report
August 2005

SIGNAL PROCESSING TECHNIQUES FOR ANTI-JAMMING GLOBAL POSITIONING SYSTEM (GPS) RECEIVERS

Villanova University

APPROVED FOR PUBLIC RELEASE; DISTRIBUTION UNLIMITED.

AIR FORCE RESEARCH LABORATORY
INFORMATION DIRECTORATE
ROME RESEARCH SITE
ROME, NEW YORK

STINFO FINAL REPORT

This report has been reviewed by the Air Force Research Laboratory, Information Directorate, Public Affairs Office (IFOIPA) and is releasable to the National Technical Information Service (NTIS). At NTIS it will be releasable to the general public, including foreign nations.

AFRL-IF-RS-TR-2005-290 has been reviewed and is approved for publication

APPROVED: /s/

DAVID H. HUGHES
Project Engineer

FOR THE DIRECTOR: /s/

WARREN H. DEBANY, JR., Technical Advisor
Information Grid Division
Information Directorate

REPORT DOCUMENTATION PAGE

Form Approved
OMB No. 074-0188

1. AGENCY USE ONLY (Leave blank)	2. REPORT DATE	3. REPORT TYPE AND DATES COVERED
	AUGUST 2005	Final May 00 – May 05

4. TITLE AND SUBTITLE
SIGNAL PROCESSING TECHNIQUES FOR ANTI-JAMMING GLOBAL POSITIONING SYSTEM (GPS) RECEIVERS

5. FUNDING NUMBERS
C - F30602-00-1-0515
PE - 62702F
PR - 4519
TA - 42
WU - P1

6. AUTHOR(S)
Moeness G. Amin

7. PERFORMING ORGANIZATION NAME(S) AND ADDRESS(ES)
Villanova University
800 Lancaster Avenue
Villanova Pennsylvania 19085

8. PERFORMING ORGANIZATION REPORT NUMBER

9. SPONSORING / MONITORING AGENCY NAME(S) AND ADDRESS(ES)
Air Force Research Laboratory/IFGC
525 Brooks Road
Rome New York 13441-4505

10. SPONSORING / MONITORING AGENCY REPORT NUMBER
AFRL-IF-RS-TR-2005-290

11. SUPPLEMENTARY NOTES
AFRL Project Engineer: David H. Hughes/IFGC/(315) 330-4122/ David.Hughes@rl.af.mil

12a. DISTRIBUTION / AVAILABILITY STATEMENT
APPROVED FOR PUBLIC RELEASE; DISTRIBUTION UNLIMITED.

12b. DISTRIBUTION CODE

13. ABSTRACT ***(Maximum 200 Words)***
The objective of this multi-year research funding is to devise new and novel methods to suppress interferers impinging on a multi-sensor GPS receiver. The research has considered chirp-like jammers as well as wideband interference. A self-coherence anti-jamming scheme is introduced which relies on the unique structure o the coarse/acquisition (C/A) code of the satellite signals. Because of the repetition of the C/A-code within each navigation symbol, the satellite signals exhibit strong self-coherence between chip-rate samples separated by integer multiples of the spreading gain. The proposed scheme utilizes this inherent self-coherence property to excise interferes that have different temporal structures from that of the satellite signals. In addition, new approaches using subspace methods and projection techniques are proposed for effective cancellation of frequency modulated jammers with minimum distortions of the desired satellite signals. The report also considers and analyzes the effect of non-Gaussian noise on the GPS receiver delay lock loops and discriminator outputs.

14. SUBJECT TERMS
Spread Spectrum, Interference Suppression, Multipath Mitigation, Subspace Estimation Methods, Anti-Jam GPS, Nonstationary Signals, Array Signal Processing

15. NUMBER OF PAGES
141

16. PRICE CODE

17. SECURITY CLASSIFICATION OF REPORT	18. SECURITY CLASSIFICATION OF THIS PAGE	19. SECURITY CLASSIFICATION OF ABSTRACT	20. LIMITATION OF ABSTRACT
UNCLASSIFIED	UNCLASSIFIED	UNCLASSIFIED	UL

Table of Contents

List of Figures

Chapter 2 Figures

Chapter 3 Figures

Chapter 4 Figures

Chapter 5 Figures

List of Tables

Summary

This report presents research work performed under the contract No. F30602-00-1-0515 with the Air Force Research Lab, Rome, NY. This report consists of five chapters, each containing introduction, numbered equations, simulations, figures, conclusion, and references.

In Chaper 1, we consider interference suppression and multipath mitigation in global navigation satellite systems (GNSS). In particular, a self-coherence anti-jamming scheme is introduced which relies on the unique structure of the coarse/acquisition (C/A) code of the satellite signals. Because of the repetition of the C/A-code within each navigation symbol, the satellite signals exhibit strong self-coherence between chip-rate samples separated by integer multiples of the spreading gain. The proposed scheme utilizes this inherent self-coherence property to excise interferers that have different temporal structures from that of the satellite signals. Using a multi-antenna navigation receiver, the proposed approach obtains the optimal set of beamforming coefficients by maximizing the cross-correlation between the output signal and a reference signal, which is generated from the received data. It is demonstrated that the proposed scheme can provide high gains towards all satellite signals in the field of view, while suppressing strong interferers. By imposing constraints on the beamformer, the proposed method is also capable of mitigating multipath that enters the receiver from or near the horizon. No knowledge of either the transmitted navigation symbols or the satellite positions is required.

In Chapter 2, we investigate the mitigation of frequency modulated (FM) interference in GPS receivers. In difference to commonly assumed wideband and narrowband interferers, the FM interferers are wideband, but instantaneously narrowband, and as such, have clear time-frequency (t-f) signatures that are distinct from the GPS C/A spread spectrum code. In the proposed technique, the estimate of the FM interference instantaneous frequency (IF) and the interference spatial signature are used to construct the spatio-temporal interference subspace. The IF estimates can be provided using existing effective linear or bilinear t-f methods. The undesired signal arrival is suppressed by projecting the input data on

the interference orthogonal subspace. With a multi-sensor receiver, the distinctions in both the spatial and time-frequency signatures of signal arrivals allow effective interference suppressions. This chapter considers the deterministic nature of the signal model and utilizes the known underlying structure of the GPS C/A code. We derive the receiver SINR under exact and perturbed IF values. The effect of IF estimation errors on both Pseudo-range measurements and navigation data recovery is analyzed. Simulation results comparing the receiver performances under IF errors in single and multi-antenna GPS receivers are provided.

In Chapter 3, we continue to address the problem of suppressing the nonstationary interference. Combined spatial and time-frequency signatures of signal arrivals at a multi-sensor array are used for nonstationary interference suppression in direct-sequence spread-spectrum (DS/SS) communications. With random PN spreading code and deterministic nonstationary interferers, the use of antenna arrays offers increased DS/SS signal dimensionality relative to the interferers. Interference mitigation through spatio-temporal subspace projection technique leads to reduced DS/SS signal distortion and improved performance over the case of a single antenna receiver. The angular separation between the interference and desired signals is shown to play a fundamental role in trading off the contribution of the spatial and time-frequency signatures to the interference mitigation process. The expressions of the receiver SINR implementing subspace projections are derived and numerical results are provided.

In Chapter 4, we study the performance of the delay lock loops (DLL) in GPS receivers in the presence of impulsive noise. The use of GPS has broadened to include mounting on or inside manned or autonomous vehicles which makes it subject to interference generated from motor emissions. Many sources of interference are typically modeled as impulsive noise whose characteristics may vary in terms of power, pulse width, and pulse occurrences. In this chapter, we examine the effect of impulsive noise on GPS DLL. We consider the DLL for the GPS Coarse Acquisition code (C/A), which is used in civilian applications, but also needed in military GPS receivers to perform signal acquisition and tracking. We focus on the statistics of the noise components of the early, late, punctual correlators, which contribute to

the discriminator error. The discriminator noise components are produced from the correlation between the impulsive noise and the early, late and punctual reference C/A code. Due to long time averaging, these components assume Gaussian distributions. The discriminator error variance is derived, incorporating the front-end precorrelation filter. It is shown that the synchronization error variance is significantly affected by the power of the received impulsive noise, the precorrelation filter, and the sample rate.

Finally, an anti-jam GPS receiver which suppresses interference by projecting the received signal on the noise subspace obtained via subspace tracking is proposed in Chapter 5. The resulting interference-free signal is then processed by a beamformer, whose weight vector is obtained by maximizing the signal-to-noise ratio at the beamformer output. It is shown that the proposed receiver can effectively eliminate interfere and enhance the GPS signals at the receiver output.

Chapter 1
A Novel Interference Suppression Scheme for Global Navigation Satellite Systems Using Antenna Array

1. Introduction

Satellite navigation is a tool to determine position, velocity, and precise time world wide. A navigation receiving device determines its three dimensional position plus time by measuring the signal traveling time from the satellite to the receiver (the so called *pseudorange* due to the clock offset at the receiver) [1]. The generic name of the satellite navigation systems is Global Navigation Satellite System (GNSS). Currently, there are two operative navigation systems, one is Global Positioning System (GPS) of the United States and the other one is Global Navigation Satellite System (GLONASS) of Russia [2].

Both GPS and GLONASS employ direct sequence spread spectrum (DS SS) signaling. The GPS satellites transmit signals at two L band frequencies: $L1$ = 1:57542GHz and $L2$ = 1:2276GHz. Each satellite broadcasts two different pseudorandom (PRN) codes, a coarse/acquisition (C/A) code and a precision (P) code, using code division multiple access (CDMA) technique. The$L1$carrier transmits both the C/A code and the P code, whereas the $L2$ carrier only transmits the P code [1]. The GPS C/A code is a Gold code with a chip rate of 1.023 Mchips/sec (or code period 1023) and repeats every millisecond, and the P code, usually encrypted for military use, has a chip rate 10.23 Mchips/sec and repeats about every week. Similar to GPS, GLONASS also has two DS SS components. However, frequency division multiple access (FDMA) technique is used in GLONASS, where each satellite transmits on a different center frequency. The C/A code of GLONASS has a length of 511 chips at a chip rate of 511 kHz, and it is the same for every GLONASS satellite. The C/A code repeats 10 times within each navigation symbol which has a rate of 100 bps. Another component of GLONASS has 10 times the chip rate (5.11 MHz) of the C/A code and uses a longer PRN code. In this chapter, we consider only the signals induced by the C/A code.

Despite the ever increasing civilian applications, the main drawback of the satellite navigation systems remains to be its high sensibility to interference and multipath [3], [4], [5], [6], [7], [8], which are the two main sources of errors in range and position estimations. The effect of interference on the GNSS receiver is to reduce the signal to noise ratio (SNR) of the navigation signal such that the receiver is unable to obtain measurements from the satellite, thus losing its ability to navigate [1]. Jammers reported to impact the GPS receivers are wideband noise, CW, pulsed noise, pulsed CW, swept tone (chirped), frequency hopping, and spoofers. Each type of jammers has advantages and drawbacks in terms of complexity and effectiveness [9]. The spread spectrum (SS) scheme, which underlines the GNSS signal structure, provides a certain degree of protection against interference. However, when the interferer power becomes much stronger than the signal power, the spreading gain alone is insufficient to yield any meaningful information. For example, for the GPS C/A signal, the receiver is vulnerable to strong interferers whose power exceeds the approximately 30 dB gain ($10\log_{10}1023 \approx 30$ dB) offered via the spreading/despreading process. It is thus desirable that the GNSS receivers operate efficiently in the presence of strong interference, whether it is intentional or unintentional.

Interference suppression in SS communication systems has been an active research topic for many years and a number of techniques have been developed (see, e.g., [4], [10], [11], [12], and references therein). In satellite navigation, interference can be combated in the time, space, or frequency domain, or in a domain of joint variables, e.g., time frequency [13], [14] or space time [15], [16]. Multiple antenna receivers allow the implementations of spatial nulling and beamsteering based on adaptive beamforming and high resolution direction finding methods. These methods are considered to be effective tools for anti jam GPS [9].

Conventional antenna arrays, which are only based on spatial processing, are among the simplest, and yet effective, techniques for narrowband interference suppression. Such techniques, however, is inadequate for broadband jammers (such as spoofer) cancellation or in the presence of multipath. In these cases, the temporal degree of freedom is required. Space time processing provides the receiver with

spatial and temporal selectivity. The spatial selectivity allows the discrimination between the navigation and interference signals based on their respective Direction of Arrivals (DOAs) [17], [18], [19], [20]. The temporal selectivity is used for broadband interference and multipath cancellation. Generally, the criteria for determining the optimal array weights include maximum signal to interference plus noise ratio (MSINR), minimum mean square error (MMSE), and minimum output power (MOP) [16]. The MSINR approach seeks the array weight vector by maximizing the receiver output SINR. The MMSE method chooses the weight vector such that the mean square difference between the array output and the desired temporal signal is minimized. Since the navigation signal power is well below the noise floor at the receiver, minimizing the output power while attempting to preserve the navigation signal is the goal of the MOP based scheme. While these methods are widely used in interference suppression in satellite navigation systems, one obvious drawback is that they all require some kind of *a priori* knowledge of the problem parameter values. For example, satellite locations are needed in order to calculate the signal power for the MSINR and MMSE methods. In [21], spatial and temporal processing techniques are applied to remove GPS like broadband jammers and recover the navigation information. The assumptions made in [21] are that the chip and bit synchronizations are achieved, implying that pseudorange measurements are obtained. However, the assumption of satellite positions or acquisitions is difficult to enforce under persistent jamming, or during the initial satellite searching stage when any synchronization is yet to be established.

In addition to interference, GPS pseudorange and carrier phase measurements also suffer from a variety of systematic biases, including satellite orbit prediction error and clock drift, ionospheric and tropospheric delay, GPS receiver clock offset, and signal multipath [22]. The satellite orbit and timing, ionospheric, and troposhperic errors can be removed by differencing techniques or significantly reduced by modeling [1]. The receiver clock offset can also be corrected by differencing but is often solved for as an unknown in the position solution. Multipath, on the other hand, is normally uncorrelated between antenna locations. As a result, differencing will not cancel the errors caused by multipath. Also, modeling multipath for each antenna location is difficult and impractical [23]. To combat signal multipath, many

techniques have been proposed. Among them, narrow correlator is one of the most widely used approaches that improve the C/A code tracking performance by reducing the space between the early and late correlator [24]. Other multipath mitigation techniques include multipath elimination delay lock loop (MEDLL) [25] and multipath estimation technology (MET) [22], etc.

This chapter proposes a new interference suppression technique for GNSS using spatial processing, but incorporating the known temporal structure of the C/A signal. A careful examination of the existing interference cancellation techniques reveals that, though efficient in most situations, they do not fully take advantage of the unique C/A signal structure, namely the replication of the C/A code. Due to the repetition of the spreading code, the GNSS C/A signal exhibits strong self coherence between chip samples that are separated by integer multiples of the spreading gain. Utilizing this feature, an anti jamming technique is developed to suppress a large class of narrowband and broadband interferers. It also has the capability of mitigating multipath, resulting in improved accuracy in pseudorange measurements. The proposed technique allows the civilian C/A code tracking and acquisition operations in the presence of strong interference, specifically at “cold start”, where there is no prior information on satellite angular positions or ranges [26]. In military applications, the encrypted P code is used instead of the C/A code. However, due to the short duration of the P code chip (10 times shorter than the C/A code chip), the synchronization in P code is usually difficult to achieve using the early late correlator, and assistance from the C/A code is needed [24]. With the receiver introduced in this chapter, initial synchronization in the P code can be established by first processing the interference suppressed C/A code. In essence, the self coherence based anti jamming approach is a blind technique, which does not require the knowledge of the navigation data or satellite locations to perform interference suppression. This makes it most applicable in the initial satellite searching phase when such information is unavailable, or in a prolonged jamming environment where the formerly obtained satellite positions are no longer reliable.

The rest of the chapter is organized as follows. In Section 2, we briefly review the concept of spectral self coherence restoral. An anti jamming GNSS scheme is presented in Section 3 and two receivers based on such scheme are developed. In Section 4, we discuss various important issues related to the

performance of the proposed GPS receiver. Numerical results are presented in Section 5 to demonstrate the performance of the proposed receiver. Finally, Section 6 concludes this chapter.

2. Overview of SCORE Algorithms

The proposed anti jamming GNSS technique builds on the basic concept of the self coherence restoral algorithm proposed in [27]. A signal $s(t)$ is referred to as spectrally self coherent at frequency separation β if the correlation between the signal and its frequency shifted version is nonzero for some lag τ, i.e., if [27], [28]

$$\rho_{ss}^{(\beta)}(\tau) = \frac{\left\langle s(t)s^*(t-\tau)e^{-j2\pi\beta t}\right\rangle_\infty}{\sqrt{\left\langle |s(t)|^2\right\rangle_\infty \left\langle |s^*(t-\tau)e^{-j2\pi\beta t}|^2\right\rangle_\infty}} = \frac{R_{ss}^{(\beta)}(\tau)}{R_{ss}(\tau)} \neq 0 \tag{1.1}$$

where $(\cdot)^*$ denotes the complex conjugate and $\langle \square \rangle_\infty$ represents the infinite time averaging operation. $\rho_{ss}^{(\beta)}(\tau)$ is the *self-coherence function* and $R_{ss}(0)$ and $R_{ss}^{(\beta)}(\tau)$ represent the average power and *cyclic autocorrelation function* of $s(t)$, respectively. For an M-element vector waveform $x(t)$, the *cyclic autocorrelation* matrix $\mathbf{R}_{ss}^{(\beta)}(\tau)$ is defined as

$$\mathbf{R}_{ss}^{(\beta)}(\tau) \square \left\langle \mathbf{x}(t)\mathbf{x}^H(t-\tau)e^{-j2\pi\beta t}\right\rangle_\infty \tag{1.2}$$

where $(\cdot)^H$ stands for the complex conjugate transpose. Complex wide sense cyclostationary waveforms exhibit spectral self coherence at discrete multiples of the time periodicities of the waveform statistics [27]. The signal waveforms that possess the self coherence feature include most communication signals, such as PCM signals and BPSK signals [28].

The spectral self coherence restoral (SCORE) beamforming techniques have been shown to blindly extract the desired signal in the presence of unknown noise and interference [27]. The SCORE algorithms seek the beamformer weight vector that maximizes a measure of the cyclic feature of the beamformer output. For example, in the presence of interference, the received signal is given by $x(t) = as(t) + v(t)$, where a is the signal amplitude and $v(t)$ is the interference, which is assumed to be independent of $s(t)$. If

$s(t)$ is spectrally self coherent at a frequency shift β, then the cyclic autocorrelation of $x(t)$ can be expressed as [27]

$$R_{xx}^{(\beta)}(\tau) = |a|^2 R_{ss}^{(\beta)}(\tau) + R_{vv}^{(\beta)}(\tau) = |a|^2 R_{ss}^{(\beta)}(\tau) \tag{1.3}$$

Equation (1.3) shows that the shift in frequency completely decorrelates the interference component in $x(t)$, given that $v(t)$ is not spectrally self-coherent at the frequency separation β.

There are several different versions of the SCORE algorithm, of which the least-squares (LS) SCORE is the simplest. The LS-SCORE algorithm determines the array weight vector by minimizing the difference between the array output and a reference signal, which is obtained by processing the delayed and frequency-shifted version of the received signal. Other SCORE algorithms include the cross-SCORE algorithm, which determines the beamformer by strengthening the cross-correlation between the output of the array and a reference signal, and the auto-SCORE algorithm, which maximizes the spectral self-coherence strength at the output of a linear combiner [27]. The self-coherence anti-jamming scheme proposed in this chapter is based on the cross-SCORE algorithm.

3. Proposed Anti-Jamming GNSS Scheme

Before introducing the proposed anti-jamming receiver, we first examine the temporal structure of the navigation signal, as the receiver is developed by exploiting the repetitive feature of the C/A signal. Figure 1 depicts the structure of the received noise-free navigation signal, where the BPSK modulated navigation symbols (simply referred to as "symbol" thereafter) are spread by a PRN code with spreading gain of P (P = 1023 for GPS and P = 511 for GLONASS) and chip-rate sampled. The code sequence (denoted as "spreading block" in Figure 1) is repeated L times (L = 20 for GPS and L = 10 for GLONASS) within each symbol. Two blocks of data are formed at the receiver: a *data block*, which spans N consecutive samples, and a *reference block* with the same number of samples as the date block. The distance between the respective samples in the data and reference blocks is set equal to jP chips, where $1 \le j < L$. Obviously, due to the repetition of the spreading code, the nth sample in the data block will

have the same value as the corresponding *n*th sample in the reference block, providing that the two samples belong to the same symbol.

From the temporal structure of the C/A signal, we observe the inherent self-coherence between samples in the data block and the reference block, due to the repetition of the spreading code. Based on this observation, a novel anti-jamming technique is developed in this chapter, and Figure 2 shows a block diagram of the proposed receiver with this technique. In Figure 2, an *M*-element array is deployed. There are two beamformers in the receiver: a main beamformer w, processing samples in the data block, and an auxiliary beamformer **f**, handling data from the reference block. An error signal $e(t)$ is formed as the difference between the beamformer output $z(t)$ and a reference signal $d(t)$, which is the output of **f** . For the proposed scheme, the weight vectors **w** and **f** are updated according to the cross-SCORE algorithm.

The signal reaching the GNSS receiver is the aggregate of the satellite navigation signals, their respective multipaths, additive white Gaussian noise (AWGN), and broadband/narrowband interferers. Thus, after carrier synchronization, the signal received at the receiver can be expressed as

$$\begin{aligned}\mathbf{x}(n) &= \sum_{q=0}^{Q} s_q(nT_s - \tau_q)\mathbf{a}_q e^{j\phi_q} + \sum_{k=1}^{K} B_k u_k(n)\mathbf{d}_k + \mathbf{v}(n) \\ &= s_0(nT_s - \tau_0)\mathbf{a}_0 e^{j\phi_0} + \sum_{q=1}^{Q} s_q(nT_s - \tau_q)\mathbf{a}_q e^{j\phi_q} + \sum_{k=1}^{K} B_k u_k(n)\mathbf{d}_k + \mathbf{v}(n)\end{aligned} \tag{1.4}$$

where T_s is the Nyquist sampling interval, Q is the number of multipath components, with subscript 0 designated to the direct-path signal. Due to the weak cross-correlation of the C/A-codes, only one satellite is considered in Equation (1.4). In the above equation, $s_q(n)$, τ_q , and ϕ_q are the signal sample, time-delay, and phase-shift of the *q*th multipath component, respectively, K is the number of interferers, $u_k(n)$ is the waveform of the *k*th interferer with amplitude B_k. The vectors $\mathbf{a}_q$ and $\mathbf{d}_k$ are, respectively, $M\times 1$ spatial signatures of the *q*th satellite multipath and the *k*th interferer, and $\mathbf{v}(n)$ consists of noise samples. Let $s(n) \triangleq s_0(nT_s - \tau_0)\mathbf{a}_0 e^{j\phi_0}$ denote the data vector across the array due to the direct-path signal. Then, Equation (1.4) can be rewritten as

$$\mathbf{x}(n) = \mathbf{s}(n) + \tilde{\mathbf{s}}(n) + \mathbf{u}(n) + \mathbf{v}(n) \tag{1.5}$$

where $\tilde{\mathbf{s}}(n) \triangleq \sum_{q=1}^{Q} s_q(nT_s - \tau_q)\mathbf{a}_q e^{j\phi_q}$ and $u(n) \triangleq \sum_{k=1}^{K} B_k u_k(n)\mathbf{d}_k$. Assuming a direct-path to the satellite at direction μ and a uniform linear array, we can express vector $\mathbf{a}_0$ in the specific format of a steering vector as

$$\mathbf{a}_0 = \mathbf{a}(\theta) \triangleq \left[1, \quad e^{j2\pi f_c \tau}, \quad \cdots, \quad e^{j2\pi f_c (M-1)\tau}\right]^T \tag{1.6}$$

where f_c is the carrier frequency, $\tau = \Delta / c \sin\theta$ is the interelement path delay of the source in the direction of θ, c is the propagation speed of the waveform, and Δ is the sensor spacing. According to the formulation of the data and reference blocks, the counterpart of $\mathbf{x}(n)$ in the reference block within the same symbol can be written as

$$\begin{aligned}
\mathbf{x}(n - jP) &= \sum_{q=0}^{Q} s_q(nT_s - \tau_q - jP)\mathbf{a}_q e^{j\phi_q} + \sum_{k=1}^{K} B_k u_k(n - jP)\mathbf{d}_k + \mathbf{v}(n - jP) \\
&= \sum_{q=0}^{Q} s_q(nT_s - \tau_q)\mathbf{a}_q e^{j\phi_q} + \sum_{k=1}^{K} B_k u_k(n - jP)\mathbf{d}_k + \mathbf{v}(n - jP) \\
&= \mathbf{s}(n) + \tilde{\mathbf{s}}(n) + \mathbf{u}(n - jP) + \mathbf{v}(n - jP)
\end{aligned} \tag{1.7}$$

where we have assumed that, when considered within the same symbol,

$$s_q(nT_s - \tau_q) = s_q(nT_s - \tau_q - jP), \; q = 0, \cdots, Q \tag{1.8}$$

Compared to the general case of self-coherence, there is no frequency difference between the signal samples in the data and reference blocks, i.e., the frequency shift $\beta = 0$.

From Figure 2, the beamformer output and the reference signal are given by $z(n) \triangleq \mathbf{w}^H \mathbf{x}(n)$ and $d(n) \triangleq \mathbf{f}^H \mathbf{x}(n - jP)$, respectively. We define the following covariances:

$$R_{zd} \triangleq E\left\{z(n)d^H(n)\right\} = \mathbf{w}^H E\left\{\mathbf{x}(n)\mathbf{x}^H(n - jP)\right\}\mathbf{f} \tag{1.9}$$

$$R_{zz} \triangleq E\left\{z(n)z^H(n)\right\} = \mathbf{w}^H E\left\{\mathbf{x}(n)\mathbf{x}^H(n)\right\}\mathbf{w} \tag{1.10}$$

$$R_{dd} \triangleq E\left\{d(n)d^H(n)\right\} = \mathbf{f}^H E\left\{\mathbf{x}(n - jP)\mathbf{x}^H(n - jP)\right\}\mathbf{f} \tag{1.11}$$

Under the assumption that the navigation signal, interference, and noise are independent, then

$$\mathbf{R}_{xx} \triangleq E\left\{\mathbf{x}(n)\mathbf{x}^H(n)\right\} = E\left\{\mathbf{x}(n-jP)\mathbf{x}^H(n-jP)\right\} = \mathbf{R}_s + \mathbf{R}_u + \mathbf{R}_v \tag{1.12}$$

The three terms on the right-hand side of Equation (1.12) denote, respectively, the covariance matrices of the C/A signal, including both the direct-path and multipath signals, interference, and noise: $\mathbf{R}_s \triangleq E\left\{\left[\mathbf{s}(n)+\tilde{\mathbf{s}}(n)\right]\left[\mathbf{s}(n)+\tilde{\mathbf{s}}(n)\right]^H\right\}$, $\mathbf{R}_u \triangleq E\left\{\mathbf{u}(n)\mathbf{u}^H(n)\right\}$, and $\mathbf{R}_v \triangleq E\left\{\mathbf{v}(n)\mathbf{v}^H(n)\right\}$. If the navigation signal is the only data component which correlates with its delayed version, then the cross-correlation matrix between the corresponding data vectors in the data and reference blocks simplifies to [cf. Equation (1.3)]

$$\mathbf{R}_{xx}^{(P)} \triangleq E\left\{\mathbf{x}(n)\mathbf{x}^H(n-jP)\right\} = \mathbf{R}_s \tag{1.13}$$

3.1. Cross-SCORE Algorithm Based Receiver

We first consider the receiver design by directly applying the cross-SCORE algorithm. For the proposed GNSS anti-jamming scheme, there are two beamformers **w** and **f** to be determined. With $d(n)$ serving as the reference signal, we define $e(n) \triangleq z(n) - d(n)$ as the difference between the receiver's output and the reference signal. The relationship between **w** and **f** can be established in the least-squares (LS) sense. For a fixed beamformer **w**, the LS solution of **f** is given by $\mathbf{f}_{\mathrm{LS}} = \mathbf{R}_{xx}^{-1}\mathbf{r}_{xx}$, where $\mathbf{r}_{xx} = E\left\{\mathbf{x}(n-jP)z^H(n)\right\} = \mathbf{R}_{xx}^{(P)H}\mathbf{w}$. Similarly, if $\boldsymbol{f}$ is fixed, then $\mathbf{w}_{\mathrm{LS}} = \mathbf{R}_{xx}^{-1}\mathbf{R}_{xx}^{(P)H}\mathbf{f}$.

According to the cross-SCORE algorithm, the beamformers w and f are obtained by maximizing the cross-correlation between $z(n)$ and $d(n)$:

$$C(\mathbf{w},\mathbf{f}) \triangleq \frac{|R_{zd}|^2}{R_{zz}R_{dd}} = \frac{\left|\mathbf{w}^H\mathbf{R}_{xx}^{(P)}\mathbf{f}\right|^2}{\left[\mathbf{w}^H\mathbf{R}_{xx}\mathbf{w}\right]\left[\mathbf{f}^H\mathbf{R}_{xx}\mathbf{f}\right]} \tag{1.14}$$

Substituting **f** and **w** in the above equation by $\mathbf{f}_{\mathrm{LS}}$ and $\mathbf{w}_{\mathrm{LS}}$, respectively, we have

$$C(\mathbf{w},\mathbf{f}_{\mathrm{LS}}) = \frac{\mathbf{w}^H\mathbf{R}_{xx}^{(P)}\mathbf{R}_{xx}^{-1}\mathbf{R}_{xx}^{(P)}\mathbf{w}}{\mathbf{w}^H\mathbf{R}_{xx}\mathbf{w}} \tag{1.15}$$

$$C(\mathbf{w}_{\mathrm{LS}}, \mathbf{f}) = \frac{\mathbf{f}^H \mathbf{R}_{xx}^{(P)} \mathbf{R}_{xx}^{-1} \mathbf{R}_{xx}^{(P)} \mathbf{f}}{\mathbf{f}^H \mathbf{R}_{xx} \mathbf{f}} \tag{1.16}$$

The weight vectors **w** and **f** that maximize $C(\mathbf{w}, \mathbf{f}_{\mathrm{LS}})$ and $C(\mathbf{w}_{\mathrm{LS}}, \mathbf{f})$, respectively, are readily shown to be the eigenvectors corresponding to the largest eigenvalues of the generalized eigenvalue problems:

$$\mathbf{R}_{xx}\mathbf{w} = \lambda \mathbf{R}_{xx}^{(P)} \mathbf{R}_{xx}^{-1} \mathbf{R}_{xx}^{(P)} \mathbf{w} \tag{1.17}$$

$$\mathbf{R}_{xx}\mathbf{f} = \kappa \mathbf{R}_{xx}^{(P)} \mathbf{R}_{xx}^{-1} \mathbf{R}_{xx}^{(P)} \mathbf{f} \tag{1.18}$$

where λ and κ are the eigenvalues.

It is observed from Equations (1.17) and (1.18) that, for the proposed receiver, the main beamformer **w**, which generates the receiver outputs, is equivalent to the auxiliary beamformer **f** that provides the reference signal. This equivalence, however, is not surprising because of the unique structure of the C/A signal. From Equations (1.4) and (1.7), we note that the self-coherence of the navigation signal is due to the time lag between the two samples which do not encounter any frequency shift after the frequency demodulation. Therefore, $\mathbf{x}(n)$ and $\mathbf{x}(n-jP)$ have the same correlation function, given by Equation (1.11). For the general case of self-coherence, on the other hand, the signal auto-correlation function does not necessarily equal to the auto-correlation function of the frequency-shifted, time-lagged version of the original signal. As a result, the cross-SCORE algorithm will not produce two identical beamformers [27], as it does for the proposed receiver.

Simulations presented in Section V show that the cross-SCORE based receiver performs fairly well in a jamming environment. It is capable of producing high gains for satellites currently in the field of view, while suppressing strong jammers. However, such a receiver provides no measures against multipath, which is one of the dominant error sources in navigation. To address the multipath issue, we modify the receiver design, as discussed in the next subsection.

3.2. Modified Cross-SCORE Algorithm Based Receiver

Since the GNSS signal multipath shares the same structure as the direct-path signal, it is expected that both the C/A signal and the undesired multipath components will appear at the receiver's output undistorted.

It is known that the satellites typically lie above the horizon, whereas the multipath is often generated from local scatters near the horizon [16]. To equip the receiver with means to combat multipath, while maintaining the self-coherent approach, we introduce constraints on **f** such that the reference signal $d(n)$ does not contain reflections from near the horizon. To do so, we define equally spaced directions γ_d, d=1,⋯,D, covering some solid angle Ω near the horizon. Let $\mathbf{B} \triangleq \left[\mathbf{b}(\gamma_1) \quad \cdots \quad \mathbf{b}(\gamma_D)\right]$ be the $M \times D$ matrix consisting of steering vectors defined as in Equation (6). To mitigate multipath in the range Ω, we require $\mathbf{B}^H\mathbf{f} = \mathbf{0}$. Then, the cost function in Equation (1.16) is rewritten as

$$\mathbf{f}_{\text{opt}} = \arg\max_{\mathbf{f}} \frac{\mathbf{f}^H \tilde{\mathbf{R}}_{xx}\mathbf{f}}{\mathbf{f}^H \mathbf{R}_{xx}\mathbf{f}}, \text{ subject to } \mathbf{B}^H\mathbf{f} = \mathbf{0} \tag{1.19}$$

where $\tilde{\mathbf{R}}_{xx} = \mathbf{R}_{xx}^{(P)}\mathbf{R}_{xx}^{-1}\mathbf{R}_{xx}^{(P)H}$. The solution of the above equation is obtained as follows. Let r = rank(***B***) ≤ min(M,D) be the rank of the **B** matrix. Performing the singular value decomposition (SVD) [29] of **B** yields

$$\mathbf{U}^H\mathbf{B}^H\mathbf{V} = \begin{bmatrix} \mathbf{\Lambda} & 0 \\ 0 & 0 \end{bmatrix} \tag{1.20}$$

where **U** and **V** are two unitary matrices with dimension $M \times M$ and $D \times D$, respectively, and

$$\mathbf{\Lambda} = \text{diag}\left\{\sigma_1, \quad \sigma_2, \quad \cdots \quad \sigma_r\right\} \tag{1.21}$$

where $\sigma_1 \geq \sigma_2 \geq \cdots \geq \sigma_r$ are eigenvalues of **B** arranged in a decreasing order. Let **A** be formed from the last M-r columns of **U**. Thus, **A** spans the null space of $\mathbf{B}^H$, i.e., $\mathbf{B}^H\mathbf{A} = \mathbf{0}$. Let **α** be a ($M$-$r$) × 1 vector such that

$$\mathbf{f} = \mathbf{A}\boldsymbol{\alpha} \tag{1.22}$$

Using vector $\boldsymbol{\alpha}$, the constrained maximization problem in Equation (1.19) is transformed to an unconstrained one:

$$\boldsymbol{\alpha} = \arg\max_{\boldsymbol{\alpha}} \frac{\boldsymbol{\alpha}^H \mathbf{A}^H \tilde{\mathbf{R}}_{xx} \mathbf{A}\boldsymbol{\alpha}}{\boldsymbol{\alpha}^H \mathbf{A}^H \mathbf{R}_{xx} \mathbf{A}\boldsymbol{\alpha}} \tag{1.23}$$

The above generalized eigendecomposition problem can be solved using Cholesky decomposition. Particularly, since $\mathbf{R}_{xx}$ is positive definite, $\mathbf{A}^H\mathbf{R}_{xx}\mathbf{A}$ is also positive definite. Then the Cholesky decomposition of $\mathbf{A}^H\mathbf{R}_{xx}\mathbf{A}$ is $\mathbf{A}^H\mathbf{R}_{xx}\mathbf{A} = \mathbf{G}\mathbf{G}^H$, where $\mathbf{G}$ is a $(M\text{-}r) \times (M\text{-}r)$ matrix with full rank [29] and, thus, invertible. Let $\boldsymbol{\alpha} = \mathbf{G}^{-H}\boldsymbol{\beta}$. Then

$$\frac{\boldsymbol{\alpha}^H \mathbf{A}^H \tilde{\mathbf{R}}_{xx} \mathbf{A}\boldsymbol{\alpha}}{\boldsymbol{\alpha}^H \mathbf{A}^H \mathbf{R}_{xx} \mathbf{A}\boldsymbol{\alpha}} = \frac{\boldsymbol{\beta}^H \mathbf{G}^{-1} \mathbf{A}^H \tilde{\mathbf{R}}_{xx} \mathbf{A}\mathbf{G}^{-H}\boldsymbol{\beta}}{\boldsymbol{\beta}^H \mathbf{G}^{-1}\mathbf{G}\mathbf{G}^H\mathbf{G}^{-H}\boldsymbol{\beta}} = \frac{\boldsymbol{\beta}^H \mathbf{G}^{-1} \mathbf{A}^H \tilde{\mathbf{R}}_{xx} \mathbf{A}\mathbf{G}^{-H}\boldsymbol{\beta}}{\boldsymbol{\beta}^H\boldsymbol{\beta}} \tag{1.24}$$

Accordingly, the maximization problem becomes

$$\max_{\boldsymbol{\alpha}} \frac{\boldsymbol{\alpha}^H \mathbf{A}^H \tilde{\mathbf{R}}_{xx} \mathbf{A}\boldsymbol{\alpha}}{\boldsymbol{\alpha}^H \mathbf{A}^H \mathbf{R}_{xx} \mathbf{A}\boldsymbol{\alpha}} = \max_{\boldsymbol{\beta}} \frac{\boldsymbol{\beta}^H \mathbf{G}^{-1} \mathbf{A}^H \tilde{\mathbf{R}}_{xx} \mathbf{A}\mathbf{G}^{-H}\boldsymbol{\beta}}{\boldsymbol{\beta}^H\boldsymbol{\beta}} = \max_{\boldsymbol{\beta}} \boldsymbol{\beta}^H \mathbf{G}^{-1} \mathbf{A}^H \tilde{\mathbf{R}}_{xx} \mathbf{A}\mathbf{G}^{-H}\boldsymbol{\beta} \tag{1.25}$$

under the standard constraint $\|\boldsymbol{\beta}\| = 1$, where $\|\cdot\|$ is the vector 2-norm [29]. Hence, $\boldsymbol{\beta}$ is given by the eigenvector associated with the maximum eigenvalue of $\mathbf{G}^{-1}\mathbf{A}^H\tilde{\mathbf{R}}_{xx}\mathbf{A}\mathbf{G}^{-H}$. And, finally,

$$\mathbf{f}_{\text{opt}} = \mathbf{A}\mathbf{G}^{-H}\boldsymbol{\beta} \tag{1.26}$$

The beamformer $\mathbf{w}$ is derived as

$$\mathbf{w}_{\text{opt}} = \mathbf{R}_{xx}^{-1}\mathbf{R}_{xx}^{(P)}\mathbf{f}_{\text{opt}} = \mathbf{R}_{xx}^{-1}\mathbf{R}_{xx}^{(P)}\mathbf{A}\boldsymbol{\alpha} \tag{1.27}$$

according to the LS relation between $\mathbf{w}$ and $\mathbf{f}$.

4. Covariance Matrix Estimations

In practice, the covariance matrices $\mathbf{R}_{xx}$ and $\mathbf{R}_{xx}^{(P)}$ are unknown and have to be replaced by their sample estimates. Define the $M \times N$ data and reference matrices as $\mathbf{X}_N \triangleq \left[\mathbf{x}(n), \quad \cdots, \quad \mathbf{x}(n-(N-1))\right]$ and

$\mathbf{X}_{N\text{ref}} \equiv \left[\mathbf{x}(n-jP), \quad \cdots, \quad \mathbf{x}(n-(N-1)-jP)\right]$, where N is the block length and $N \le P$. The sample covariance matrices are then given by

$$\hat{\mathbf{R}}_{xx} = \frac{1}{N}\mathbf{X}_N \mathbf{X}_N^H \tag{1.28}$$

$$\hat{\mathbf{R}}_{xx}^{(P)} = \frac{1}{N}\mathbf{X}_N \mathbf{X}_{N\text{ref}}^H \tag{1.29}$$

And, the beamformers **w** and **f** are calculated correspondingly.

It is noted from Equation (1.16) that the covariance matrices $\mathbf{R}_{xx}$ and $\mathbf{R}_{xx}^{(P)}$ determine the performance of the proposed receiver. In practical implementations, the data and reference blocks $\mathbf{X}_N$ and $\mathbf{X}_{N\text{ref}}$ are used to estimate $\mathbf{R}_{xx}$ and $\mathbf{R}_{xx}^{(P)}$, and subsequently provide the weight vector **w**, which is then applied to process signal samples in the data block. The key assumption made for the proposed GPS receiver in Section III is that both the data and reference samples, $\mathbf{x}(n)$ and $\mathbf{x}(n- jP)$, $1 \le j < 20$, belong to the same navigation symbol. However, since the data samples used for covariance matrix estimations are selected randomly, and interference suppression is performed prior to any symbol synchronization process, there is no guarantee that the data and reference samples belong to the same symbol. Questions arise as how will the receiver perform when the above assumption fails, i.e., the data and reference samples lie in two adjacent symbols?

To answer the above question, we relax the condition imposed in Section 3, and develop the general expression of the covariance matrices between the data and reference samples, $\mathbf{x}(n)$ and $\mathbf{x}(n-jP)$. Define the following events:

$$\begin{aligned}
&A_1 : x(n) \ \& \ x(n-jP) \text{ are within the same symbol,} \\
&A_2 : x(n) \ \& \ x(n-jP) \text{ are in two adjacent symbols,} \\
&A_{21} : x(n) \ \& \ x(n-jP) \text{ are in two symbols with the same sign,} \\
&A_{22} : x(n) \ \& \ x(n-jP) \text{ are in two symbols with different signs}
\end{aligned} \tag{1.30}$$

With random selection of time n, and using the repetitive property of the C/A-code, it is straightforward to show that the corresponding probabilities of the above events are

$\Pr\{A_1\} = \dfrac{T - jP}{T} = 1 - \dfrac{jP}{T}$, $\Pr\{A_2\} = \dfrac{jP}{T}$, $\Pr\{A_{21}\} = \dfrac{jP}{2T}$, and $\Pr\{A_{22}\} = \dfrac{jP}{2T}$, respectively, where T = 20P is the total number of samples in one symbol. The exact expression of the cross-correlation function $\mathbf{R}_{xx}^{(P)}$ can be written in terms of the above probabilities and conditional expectations as

$$\begin{aligned}\mathbf{R}_{xx}^{(P)} &= E\left\{\mathbf{x}(n)\mathbf{x}^H(n - jP)\middle|A_1\right\}\Pr\{A_1\} + E\left\{\mathbf{x}(n)\mathbf{x}^H(n - jP)\middle|A_2\right\}\Pr\{A_2\} \\ &= E\left\{\mathbf{x}(n)\mathbf{x}^H(n - jP)\middle|A_1\right\}\Pr\{A_1\} \\ &\quad + E\left\{\mathbf{x}(n)\mathbf{x}^H(n - jP)\middle|A_{21}\right\}\Pr\{A_{21}\} + E\left\{\mathbf{x}(n)\mathbf{x}^H(n - jP)\middle|A_{22}\right\}\Pr\{A_{22}\}\end{aligned} \tag{1.31}$$

Since $E\left\{\mathbf{x}(n)\mathbf{x}^H(n - jP)\middle|A_1\right\} = E\left\{\mathbf{x}(n)\mathbf{x}^H(n - jP)\middle|A_{21}\right\} = \mathbf{R}_s$ and $E\left\{\mathbf{x}(n)\mathbf{x}^H(n - jP)\middle|A_{22}\right\} = -\mathbf{R}_s$, then

$$\mathbf{R}_{xx}^{(P)} = \mathbf{R}_s\left(\Pr\{A_1\} + \Pr\{A_{21}\}\right) - \mathbf{R}_s\Pr\{A_{22}\} = \left(1 - \frac{jP}{T}\right)\mathbf{R}_s \tag{1.32}$$

Equation (1.32) shows that the covariance matrix $\mathbf{R}_{xx}^{(P)}$ depends on the distance between the data and reference samples jP. The maximum value of $\mathbf{R}_{xx}^{(P)}$ is achieved when j = 1, representing the closest possible data and reference blocks.

In practice, however, sample estimates, obtained from Equations (1.27) and (1.28) using the data and reference blocks $\mathbf{X}_N$ and $\mathbf{X}_{N\text{ref}}$, replace the exact values in Equation (1.32). It can be readily shown that if $\mathbf{X}_N$ and $\mathbf{X}_{N\text{ref}}$ are jP samples apart, $1 \le j < 20$, the probability of the two blocks belonging to the same symbol or, equivalently, in two adjacent symbols with the same sign, is $1 - \dfrac{jP + N}{2T}$. On the other hand, the probability that $\mathbf{X}_N$ and $\mathbf{X}_{N\text{ref}}$ are in two adjacent symbols with opposite signs is $\dfrac{jP - N}{2T}$. Using the above probabilities, the expected values of $\hat{\mathbf{R}}_{xx}$ and $\hat{\mathbf{R}}_{xx}^{(P)}$ are derived in Appendix A as:

$$\bar{\hat{\mathbf{R}}}_{xx} = \mathbf{R}_s + \mathbf{R}_u + \mathbf{R}_v \tag{1.33}$$

$$\bar{\hat{\mathbf{R}}}_{xx}^{(P)} = \left(1 - \frac{jP}{T}\right)\mathbf{R}_s \tag{1.34}$$

which show the same dependency on jP as in Equation (1.32) and that $\hat{\mathbf{R}}_{xx}$ and $\hat{\mathbf{R}}_{xx}^{(P)}$ are unbiased estimates of $\mathbf{R}_{xx}$ and $\mathbf{R}_{xx}^{(P)}$, respectively.

The above covariance matrix estimations use only one data block and its replicated reference block. To fully take advantage of the repetitive feature of the C/A-code, multiple data/reference blocks can be used in the time-averaging. Particularly, using G data and reference blocks, Equations (1.27) and (1.28), respectively, become

$$\hat{\mathbf{R}}_{xxG} = \frac{1}{G}\sum_{g=1}^{G}\mathbf{X}_N(g)\mathbf{X}_N^H(g)/N \tag{1.35}$$

$$\hat{\mathbf{R}}_{xxG}^{(P)} = \frac{1}{G}\sum_{g=1}^{G}\mathbf{X}_N(g)\mathbf{X}_{N\text{ref}}^H(g)/N \tag{1.36}$$

In the case when one of the data blocks (and, respectively, a reference block) is split between two adjacent symbols with opposite signs, a maximum of only two of the G terms in the above equation may suffer from symbol transition, whereas the rest of the terms will be coherently combined. Appendix A and B derive the mean and variance of the above estimations, showing the value of using a higher value of G.

5. Numerical Results

In this section, we evaluate the performance of the proposed self-coherence anti-jamming receiver using the GPS C/A signals.

A uniform linear array (ULA) consisting of M = 7 sensors with half-wavelength spacing is used in simulations with one satellite and no multipath. We set M = 11 for simulations with multiple satellites or multipath. The GPS navigation symbols are in the BPSK format and spread by C/A-codes (Gold codes) with processing gain of P = 1023. We select the first satellite C/A-code for concept demonstration. At the receiver, chip-rate sampling is performed and N = 800 samples are collected in both the data and reference blocks for covariance matrix estimations. The signal-to-noise ratio (SNR) and signal-to-

interference-plus-noise ratio (SINR) are defined, respectively, as $\mathrm{SNR} = 10\log_{10} 1/P_v$ and $\mathrm{SINR} = 10\log_{10} 1/\left(P_i + P_v\right)$, all in dB, where unit signal power is assumed for simplicity, P_v is the noise power, and P_i is the interference power. The jammer-to-signal ratio (JSR) is defined as $\mathrm{JSR} = 10\log_{10} P_i$ dB. Interferers used in the simulations are generated as broadband binary signals having the same rates as the C/A-codes, but with a different structure than that of the C/A signals.

5.1. Antenna Beam Pattern without Interference

We first consider the scenarios in which no interference presents at the receiver. SNR is -30 dB. Covariance matrices are estimated using one data block and one reference block taken within the same symbol. The performance of the cross-SCORE based receiver is shown in Figure 3, where the antenna pattern is formed towards the satellite located at $\theta = 30^\circ$.

We recall the discussions in Section 4 which suggest that better performance can be expected when multiple data and reference blocks are used to estimate the covariance matrices. In Appendix B, the variances of the sample estimates of $\mathbf{R}_{xxG}^{(P)}$ are calculated and it shows that using multiple data/reference blocks can indeed reduce the estimation variance. We now demonstrate experimentally the effect of multi-block estimation on the receiver performance. Particularly, a very special situation is created where one of the data blocks is evenly split between two symbols having opposite signs. SNR is set at -40 dB. If G = 2 and the split data block happens to be the second one, the receiver fails to provide any substantial gain for the satellite located at 30°, as shown in Figure 4(a). This is because that elements in the time-averaging of $\hat{\mathbf{R}}_{xxG}^{(P)}$ given by Equation (1.35) cancel each other, resulting in significantly weak cross-correlation between $z(n)$ and $d(n)$ [cf. Equation (1.14)]. If, on the other hand, G > 2 data and reference blocks are involved in the estimation, the split of one block will not have such a dramatic impact on the receiver performance as in the G = 2 case, as only two among G blocks are affected due to the split. It is clear from Figure 4(b) that a beam is generated towards the satellite with G = 7 despite the split.

Generally, to avoid the performance degradation, it is recommended that odd number of samples (N) should be chosen for each data/reference block and $2 < G < D$.

It is known that in satellite navigation, at least four satellites are needed simultaneously in the field of view in order to calculate the receiver's three-dimensional position and time. Since the proposed receiver relies on the special structure of the C/A signals to suppress interference and all satellite emitted C/A signals share the same repetitive feature, it is expected that the receiver will pass the signals from all satellites with high gains. In the simulation, the satellites are located at $\theta_1 = 10^\circ$, $\theta_2 = 30^\circ$, $\theta_3 = 50^\circ$, and $\theta_4 = 70^\circ$, with SNR = -30 dB. As shown in Figure 5, four clear beams are generated towards the four satellites.

A point worth mentioning is that the receiver presented in this chapter is able to suppress interference for all satellites at once. In GNSS, since the satellite spreading codes are known at the receiver, it may be intuitive to consider using the spreading code as the reference instead of generating one from the received data. Even though the locally generated spreading code is noise and interference free, it cannot serve as the reference signal in the proposed receiver because 1) the alignment of the incoming signal and the local reference code may not be established during the interference removal stage, hence there is no guarantee that the data block and reference blocks are separated by integer multiples of P chips; 2) it is not possible to use one specific satellite's spreading code as the reference signal to remove interference for all satellites. Therefore, interference suppression must occur in a serial manner. The disadvantage is obvious as compared to the simultaneous interference removal the proposed receiver offers.

5.2. Interference Suppression

We next investigate the receiver's interference suppression capability by comparing it with the MMSE receiver of [16]. The MMSE receiver determines the weight vector by minimizing the mean square difference between the array output and the desired signal. The latter approach, however, requires the knowledge of the satellite direction. This condition is eliminated in the proposed scheme. If the jammers have explicit bearings, we can generate the received signals according to Equation (1.4), but replacing the

spatial signature $\mathbf{d}_k$ by the respective steering vector defined in Equation (1.6). The direction of the satellite is 20°, while two jammers are located at 40° and 60°. The weight vector in the MMSE method is obtained by using the exact transmitted navigation signal. Figure 6 clearly shows that deep nulls are placed at the jammer locations, whereas high gains are generated towards the direction of the satellite in both schemes. The advantage of the proposed receiver is that neither prior synchronization nor known satellite location is required.

5.3. Multipath Effects

The purpose of the simulations performed in this subsection is to demonstrate the difference between the receiver that solely relies on the cross-SCORE algorithm and the receiver with additional constraint in the presence of multipath. As discussed in Section 3.1, the cross-SCORE based receiver is unable to mitigate the signal multipath, though very efficient in suppressing interference, as shown by simulations presented so far. This drawback has motivated a constrained receiver design and resulted in the modified cross-SCORE algorithm based receiver in Section 3.2.

We assume that multipath reaches the receiver from the 15-degree range (Ω as defined in Section 3.2) above the horizon. We divide Ω into seven 2-degree spaced angles and form the corresponding matrix $\boldsymbol{B}$. The power of the multipath component is one fifth of the direct-path signal power.

We first consider the case when there is no interference. The direct-path signal is incident on the array with 50° angle. One multipath component (half-chip relative delay and half the direct-path signal power) arrives from the 9° direction. Using the cross-SCORE based receiver, both the direct-path signal and the multipath component receive high gain at the receiver output [Figure 7(a)]. If, instead, the modified cross-SCORE based receiver is employed, the multipath contribution is significantly reduced from the output of the receiver, which is evident from Figure 7(b).

In the next case, a jammer enters into the system from 30°. Figure 8 shows how the two different receivers respond in this environment. We note from Figure 8(a) that both receivers can successfully

place deep null at the jammer location. However, the two receivers' responses to multipath are just opposite. While the cross-SCORE based receiver generates a beam towards the multipath component, the modified cross-SCORE algorithm based receiver creates a null at the same direction.

The multipath mitigation performance of the proposed receiver is also evaluated by feeding the output of the receiver to a conventional early-late delay lock loop (DLL) [24]. We consider the discriminator functions of the receiver outputs without multipath mitigation and the outputs with the modified cross-SCORE algorithm. We compare the results with the case where there is no multipath. The early-late spacing is set to be half of the C/A chip interval. The simulation results are depicted in Figure 8(b), which clearly shows that, without any multipath mitigation process, the zero-crossing point of the discriminator function drifts away from the origin, indicating the pseudorange measurement error [30]. If, on the other hand, the modified cross-SCORE receiver is used first to mitigate multipath contributions, the zero-crossing point of the corresponding discriminator function almost overlaps with the zero-crossing point obtained using the direct-path only signal, suggesting that the proposed technique can significantly reduce the multipath effect on pseudorange measurement.

These simulations prove that both receivers have the capability of canceling strong jammers. However, for multipath mitigation, only the modified cross-SCORE algorithm based receiver can reject multipath coming from near the horizon.

5.4. Synchronization Process

In satellite navigation, the receiver is ultimately evaluated by its ability to provide accurate pseudorange measurements. This is achieved by establishing synchronization between the receiver and the satellite, which is decided based on the cross-correlation between the beamformer outputs and a locally generated spreading sequence [31]. When the phase of the receiver replica code matches that of the code sequence emitted from the satellite, there is a maximum correlation. The high-gain beams towards the satellites provided in the previous examples should be examined in the context of their effects on the post-processing pseudorange calculations.

In the simulation, the satellite is located at 20° and the two jammers are at 40° and 60°. The figure of merit is the cross-correlation between the receiver output and the Gold code sequence:

$$C = \frac{E\left\{\mathbf{z}^H\mathbf{c}\right\}}{\sqrt{E\left\{\mathbf{z}^H\mathbf{z}\right\}E\left\{\mathbf{c}^H\mathbf{c}\right\}}} \tag{1.37}$$

where **c** denotes the $P \times 1$ receiver Gold code, **z** is a $P \times 1$ vector with elements given by $z(n) = \mathbf{w}^H\mathbf{x}$ and **w** is the beamformer coefficient vector discussed in Section 3.1. The normalized cross-correlation with the respective antenna beam pattern for SNR = -25 dB and JSR = 30 dB and 50 dB are shown in Figures 9 and 10, respectively. Also shown in these figures are the normalized cross-correlations obtained before the jammers are removed. It is observed from Figure 9(b) that synchronization can be achieved in the presence of interference when JSR = 30 dB. Figure 10 shows that the proposed receiver can effectively cancel directional jammers and achieve synchronization even when the JSR is as high as 50 dB [Figure 10(c)]. Without interference suppression, however, synchronization fails as shown in Figure 10(b).

5.5. Circular Array

In addition to the uniform linear array, we also implemented the proposed receiver with a uniform circular array (UCA), whose configuration is shown in Figure 11(a). Let (θ, ϕ) denote the elevation angle and the azimuth angle of the satellite. Then, the steering vector of the satellite for the *M*-element UCA is given by

$$\mathbf{a}(\theta,\phi) = \left[e^{j\frac{2\pi r}{\lambda}\sin\theta\cos\phi}, \quad \cdots, \quad e^{j\frac{2\pi r}{\lambda}\sin\theta\cos\left(\phi - 2\pi\frac{M-1}{M}\right)} \right]^T \tag{1.38}$$

where *r* is the radius of the circular array and λ is the wavelength. The steering vector of the jammer has the same form as **a**(θ, ϕ) given above. In the simulation, the satellite signal reaches the array from ($10^\circ, 20^\circ$), whereas a jammer is located at ($60^\circ, 40^\circ$). The beam pattern is shown in Figure 11(b) for $r = \lambda$, and SNR = -30 dB and JSR = 30 dB. It is observed from Figure 11(b) that the receiver has the ability to reject jammers from arbitrary directions.

6. Conclusions

In this chapter, we addressed the issue of interference suppression in global satellite navigation system. Specifically, the unique structure of the GNSS C/A signal is exploited. Due to the repetition of the C/A-code within each navigation symbol, strong self-coherence is observed between chip-rate sampled signals. It is shown that the use of this self-coherence feature allows the development of an anti-jamming GNSS receiving scheme which is built on the cross-SCORE algorithm. The proposed scheme incorporates multiple data and reference blocks, separated by integer multiples of the spreading code length, to generate the array weight vectors. Its performance is analyzed in view of its dependency on the number of blocks and the number of samples in each block. Two receivers are constructed based on the proposed scheme. One directly applies the cross-SCORE algorithm which seeks the optimal beamformers by maximizing the cross-correlation between the receiver output and a reference signal, derived from the receiver signal. The other one applies constraints on the beamformer such that it can also reject multipath arriving from and near the horizon. Numerical results have shown that the proposed scheme is capable of suppressing strong wide class of narrowband and broadband interferers while preserving signals and no *a priori* knowledge of either the transmitted signals or the satellite locations is required.

Appendix A Mean Calculation

To simplify the derivation, we rewrite the received signal vector as

$$\mathbf{x}(n) = s(n)\mathbf{a}(\theta) + \mathbf{v}(n) \tag{A.1}$$

where we consider only the direct-path signal with an explicit direction θ of the satellite. The vector $\mathbf{v}(n)$ contains samples of interference and noise, with zero mean and variance σ_v^2. Both components of $\mathbf{v}(n)$ are assumed to be independent of the GPS signal. Accordingly, $\mathbf{R}_s = E\left\{s(n)\mathbf{a}(\theta)\mathbf{a}^H(\theta)s^H(n)\right\} = \mathbf{a}(\theta)\mathbf{a}^H(\theta)\,\square\,\mathbf{R}_a$, where it is assumed $E\left\{s(n)s^H(n)\right\} = E\left\{\left|s(n)\right|^2\right\} = 1$.

From Section 3, the estimates of the covariance matrices $\mathbf{R}_{xx}$ and $\mathbf{R}_{xx}^{(P)}$ are obtained using the data and reference blocks $\mathbf{X}_N$ and $\mathbf{X}_{N\text{ref}}$ as $\hat{\mathbf{R}}_{xx} = \mathbf{X}_N\mathbf{X}_N^H/N$ and $\hat{\mathbf{R}}_{xx}^{(P)} = \mathbf{X}_N\mathbf{X}_{N\text{ref}}^H/N$, respectively. Taking the expected value $\hat{\mathbf{R}}_{xx}$ yields

$$\bar{\hat{\mathbf{R}}}_{xx} = E\left\{\hat{\mathbf{R}}_{xx}\right\} = \frac{1}{N}\sum_{i=0}^{N-1} E\left\{\mathbf{x}(n-i)\mathbf{x}^H(n-i)\right\} = \mathbf{R}_s + \mathbf{R}_v \tag{A.2}$$

The expected value of $\hat{\mathbf{R}}_{xx}^{(P)}$ is obtained as follows. Define the following events:

$$\begin{aligned}
&B_1 : \mathbf{X}_N \ \&\ \mathbf{X}_{N\text{ref}} \text{ are within the same symbol,}\\
&B_2 : \mathbf{X}_N \text{ or } \mathbf{X}_{N\text{ref}} \text{ is split between two adjacent symbols}\\
&\qquad \&\ N_1 < N \text{ samples are in the first symbol,}\\
&B_3 : \text{ the entire } \mathbf{X}_N \text{ and } \mathbf{X}_{N\text{ref}} \text{ are in two adjacent symbols.}
\end{aligned} \tag{A.3}$$

The corresponding probabilities of the above events are: $\Pr\{B_1\} = 1 - \frac{jP+N}{T}$, $\Pr\{B_2\} = \frac{2N}{T}$, and $\Pr\{B_3\} = \frac{jP-N}{T}$, respectively. In addition, we define the following events regarding the two adjacent symbols:

$$\begin{aligned} C_1 &: \text{the two adjacent symbols have the same sign,} \\ C_2 &: \text{the two adjacent symbols have opposite signs.} \end{aligned} \tag{A.4}$$

The expected value of $\hat{\mathbf{R}}_{xx}^{(P)}$ is calculated as

$$\bar{\hat{\mathbf{R}}}_{xx}^{(P)} = E\left\{\hat{\mathbf{R}}_{xx}^{(P)}\right\} = \frac{1}{N}\sum_{i=1}^{N} E\left\{\mathbf{x}(n-i)\mathbf{x}^H(n-i-jP)\right\} = \bar{\hat{\mathbf{R}}}_{xx|B_1}^{(P)} + \bar{\hat{\mathbf{R}}}_{xx|B_2}^{(P)} + \bar{\hat{\mathbf{R}}}_{xx|B_3}^{(P)} \tag{A.5}$$

where

$$\bar{\hat{\mathbf{R}}}_{xx|B_1}^{(P)} = \frac{1}{N}\sum_{i=1}^{N} E\left\{\mathbf{x}(n-i)\mathbf{x}^H(n-i-jP)\middle| B_1\right\}\Pr\{B_1\} = \left(1 - \frac{jP+N}{T}\right)\mathbf{R}_s \tag{A.6}$$

Because the GPS symbols are equi-probable, then the occurrence of B_3 implies

$$\bar{\hat{\mathbf{R}}}_{xx|B_3}^{(P)} = \frac{1}{N}\sum_{i=1}^{N} E\left\{\mathbf{x}(n-i)\mathbf{x}^H(n-i-jP)\middle| B_3\right\}\Pr\{B_3\} = 0 \tag{A.7}$$

On the other hand, when event B_2 occurs,

$$\bar{\hat{\mathbf{R}}}_{xx|B_2}^{(P)} = \frac{1}{N}\sum_{i=1}^{N} E\left\{\mathbf{x}(n-i)\mathbf{x}^H(n-i-jP)\middle| B_2\right\}\Pr\{B_2\} = \frac{N}{T}\mathbf{R}_s \tag{A.8}$$

From Equations (A.5 - A.8), the expected value of $\hat{\mathbf{R}}_{xx}^{(P)}$ is given by

$$\bar{\hat{\mathbf{R}}}_{xx}^{(P)} = \left(1 - \frac{jP+N}{T}\right)\mathbf{R}_s + \frac{N}{T}\mathbf{R}_s = \left(1 - \frac{jP}{T}\right)\mathbf{R}_s \tag{A.9}$$

which is exactly the one shown in Equation (1.32).

When using *G* data and reference blocks, the estimate of the covariance matrix $\mathbf{R}_{xx}^{(P)}$ is given by

$$\hat{\mathbf{R}}_{xxG}^{(P)} = \frac{1}{G}\sum_{g=1}^{G} \mathbf{X}_N(g)\mathbf{X}_{N\text{ref}}^H(g)/N \tag{A.10}$$

To calculate $\overline{\hat{\mathbf{R}}}_{xxG}^{(P)}$, the expected value of $\hat{\mathbf{R}}_{xxG}^{(P)}$, we define the following events:

F_1: the first data block or the last reference block is split,
F_2: one of the other G-1 data/reference blocks is split
& $G_1 < G$ data blocks (respectively, G_1-1 reference blocks) are in one symbol, (A.11)
F_3: the data blocks and reference blocks are within the same symbol,
F_4: no split block and the data and reference blocks are in two adjacent symbols.

The corresponding probabilities are $\Pr\{F_1\} = \frac{N}{T}$, $\Pr\{F_2\} = \frac{N}{T}$, $\Pr\{F_3\} = 1 - \frac{N + GjP}{T}$, and $\Pr\{F_4\} = \frac{GjP - N}{T}$. We maintain that

$$\hat{\mathbf{R}}_{xxG|F_1}^{(P)} = \frac{1}{G}\sum_{g=1}^{G} E\left\{\mathbf{X}_N(g)\mathbf{X}_{N\text{ref}}^H(g)\middle|F_1\right\}\Pr\{F_1\}/N = \frac{N}{T}\frac{G-1}{G}\mathbf{R}_s + \frac{N}{T}\mathbf{R}_s \tag{A.12}$$

and

$$\hat{\mathbf{R}}_{xxG|F_2}^{(P)} = \frac{1}{G}\sum_{g=1}^{G} E\left\{\mathbf{X}_N(g)\mathbf{X}_{N\text{ref}}^H(g)\middle|F_2\right\}\Pr\{F_2\}/N = \frac{(G-1)N}{2T}\frac{G-2}{G}\mathbf{R}_s + \frac{(G-1)N}{2T}\mathbf{R}_s \tag{A.13}$$

Further,

$$\hat{\mathbf{R}}_{xxG|F_3}^{(P)} = \frac{1}{G}\sum_{g=1}^{G} E\left\{\mathbf{X}_N(g)\mathbf{X}_{N\text{ref}}^H(g)\middle|F_3\right\}\Pr\{F_3\}/N = \left(1 - \frac{N + GjP}{T}\right)\mathbf{R}_s \tag{A.14}$$

and

$$\hat{\mathbf{R}}_{xxG|F_4}^{(P)} = \frac{1}{G}\sum_{g=1}^{G} E\left\{\mathbf{X}_N(g)\mathbf{X}_{N\text{ref}}^H(g)\middle|F_4\right\}\Pr\{F_4\}/N = \frac{GjP - N}{2T}\frac{G-2}{G}\mathbf{R}_s + \frac{GjP - N}{2T}\mathbf{R}_s \tag{A.15}$$

Finally, $\overline{\hat{\mathbf{R}}}_{xxG}^{(P)}$ is given by

$$\overline{\hat{\mathbf{R}}}_{xxG}^{(P)} = \overline{\hat{\mathbf{R}}}_{xxG|F_1}^{(P)} + \overline{\hat{\mathbf{R}}}_{xxG|F_2}^{(P)} + \overline{\hat{\mathbf{R}}}_{xxG|F_3}^{(P)} + \overline{\hat{\mathbf{R}}}_{xxG|F_4}^{(P)} = \left(1 - \frac{jP}{T}\right)\mathbf{R}_s \tag{A.16}$$

which is equivalent to the expected value given in Equation (1.32).

Appendix B Variance Calculation

The variance of $\hat{\mathbf{R}}_{xx}^{(P)}$ is given by [32]

$$\mathrm{var}\left[\hat{\mathbf{R}}_{xx}^{(P)}\right] = E\left\{\hat{\mathbf{R}}_{xx}^{(P)}\hat{\mathbf{R}}_{xx}^{(P)H}\right\} - E^2\left\{\hat{\mathbf{R}}_{xx}^{(P)}\right\} \tag{A.17}$$

In Appendix A, we have shown that the covariance estimates are unbiased. In what follows, we concentrate on evaluating $E\left\{\hat{\mathbf{R}}_{xx}^{(P)}\hat{\mathbf{R}}_{xx}^{(P)H}\right\}$.

Using one data and reference block, we let $\boldsymbol{\Psi}_{1|B_1} \triangleq E\left\{\hat{\mathbf{R}}_{xx}^{(P)}\hat{\mathbf{R}}_{xx}^{(P)H}\middle| B_1\right\}\Pr\{B_1\}$, where events B_l, $l \in [1,3]$, are defined in Equation (A.3). Then,

$$\boldsymbol{\Psi}_1 \triangleq E\left\{\hat{\mathbf{R}}_{xx}^{(P)}\hat{\mathbf{R}}_{xx}^{(P)H}\right\} = \boldsymbol{\Psi}_{1|B_1} + \boldsymbol{\Psi}_{1|B_2} + \boldsymbol{\Psi}_{1|B_3} \tag{A.18}$$

When the data and reference blocks are within the same symbol or, equivalently, in two adjacent symbols with the same sign (i.e., event C_1), we have

$$E\left\{\hat{\mathbf{R}}_{xx}^{(P)}\hat{\mathbf{R}}_{xx}^{(P)H}\middle| C_1\right\} = \frac{1}{N^2}E\left\{\sum_{i=0}^{N-1}\sum_{l=0}^{N-1}\mathbf{x}(n-i)\mathbf{x}^H(n-i-jP)\mathbf{x}(n-l-jP)\mathbf{x}^H(n-l)\middle| C_1\right\} \tag{A.19}$$

Substituting **x**(n) from Equation (1.39) and after some straightforward calculations, we have

$$E\left\{\hat{\mathbf{R}}_{xx}^{(P)}\hat{\mathbf{R}}_{xx}^{(P)H}\middle| C_1\right\} = \frac{M(N+\sigma_v^2)}{N}\mathbf{R}_a + \frac{M(1+\sigma_v^2)}{N}\mathbf{R}_v \triangleq \tilde{\mathbf{R}} \tag{A.20}$$

where we have used $\mathbf{a}^H(\theta)\mathbf{a}(\theta) = M$ and $E\left\{\mathbf{v}^H(n)\mathbf{v}(n)\right\} = M\sigma_v^2$. When event B_1 occurs,

$$\boldsymbol{\Psi}_{1|B_1} = \left(1 - \frac{jP+N}{T}\right)\tilde{\mathbf{R}} \tag{A.21}$$

Similarly,

$$\boldsymbol{\Psi}_{1|B_2} = \frac{2N}{T}\tilde{\mathbf{R}} \tag{A.22}$$

and in case of event B_3, we have

$$\boldsymbol{\Psi}_{1|B_3} = \frac{(jP-N)}{T}\tilde{\mathbf{R}} \tag{A.23}$$

Finally, the variance of $\hat{\mathbf{R}}_{xx}^{(P)}$ is

$$\begin{aligned}\mathrm{var}\left[\hat{\mathbf{R}}_{xx}^{(P)}\right] &= E\left\{\hat{\mathbf{R}}_{xx}^{(P)}\hat{\mathbf{R}}_{xx}^{(P)H}\right\} - E^2\left\{\hat{\mathbf{R}}_{xx}^{(P)}\right\} \\ &= \frac{M(N+\sigma_v^2)}{N}\mathbf{R}_a + \frac{M(1+\sigma_v^2)}{N}\mathbf{R}_v - \left(1-\frac{jP}{T}\right)^2\mathbf{R}_s^2\end{aligned} \tag{A.24}$$

For *G* data and reference blocks we can similarly define, using the events in Equation (A.11),

$$\boldsymbol{\Psi}_G \triangleq E\left\{\hat{\mathbf{R}}_{xxG}^{(P)}\hat{\mathbf{R}}_{xxG}^{(P)H}\right\} = \boldsymbol{\Psi}_{G|F_1} + \boldsymbol{\Psi}_{G|F_2} + \boldsymbol{\Psi}_{G|F_3} + \boldsymbol{\Psi}_{G|F_4} \tag{A.25}$$

where $\boldsymbol{\Psi}_{G|F_l} \triangleq E\left\{\hat{\mathbf{R}}_{xxG}^{(P)}\hat{\mathbf{R}}_{xxG}^{(P)H}\middle|F_l\right\}\Pr\{F_{l1}\}$, $l\in[1,4]$. Following the same procedure we adopted in calculating the expected value of $\hat{\mathbf{R}}_{xx}^{(P)}$, it can be readily shown that

$$\begin{aligned}\boldsymbol{\Psi}_{G|F_1} &= \left[\frac{N}{T}\frac{(G-1)^2}{G^2} + \frac{N}{T}\right]\tilde{\mathbf{R}} \\ \boldsymbol{\Psi}_{G|F_2} &= \left[\frac{(G-1)N}{2T}\frac{(G-1)^2}{G^2} + \frac{(G-1)N}{2T}\right]\tilde{\mathbf{R}} \\ \boldsymbol{\Psi}_{G|F_3} &= \left(1-\frac{N-GjP}{T}\right)\tilde{\mathbf{R}} \\ \boldsymbol{\Psi}_{G|F_4} &= \left[\frac{G(jP-N)}{2T}\frac{(G-1)^2}{G^2} + \frac{G(jP-N)}{2T}\right]\tilde{\mathbf{R}}\end{aligned} \tag{A.26}$$

from which we obtain

$$E\left\{\hat{\mathbf{R}}_{xxG}^{(P)}\hat{\mathbf{R}}_{xxG}^{(P)H}\right\} = \left(1-2\frac{jP}{T}+2\frac{jP}{GT}\right)\left[\frac{M(N+\sigma_v^2)}{N}\mathbf{R}_a + \frac{M(1+\sigma_v^2)}{N}\mathbf{R}_v\right] \tag{A.27}$$

Finally, the variance is

$$\begin{aligned}\mathrm{var}\left[\hat{\mathbf{R}}_{xx}^{(P)}\right] &= E\left\{\hat{\mathbf{R}}_{xx}^{(P)}\hat{\mathbf{R}}_{xx}^{(P)H}\right\} - E^2\left\{\hat{\mathbf{R}}_{xx}^{(P)}\right\} \\ &= \left(1-2\frac{jP}{T}+2\frac{jP}{GT}\right)\left[\frac{M(N+\sigma_v^2)}{N}\mathbf{R}_a + \frac{M(1+\sigma_v^2)}{N}\mathbf{R}_v\right] - \left(1-\frac{jP}{T}\right)^2\mathbf{R}_s^2\end{aligned} \tag{A.28}$$

The above equation clearly shows that the larger the number of data and reference blocks used in the time-averaging, the smaller the variance.

References

[1] E. D. Kaplan (eds.), *Understanding GPS: Principles and Applications.*1em plus 0.5em minus 0.4emArtech House Publisher, 1996.

[2] P. Enge and P. Misra, "Scanning the issue/technology," *Proceedings of The IEEE*, vol. 87, no. 1, pp. 3–15, January 1999.

[3] J. McNeff, "The global positioning system," *IEEE Transactions on Microwave Theory and Techniques*, vol. 50, no. 3, pp. 645–652, March 2002.

[4] R. Van Nee, "Spread spectrum code and carrier synchronization errors caused by multipath and interference," *IEEE Transactions on Aerospace and Electronic Systems*, vol. 29, no. 4, pp. 1359–1365, October 1993.

[5] P. W. Ward, "GPS receiver interference monitoring, mitigation and analysis techniques," *Journal of the Institute of Navigation*, vol. 41, no. 4, pp. 367–391, Winter 1995.

[6] D. Moelker, E. van der Pol, and Y. Bar-Ness, "Multiple antennas for advanced GNSS multipath mitigation and multipath direction finding," in *Proceedings of ION GPS 97*, 1997, pp. 541–550.

[7] M. S. Braasch and A. J. V. Dierendonck, "GPS receiver architectures and measurements," *Proceedings of the IEEE*, vol. 87, no. 1, pp. 48–64, January 1999.

[8] M. Braasch and M. DiBenedetto, "Spread spectrum ranging multipath model and validation," *IEEE Transactions on Aerospace and Electronic Systems*, vol. 37, pp. 298–303, January 2001.

[9] P. Ward, "GPS interference and jamming issues for civil and military users," in *Short Course 323, Navtech Seminars and GPS Supply, Inc.*, Annapolis, MD, 2003.

[10] R. Iltis and L. Milstein, "Performance analysis of narrowband interference rejection techniques in DS spread-spectrum systems," *IEEE Transactions on Communications*, vol. 32, no. 11, pp. 1169–1177, November 1984.

[11] L. Rusch and H. Poor, "Narrowband interference suppression in CDMA spread spectrum communications," *IEEE Transactions on Communications*, vol. 42, no. 2, pp. 1969–1979, February/March/April 1994.

[12] L. Rusch and H. Poor, "Multiuser detection techniques for narrowband interference suppression in spread spectrum communications," *IEEE Transactions on Communications*, vol. 43, no. 2, pp. 1725–1737, February/March/April 1995.

[13] Y. Zhang, M. G. Amin, and A. R. Lindsey, "Anti-jamming GPS receivers based on bilinear signal distributions," in *Proceedings of the 2001 Military Communications Conference (MILCOM 2001)*, vol. 2, 2001, pp. 1070–1074.

[14] M. G. Amin and Y. Zhang, "Spatial time-frequency distributions and their applications," in *Proceedings of the 6th International Symposium on Signal Processing and its Applications*, vol. 1, 2001, pp. 254–255.

[15] M. D. Zoltowski and A. S. Gecan, "Advanced adaptive null steering concepts for GPS," in *Proceedings of the 1995 Military Communications Conference (MILCOM 1995)*, vol. 3, 1995, pp. 1214–1218.

[16] R. L. Fante and J. J. Vaccaro, "Wideband cancellation of interference in a GPS receive array," *IEEE Transactions on Aerospace and Electronic Systems*, vol. 36, no. 2, pp. 549–564, April 2000.

[17] R. L. Fante and J. J. Vacarro, "Cancellation of jammers and jammer multipath in a GPS receiver," *IEEE Aerospace and Electronic System Magazine*, vol. 13, no. 11, pp. 25–28, November 1998.

[18] D. Moelker, E. Van Der Pol, and Y. Bar-Ness, "Adaptive antenna arrays for interference cancellation in GPS and GLONASS receivers," in *Proceedings of the IEEE 1996 Position Location and Navigation Symposium*, 1996, pp. 191–198.

[19] Y. Zhang, M. Amin, and A. R. Lindsey, "Anti-jamming GPS receivers based on bilinear signal distributions," in *Proceedings of the MILCOM 2001*, vol. 2, 2001, pp. 1070–1074.

[20] G. Hatke, "Adaptive array processing for wideband nulling in GPS systems," in *Proceedings of the 32nd Asilomar Conference on Signals, Systems and Computers*, vol. 2, 1998, pp. 1332–1336.

[21] P. Xiong, M. J. Medley, and S. N. Batalama, "Spatial and temporal processing for global navigation satellite systems: The GPS receiver paradigm," *IEEE Transactions on Aerospace and Electronic Systems*, vol. 39, no. 4, pp. 1471–1484, October 2003.

[22] B. Townsend and P. Fenton, "A practical approach to the reduction of pseudorange multipath errors in a L1 GPS receiver," in *Proceedings of the 1994 ION GPS Conference*, 1994, pp. 20–23.

[23] B. Townsend and P. Fenton, "Performance evaluation of the multipath estimating delay lock loop," in *Proceedings of the 1995 ION National Technical Meeting*, 1995.

[24] A. Van Dierendonck, P. Fenton, and T. Ford, "Theory and performance of narrow correlator spacing in a GPS receiver," *Journal of The Institute of Navigation*, vol. 39, no. 2, pp. 265–283, 1992.

[25] R. J. Van Nee, "The multipath estimation delay lock loop: Approaching theoretical limits," in *Proceedings of the 2nd IEEE Symposium on Spread Spectrum Techniques and Applications*, 1992, pp. 39–42.

[26] P. Misra and P. Enge, *Global Positioning System, signals, Measurements, and performance*. Lincoln, Massachusetts: Ganga-Jamuna Press, 2001.

[27] B. Agee, S. Schell, and W. Gardner, "Spectral self-coherence restoral: A new approach to blind adaptive signal extraction using antenna array," *Proceedings of the IEEE*, vol. 78, no. 4, pp. 753–767, April 1990.

[28] B. Agee, S. Schell, and W. Gardner, "The score approach to blind adaptive signal extraction: An application of the theory of spectral correlation," in *Proceedings of the Fourth Annual ASSP Workshop on Spectrum Estimation and Modeling*, 1988, pp. 277–282.

[29] G. H. Golub and C. F. Van Loan, *Matrix Computations*, 3rd ed. Baltimore, MD: Johns Hopkins University Press, 1996.

[30] M. S. Braasch and A. J. V. Dierendonck, “GPS receiver architectures and measurements,” *Proceedings of the IEEE*, vol. 87, no. 1, pp. 48–64, January 1999.

[31] B. W. Parkinson and J. J. Spilker Jr. (eds.), *Global positioning system: Theory and applications, Vol I*. American Institute of Aeronautics, Inc,. Washington, DC: Progress in Astronautics and Aeronautics, 1996.

[32] A. Papoulis, *Probability, Random Variables, and Stochastic Processes*, 3rd ed. McGraw-Hill, 1991.

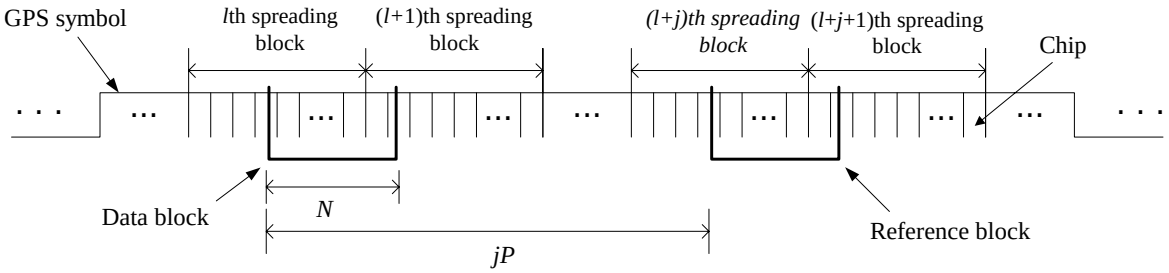

Figure 1. Noise-free C/A signal structure and data and reference blocks formation.

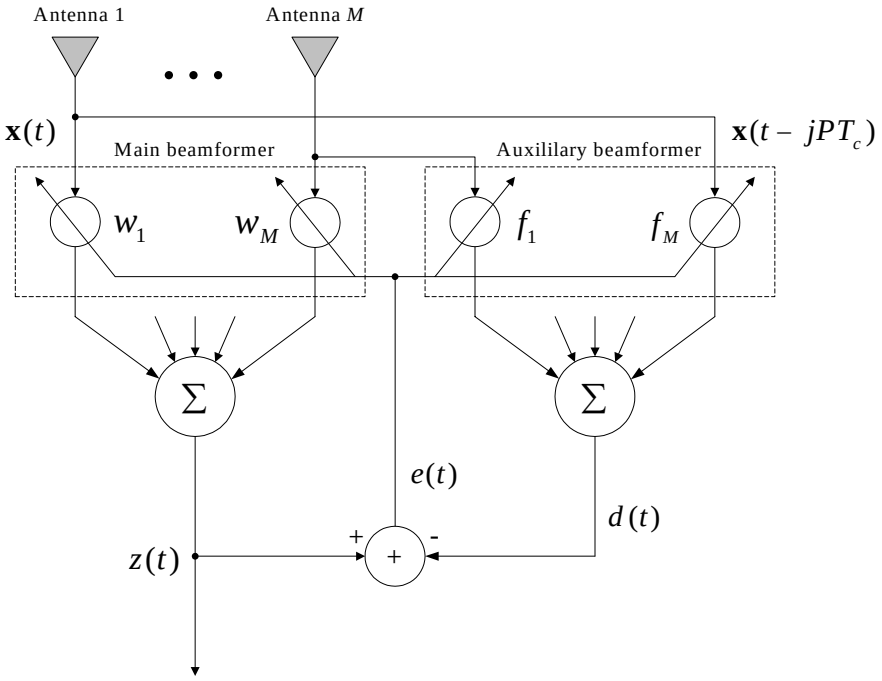

Figure 2. Structure of the proposed anti-jamming scheme.

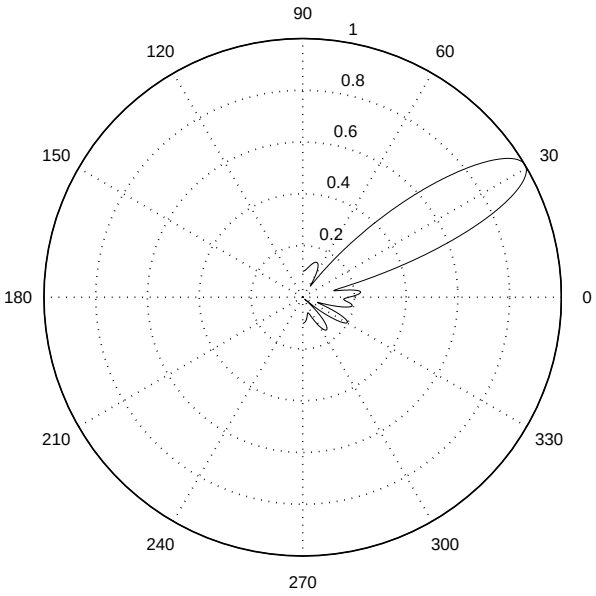

Figure 3. Beam pattern generated by the cross-SCORE based receiver with SNR = -30 dB and one data and one reference block taking within the same symbol.

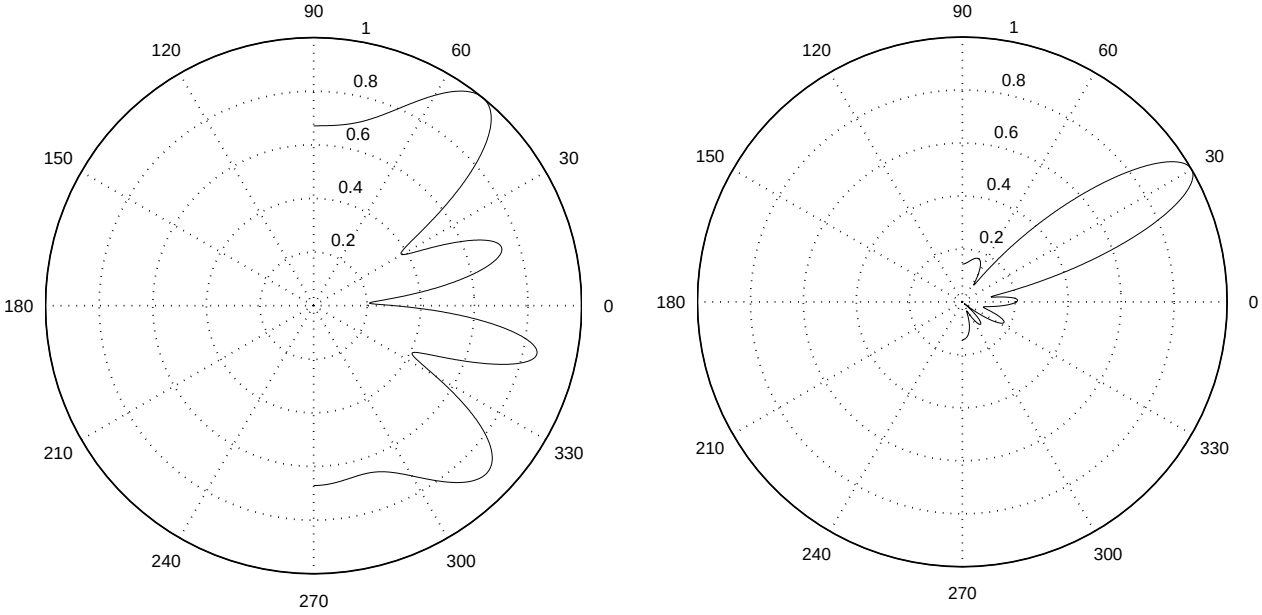

Figure 4. Beam pattern generated by the cross-SCORE based receiver with multiple data and reference blocks and SNR = -40 dB. (a) G = 2; (b) G = 7.

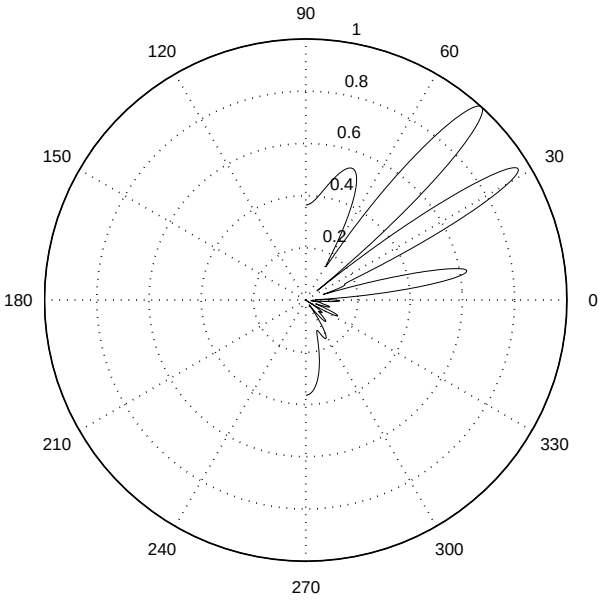

Figure 5. Beam pattern generated by the cross-SCORE based receiver with four satellites, SNR =-30 dB, and *G* = 7.

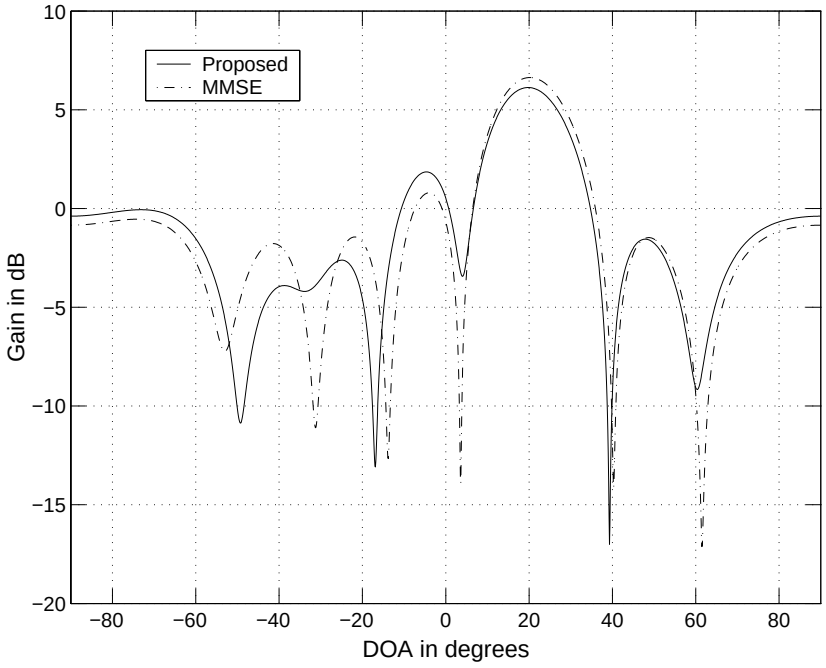

Figure 6. Antenna gains of the proposed scheme and the MMSE scheme with SINR = -33 dB, JSR = 30 dB, and *G* = 3.

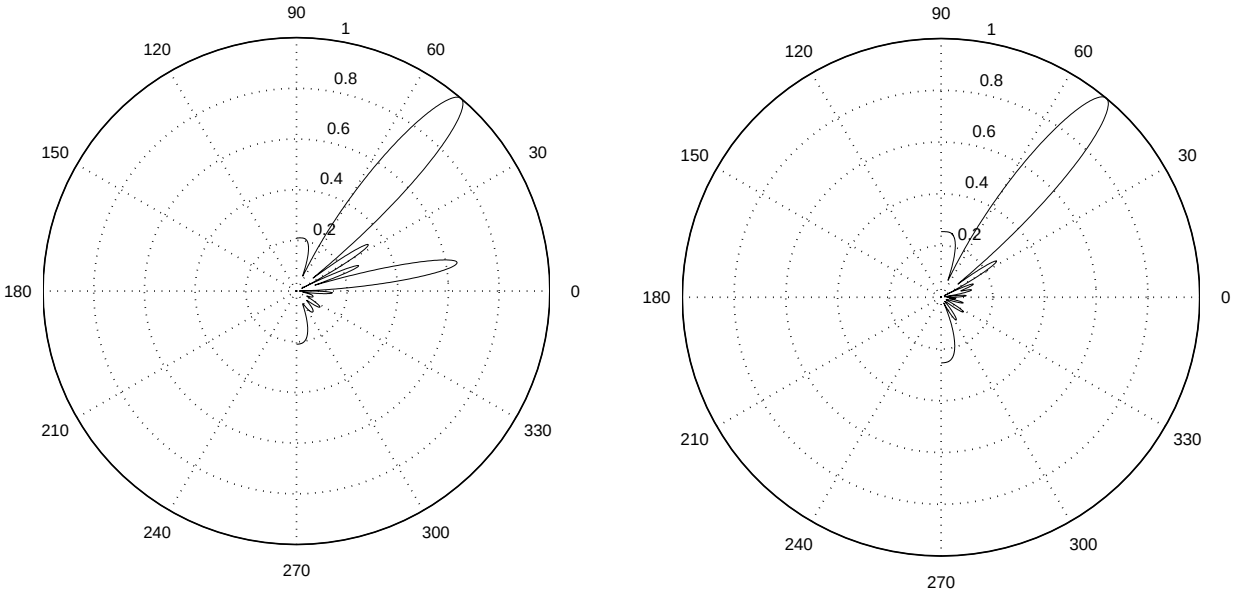

(a) (b)

Figure 7. In the presence of multipath with SNR = -30 dB and *G* = 7. (a) Cross-SCORE based receiver; (b) Modified cross-SCORE based receiver.

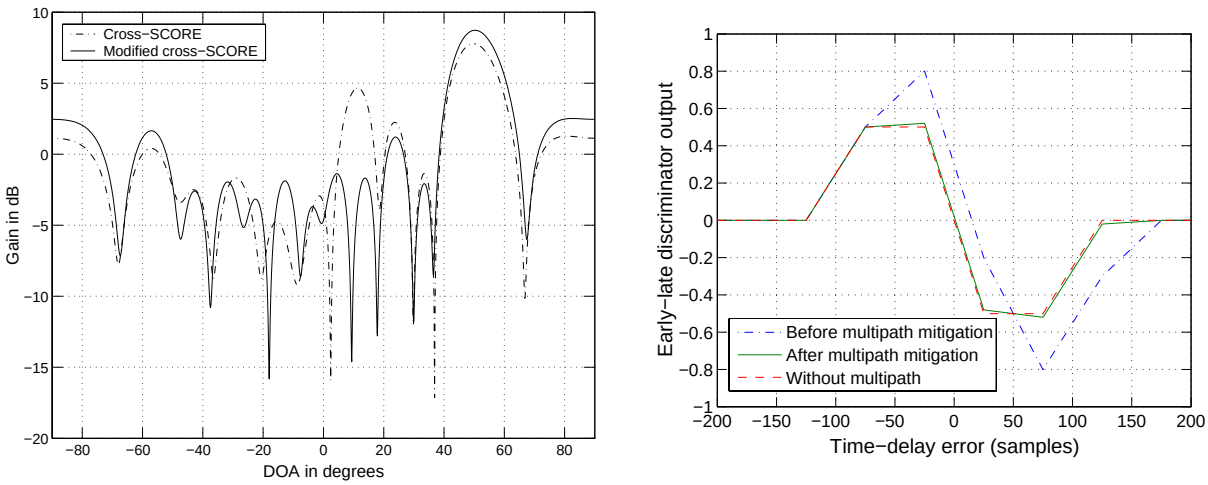

(a) (b)

Figure 8. (a) Comparison between the cross-SCORE based receiver and the modified cross-SCORE based receiver SINR = - 33 dB, JSR = 30 dB, and *G* = 7; (b) Comparison of the discriminator functions of the early-late delay lock loop.

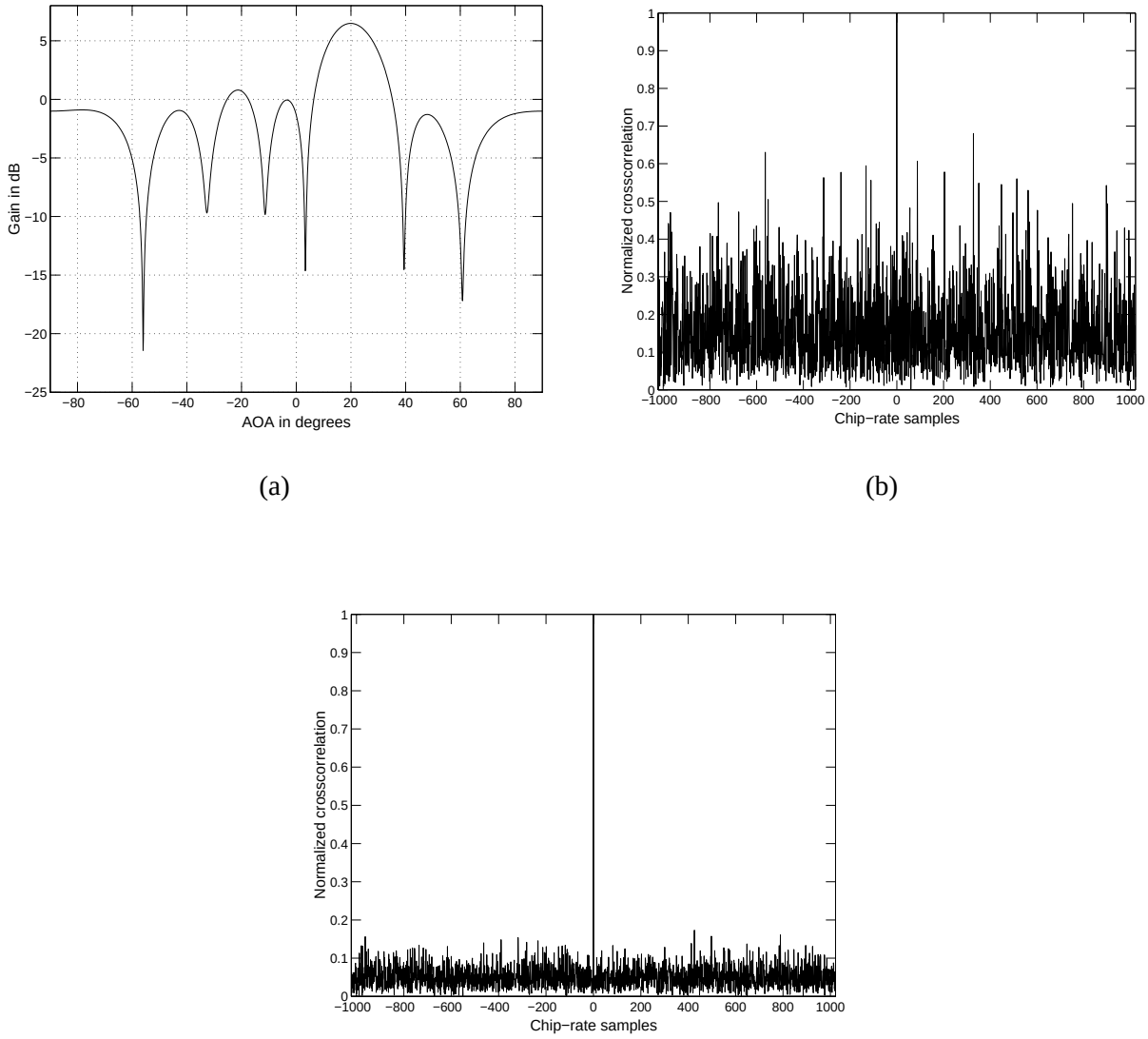

Figure 9. Synchronization of the cross-SCORE based receiver with SNR = -25 dB, JSR = 30 dB, and *G* = 7. (a) Beam pattern; (b) Normalized cross-correlation before jammer removal; (c) Normalized cross-correlation after jammer removal.

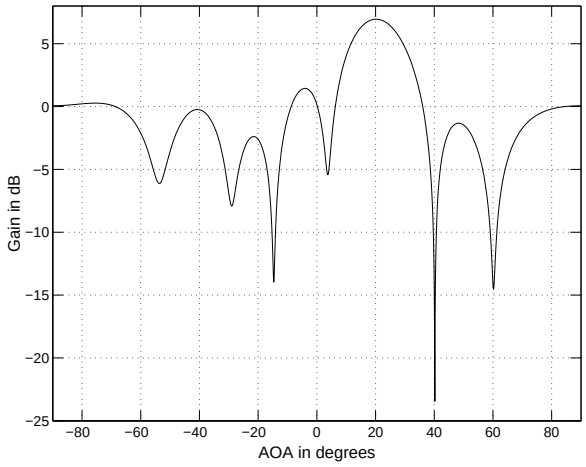

(a)

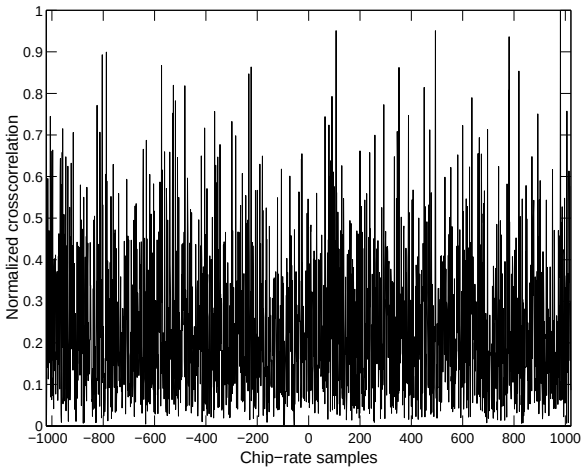

(b)

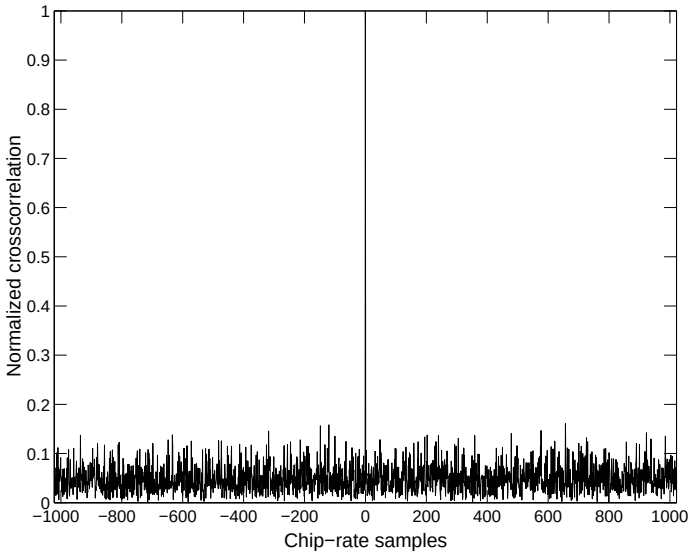

(c)

Figure 10. Synchronization of the cross-SCORE based receiver with SNR = -25 dB, JSR = 50 dB, and *G* = 7. (a) Beam pattern; (b) Normalized cross-correlation before jammer removal; (c) Normalized cross-correlation after jammer removal.

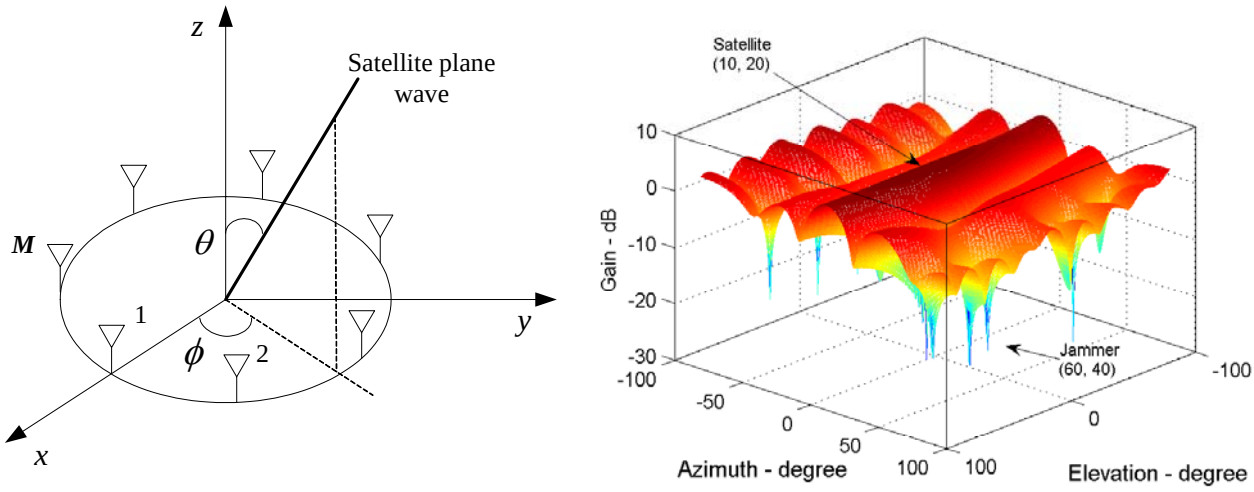

(a) (b)

Figure 11. Performance of the receiver with a circular array. (a) Circular array configuration; (b) Beam pattern.

Chapter 2
Subspace Array Processing for the Suppression of FM Jamming in GPS Receivers

1. Introduction

Signals with rapidly time-varying frequency characteristics can be the preferred option at different transmitters or generated as a consequence of moving targets and scatterers of fixed-frequency emitters [12]. These signals are difficult to analyze, track, and remove using conventional methods assuming stationary or quasi-stationary environments. Recent developments in time-frequency signal representations [9], [13], [25] have allowed accurate estimations of the signal time-frequency signature, including the signal instantaneous frequency and instantaneous bandwidth, leading to effective suppression of undesired nonstationary signals [1], [5], [15], [27]. Previous work has addressed the general case of direct sequence spread spectrum receivers. In this chapter, we consider the specific case of suppressing a class of frequency-modulated jammers incident on a Global Position System (GPS) receiver using the jammer spatial and time-frequency signatures in conjunction with methods of subspace projections.

The GPS uses a direct sequence spread spectrum (DSSS) signal that is highly susceptible to interference [16], [24]. There are both intentional and non-intentional forms of interference. The primary area of concern in both commercial and military application is intentional interferers. Development of techniques for protection of GPS from interference and jamming is an area of active research.

GPS DSSS signals have some degree of jamming protection, via processing gain, built in to the signal structure itself; however, due to the fact that the GPS signal originates in a half-geosynchronous orbit, it is relatively weak when it reaches the earth. The weak signal strength of the GPS signal makes it easy for an intentional jammer to overcome the inherent jamming protection of the DSSS signal.

Depending on the GPS receiver, the jammer-to-signal ratio (JSN) of greater than 40 to 50dB will prevent the GPS receiver from being able to obtain a position. There are several approaches to mitigating this susceptibility including frequency-domain techniques [6], [11], time-domain techniques [17], [21], and adaptive antennas [14], [23]. Frequency- and time-domain techniques are only effective against partial band interference. Further, neither of these techniques is capable of effectively incorporating the suddenly- changing or evolutionary rapidly time-varying nature of the frequency characteristics of the interference. In both techniques, there is a lack of intelligence about interference behavior in the joint time-frequency (t-f) domain, rendering them limited in results and applicability. For the time-varying interference depicted in Figure 1, frequency-domain methods remove the frequency band Δf and ignore the fact that only few frequency bins are contaminated by the interference at a given time. Dually, time-domain excision techniques, through gating or clipping the interference over ΔT, do not account for the cases where only few time samples are contaminated by the interference for a given frequency. Applying either method will indeed eliminate the interference but at the cost of unnecessarily reducing the desired signal energy.

Adaptive excision methods might be able to track and remove the nonstationary interference, but would fail if the interference is highly nonlinear FM or linear FM, as in Figure 1, with high sweep rates. Further, the adaptive filtering length or block transform length trades off the temporal and the spectral resolutions of the interference. Increasing the step size parameter increases the filter output errors at convergence, and causes an unstable estimate of the interference waveform.

The above example clearly demonstrates that nonstationary interferers, which have model parameters that rapidly change with time, are particularly troublesome due to the inability of single-domain mitigation algorithms to adequately ameliorate their effects. In this challenging situation, and others like it, joint t-f techniques can provide significant performance gains, since the instantaneous frequency (IF), the instantaneous bandwidth, and the energy measurement, in addition to myriad other parameters, are available. The objective is then to estimate the t-f signature of the received data using t-f analysis,

attenuating, or removing, the received signal in those t-f regions that contain strong interference. This is depicted by the region in between the dashed lines in Figure 1.

Recently, several techniques based on linear transforms and quadratic distributions have been devised for FM interference excision in direct-sequence spread-spectrum (DSSS) communication systems [1] – [5], [15], [18], [19], [27], [28]. These techniques assume clear jammer time-frequency signatures and rely on the distinct differences in the localization properties between the jammer and the spread spectrum signals. An important class of these t-f based methods applies subspace projection techniques for interference mitigation [4], [26], [31], [32]. In essence, the jammer instantaneous frequency, whether provided by the time-frequency distributions or any other IF estimator, is used to define the temporal signature of the interference, with one-dimensional signal space per interference source. This, in turn, is used to construct a subspace orthogonal to the jammer. The respective projection matrix is used to excise the jammer power in the incoming signal prior to correlation with the receiver pseudorandom noise (PN) sequence. The result is improved receiver signal-to-interference-plus-noise ratio (SINR) and reduced BERs. Compared with the subspace projection techniques in the single-sensor case, the use of multi-sensor array greatly increases the dimension of the available signal subspace. It allows both the distinctions in the spatial and time-frequency (temporal) signatures of the GPS signals from those of the interferers to play equal roles in suppressing the jammer with a minimum distortion of the desired signal.

In this chapter, we examine the applicability of multi-sensor subspace projection techniques for suppressing nonstationary jammers in GPS receivers. We rely on IF estimators, specifically the TFDs, to provide accurate estimates of the jammer signal parameters. With any employed IF estimator, the jammer parameters are deemed to be perturbed. Due to inaccuracies in IF, the GPS receiver anti-jamming performance is degraded, lowering the receiver SINR. This chapter analyzes the multi-antenna GPS receiver performance in the presence of zero-mean identical and independent Gaussian IF estimation errors. The single antenna receiver case is derived as a special case of the multi-antenna receiver. It is shown that the use of several antennas at the receivers reduce the impact of IF estimation errors on degrading the receiver performance. The angular location of each GPS satellite is assumed known and is

used to design an appropriate jammer mitigation technique. In addition, accurate estimates of the jammer spatial signatures are assumed, and stem from recently developed successful direction finding techniques of FM signals [7], [8], [30]. In comparing the single and multi-antenna cases, the chapter shows that the use of antenna arrays effectively improves the receiver SINR by exploiting the difference in spatial signatures as well as the t-f signatures.

This chapter is organized as follows. Section 2 gives a description of the GPS signal structure. It also briefly discusses nonstationary signal parameter estimations, and provides key references on the subject. FM jammer suppression using subspace projection is introduced and analyzed in Section 3 for multi-antenna GPS receivers. The effect of inaccuracies in IF estimation on receiver performance is analyzed in Section 4 for the single-jammer case. Appendix A presents the generalization of the analysis of Section 4 to multiple jammers. All jammers are modeled as frequency modulated signals with no instantaneous bandwidth. AM/FM jammers are outside the scope of this chapter and require a different analytical approach.

2. Background

2.1. GPS C/A Signal Structure

GPS employs BPSK-modulated DSSS signals. The navigation data is transmitted at a symbol rate of 50 bps. It is spread by a coarse acquisition (C/A) code and a precision (P) code. The C/A code is a Gold sequence with a chip rate of 1.023 MHz and a period of 1023 chips, i.e. its period is 1 ms, and there are 20 periods within one data symbol. The P code is a PN code at the rate of 10.23 MHz and with a period of 1 week. These two spreading codes are multiplexed in quadrature phases[10,16,24]. Figure 2 shows the signal structure. The carrier L1 is modulated by both the C/A code and the P code and the carrier L2 is only modulated by P code. It is commonly assumed that the C/A code and the P code are perfectly separated. The peak power spectral density of the C/A signal exceeds that of the P code by 13dB. The GPS signal is typically very weak. The jammer-to-signal ratio (JSR) is often larger than 40 dB, whereas

the signal-to-noise ratio (SNR) is about -14 to -20dB. Due to the high JSR, the jammer depicts a clear signature in the time-frequency domain.

We mainly address the problem of anti-jamming for the C/A code. This code has unique properties due to the fact that it is periodic within one data symbol and fixed for each satellite signal. It is shown that this periodicity has a considerable effect on the receiver performance.

2.2. Instantaneous Frequency Estimation

As stated previously, there are several linear and bilinear t-f methods for IF estimation, most notably, those based on Wigner-Ville distribution and its generalization into Cohen's class. The Wigner distribution (WD) (also known as Wigner-Ville distribution), which was the first distribution introduced in the context of quantum mechanics, has paved the way to several key contributions to advances in the area of time-frequency analysis as well as representations of signals with time-varying characteristics. These contributions have aimed at overcoming the drawbacks of the WD and sought new, more effective tools for nonstationary signal analysis, synthesis, and processing.

Cohen [13] provided a consistent set of definitions for a desirable class of time-frequency distributions (TFDs), often referred as Cohen's class. Cohen's class of time-frequency (t,ω) distributions for the signal x(t) may be presented in different forms, including

$$\rho(t,\omega;\phi) = \int_{-\infty}^{\infty}\int_{-\infty}^{\infty} \phi(t-u,\tau)x(u+\tau/2)x(u-\tau/2)\, e^{-j\omega\tau} du\, d\tau \qquad (2.1)$$

Different distributions are obtained by selecting different kernels, $\phi(t,\tau)$. Both the Wigner distribution and the spectrogram are prominent members of Cohen's class. The WD, and its widowed approximation, is obtained from (2.1) by setting the kernel to be an impulse in time, *t*. TFDs have been successfully applied to areas where signals are localizable in the time frequency domain and have fixed distinct signatures that permit their classification and separation. Many of these applications are discussed in the book by Cohen [13] and also in the book by Qian and Chen [25]. One successful offering of TFD is in the area of instantaneous frequency estimation for FM signals [9]. TFD can be used to provide an

accurate estimate of a jammer uniquely characterized by its instantaneous frequency. The distinctions between the FM and the Gold code time-frequency signatures as well as the relative high strength of the jammer and weak GPS signal power, simplify the jammer IF estimation. Figure 3 shows the Wigner distribution of a chirp signal in noise with SNR = -20 dB. Added to the chirp signal, a spread spectrum signal of JSR = 40 dB. The chirp t-f signature is clear in the figure, and its parameters can be easily identified and used for subspace construction. We maintain that the proposed technique for GPS FM jammer suppression does not require the application of any particular IF estimator. However, TFD has been shown to outperform other estimators, specifically for signals with rapidly-changing frequency characteristics [9], with increased computational cost.

3. Subspace Projection Array Processing

The concept of subspace projection for instantaneously narrowband jammer suppression is to remove the jammer components by projecting the received data onto the subspace that is orthogonal to the jammer subspace, as illustrated in Figure 4.

In GPS, the PN sequence of length L (1023) repeats itself Q (20) times within one symbol of the 50 bps navigation data. We use discrete-time form, where all the signals are sampled at the chip-rate of the C/A code. We consider an antenna array of N sensors, and the communication channel is restricted to flat-fading. In the proposed interference excision approach, the LNQ sensor output samples are partitioned into Q blocks, each of L chips and LN samples. The jammer can be consecutively removed from the 20 blocks that constitute one symbol. This is achieved by projecting the received data in each block on the corresponding orthogonal subspace of the jammer. The jammer-free signal is then correlated with the replica PN sequence on a symbol-by-symbol basis. We first consider the subspace projection within each block. The array output vector at the k^{th} sample is given by

$$\mathbf{x}(k) = \mathbf{x}_s(k) + \mathbf{x}_u(k) + \mathbf{b}(k) = c(k)\mathbf{h} + \sum_{i=1}^{D} A_i u_i(k)\mathbf{a}_i + \mathbf{b}(k) \tag{2.2}$$

where $\mathbf{x}_s$, $\mathbf{x}_u$, and $\mathbf{b}$ are the signal, the jammer and the white Gaussian noise contributions, respectively. $\mathbf{h}$ is the signal spatial signature, and $c(k)$ is the spreading PN sequence. The number of jammers is D. All jammers are considered as instantaneously narrowband FM signals with constant amplitude $u_i(k)=\exp[j\varphi_i(k)]$. A_i and $\mathbf{a}_i$ are the i-th jammer amplitude and the spatial signature, respectively. Furthermore, we normalize the channels and set $\|\mathbf{h}\|_F^2 = N$ and $\|\mathbf{a}\|_F^2 = N$, where $\|\cdot\|_F^2$ is the Frobenius norm of a vector. The noise vector $\mathbf{b}(k)$ is zero-mean, temporally and spatially white with

$$\begin{aligned} E[\mathbf{b}(k)\mathbf{b}^T(k+l)] &= 0 \\ E[\mathbf{b}(k)\mathbf{b}^H(k+l)] &= \sigma^2\delta(l)\mathbf{I}_N \end{aligned} \tag{2.3}$$

where σ^2 is the noise power, and $\mathbf{I}_N$ is the $N\times N$ identity matrix. Using L sequential array vector samples within the block, we obtain the following LN-by-1vector

$$\begin{aligned} \mathbf{X} &= [\mathbf{x}^T(1) \;\; \mathbf{x}^T(2) \;\; ... \;\; \mathbf{x}^T(L)]^T \\ &= \mathbf{X}_s + \mathbf{X}_u + \mathbf{B} \end{aligned} \tag{2.4}$$

The vector $\mathbf{X}_u$ consists of the D jammer signals, and is expressed as

$$\mathbf{X}_u = \sum_{i=1}^{U} \mathbf{V}_i \tag{2.5}$$

with

$$\mathbf{V}_i = \mathbf{u}_i \otimes \mathbf{a}_i = \frac{1}{\sqrt{L}}[u_i(1) \;\; u_i(2) \;\; ... \;\; u_i(L)]^T \otimes \mathbf{a}_i \tag{2.6}$$

where $\otimes$ denotes the Kronecker product. Therefore,

$$\mathbf{V} = [\mathbf{V}_1 \;\; \mathbf{V}_2 \;\; ... \;\; \mathbf{V}_D] \tag{2.7}$$

spans the jammer signal subspace, and its orthogonal subspace projection matrix is given by

$$\mathbf{P} = \mathbf{I}_{LN} - \mathbf{V}(\mathbf{V}^H\mathbf{V})^{-1}\mathbf{V}^H = \mathbf{I}_{LN} - \frac{1}{N}\mathbf{V}\mathbf{V}^H \tag{2.8}$$

The projection of the received signal vector onto the orthogonal subspace yields

$$\mathbf{X}_\perp = \mathbf{P}\mathbf{X} = \mathbf{P}\mathbf{X}_s + \mathbf{P}\mathbf{B} \tag{2.9}$$

which excises the jammers entirely. The signal vector $\mathbf{X}_s$, assuming symbol "1" is transmitted, can be rewritten as

$$\mathbf{X}_s = [\,p(1) \quad p(2) \quad \ldots \quad p(L)]^T \otimes \mathbf{h} \;\triangleq\; \mathbf{q} \tag{2.10}$$

where $p(n)$ is the C/A code and the vector $\mathbf{q}$ represents the spatial-temporal signature of the GPS signal. The result of despreading in the subspace projection based array system over one block is

$$y = \mathbf{q}^H \mathbf{X}_\perp = \mathbf{q}^H \mathbf{P}\mathbf{q} + \mathbf{q}^H \mathbf{P}\mathbf{B} \;\triangleq\; y_1 + y_2 \tag{2.11}$$

where y_1 and y_2 are the contributions of the PN and the noise sequences to the decision variable, respectively. Equation (2.11) assumes that the received satellite signal is aligned with its receiver replica. Appendix A shows that the projection operation does not cause a shift of the correlation peak, and as such, there is no bias in the pseudorange. For simplification, we assume that the jammers share the same period as the GPS data symbol. In GPS systems, due to the fact that each satellite is assigned a fixed Gold code [3], and that the Gold code is the same for every data symbol, y_1 is a deterministic value, rather than a random variable assumed in many spread spectrum applications. The value of y_1 is given by

$$\begin{aligned} y_1 &= \mathbf{q}^H \mathbf{P}\mathbf{q} = \mathbf{q}^H (\mathbf{I}_{LN} - \frac{1}{N}\mathbf{V}\mathbf{V}^H)\mathbf{q} \\ &= \mathbf{q}^H\mathbf{q} - \frac{1}{N}\mathbf{q}^H \begin{pmatrix} \mathbf{V}_1 & \mathbf{V}_2 & \ldots & \mathbf{V}_D \end{pmatrix} \begin{pmatrix} \mathbf{V}_1^H \\ \mathbf{V}_2^H \\ \vdots \\ \mathbf{V}_D^H \end{pmatrix} \mathbf{q} \\ &= LN - \frac{1}{N}\mathbf{q}^H \left(\sum_{i=1}^{D} \mathbf{V}_i \mathbf{V}_i^H \right) \mathbf{q} = LN - \frac{1}{N} \sum_{i=1}^{D} \mathbf{q}^H \mathbf{V}_i \mathbf{V}_i^H \mathbf{q} \end{aligned} \tag{2.12}$$

where

$$\mathbf{q}^H \mathbf{V}_i = (\boldsymbol{p} \otimes \mathbf{h})^H (\mathbf{u}_i \otimes \mathbf{a}_i) = (\boldsymbol{p}^H \mathbf{u}_i)(\mathbf{h}^H \mathbf{a}_i) \tag{2.13}$$

Define

$$\alpha_i = \frac{\mathbf{h}^H \mathbf{a}_i}{N} \tag{2.14}$$

as the spatial cross-correlation coefficient between the signal and the i^{th} jammer, and

$$\beta_i = \frac{\mathbf{p}^T \mathbf{u}_i}{\sqrt{L}} \tag{2.15}$$

as the temporal cross-correlation coefficient between the PN sequence and the i^{th} jammer vector. Accordingly,

$$\mathbf{q}^H \mathbf{V}_i = \sqrt{L} N \alpha_i \beta_i \tag{2.16}$$

$$y_1 = LN - LN \sum_{i=1}^{D} |\alpha_i|^2 |\beta_i|^2 = LN \left(1 - \sum_{i=1}^{D} |\alpha_i|^2 |\beta_i|^2 \right) \tag{2.17}$$

From the above equation, it is clear that y_1 is real, which is due to the Hermitian property of the projection matrix $\mathbf{P}$. From the assumptions in (2.3), y_2 is complex Gaussian with zero-mean. Accordingly,

$$E[y] = y_1 = LN \left(1 - \sum_{i=1}^{D} |\alpha_i|^2 |\beta_i|^2 \right) \tag{2.18}$$

$$\begin{aligned} Var[y] &= Var[y_2] = E[|y_2|^2] \\ &= E[\mathbf{q}^H \mathbf{P} \mathbf{B} \mathbf{B}^H \mathbf{P}^H \mathbf{q}] = \mathbf{q}^H \mathbf{P} E[\mathbf{B}\mathbf{B}^H] \mathbf{P} \mathbf{q} \\ &= \sigma^2 \mathbf{q}^H \mathbf{P} \mathbf{P} \mathbf{q} = \sigma^2 \mathbf{q}^H \mathbf{P} \mathbf{q} \\ &= \sigma^2 y_1 = \sigma^2 LN \left(1 - \sum_{i=1}^{D} |\alpha_i|^2 |\beta_i|^2 \right) \end{aligned} \tag{2.19}$$

The above two equations are derived for only one block of the GPS signal symbol. Below, we add subscript m to identify y with block m (m=1, 2, …, Q). By summing all Q blocks, we obtain the output of the symbol-level despreading,

$$y = \sum_{m=1}^{Q} y_m \tag{2.20}$$

Since y_m is Gaussian with zero-mean, then y is also a zero-mean Gaussian random variable. The decision variable y_r is the real part of y,

$$y_r = \text{Re}[y] \tag{2.21}$$

The expected value of y_r is

$$
\begin{aligned}
E[y_r] = E[y] &= \sum_{m=1}^{Q} E[y_m] \\
&= LN\left(Q - \sum_{m=1}^{Q}\sum_{i=1}^{D} |\alpha_{mi}|^2 |\beta_{mi}|^2 \right) \\
&= LN\left[Q - \sum_{i=1}^{D}\left(|\alpha_i|^2 \sum_{m=1}^{Q} |\beta_{mi}|^2 \right) \right]
\end{aligned}
\tag{2.22}
$$

where α_{mi} and β_{mi} are the spatial and temporal cross-correlation coefficients between the signal and the i^{th} jammer over block m. Since the changes in the spatial signatures of the signals and jammers are very small compared with the period of one GPS symbol (20 ms), α_{mi} can be simplified to α_I for the last step in (2.22). The variance of y_r is

$$
\begin{aligned}
\sigma_{y_r}^2 &= \frac{1}{2}\sigma_y^2 = \frac{1}{2}\sum_{m=1}^{Q}\sigma_{y_m}^2 \\
&= \frac{1}{2}\sigma^2 LN\left[Q - \sum_{i=1}^{D}\left(|\alpha_i|^2 \sum_{m=1}^{Q} |\beta_{mi}|^2 \right) \right]
\end{aligned}
\tag{2.23}
$$

Therefore, the receiver SINR expression [17] after projection and despreading is given by

$$
\begin{aligned}
SINR &= \frac{E^2[y]}{Var[y]} \\
&= \frac{2LN\left[Q - \sum_{i=1}^{D}\left(|\alpha_i|^2 \sum_{m=1}^{Q} |\beta_{mi}|^2 \right) \right]}{\sigma^2}
\end{aligned}
\tag{2.24}
$$

The temporal and spatial coefficients appear as multiplicative products in (2.24). This implies that the spatial and temporal signatures play equivalent roles in the receiver performance. In the absence of the jammers, no excision is necessary, and the SINR of the receiver output will become $2LNQ/\sigma^2$, which represents the upper bound of the interference suppression performance. Clearly, the term

$$
2LN\sum_{i=1}^{D}\left(|\alpha_i|^2 \sum_{m=1}^{Q} |\beta_{mi}|^2 \right) \tag{2.25}
$$

in equation (2.24) is the reduction in the receiver performance caused by the proposed interference suppression technique. It reflects the energy of the signal component that is in the jammer subspace. We note that if the jammers and the DSSS signal are orthogonal, either in spatial domain (α_i=0) or in

temporal domain (β_{mi}=0), the interference excision is achieved with no loss in performance. In the general case, $\beta_{mi,}$ for FM interference, takes a small value, which is much smaller than α_i. Therefore, the difference in the temporal signatures of the incoming signals allows the proposed projection technique to excise FM jammers effectively with only insignificant signal loss. The spatial cross-correlation coefficients α_i are fractional values and, as such, further reduce the undesired term in (2.25).

Interference suppression using arrays is improved in several ways. First, the employment of an antenna array can lead to an accurate IF estimation of the jammers [19]. Second, in comparison to the single sensor case [$N=1,\ \alpha_i=1$],

$$SINR=\frac{2L\left(Q-\sum_{i=1}^{D}\sum_{m=1}^{Q}\left|\beta_{mi}\right|^2\right)}{\sigma^2} \tag{2.26}$$

multi-sensor receivers, at minimum, improve SINR by the array gain. This is true, independent of the underlying fading channels and scattering environment. Finally, spatial selectivity, highlighted by the role of α is used to discriminate against the jammer signal.

4. Effects of IF Errors on the Projection Operation

Errors in IF may occur in many situations, where it becomes difficult to determine the IF due to a drop in the jammer power, presence of amplitude modulations, or high levels of cross-terms in the t-f domain. When IF estimation errors exist, the subspace projection operation will not entirely remove the jammer. The un-excised residual jammer at the projection filter output is often significant, specifically for high JSR. With no specific focus on any particular IF estimator, the phase errors in this section are modeled as a zero-mean Gaussian white noise process, motivated by the fact that phase errors, directly obtained from the analytic signal of FM in complex Gaussian additive noise, have wrapped Gaussian distributions [20]. For high jammer power, the distribution variance becomes very small and the phase errors assume a Gaussian distribution. Consider a single jammer with an estimated unit vector represented as

$$\hat{\mathbf{u}}^T = \frac{1}{\sqrt{L}}\left[e^{j(\phi(1)+\Delta(1))} \quad e^{j(\phi(2)+\Delta(2))} \quad \cdots \quad e^{j(\phi(L)+\Delta(L))} \right] \tag{2.27}$$

The phase estimation errors Δ(i) at different chips are assumed to be i.i.d random variables with a zero mean Gaussian distribution and variance σ_ε^2. The variance σ_ε^2 is assumed to be sufficiently small such that most errors lie inside the interval [$-\pi$, π]. The projection matrix, constructed from the inaccurate jammer vector, is

$$\hat{\boldsymbol{P}} = \mathbf{I}_{LN} - \frac{1}{N}\hat{\mathbf{U}}\hat{\mathbf{U}}^H \tag{2.28}$$

where $\hat{\mathbf{U}} = \hat{\mathbf{u}} \otimes \mathbf{a}$. In this case, the output of the correlator in one block is

$$\hat{y} = \mathbf{X}_s^H \hat{\boldsymbol{P}} \mathbf{X}_s + \mathbf{X}_s^H \hat{\boldsymbol{P}} \mathbf{W} + \mathbf{X}_s^H \hat{\boldsymbol{P}} \mathbf{X}_u \triangleq \hat{y}_1 + \hat{y}_2 + \hat{y}_3 \tag{2.29}$$

where $\hat{y}_1$, $\hat{y}_2$ and $\hat{y}_3$ represent, respectively, the contributions of the spreading code, the noise sequence, and the interfering signal. Due to phase estimation errors, these three variables are random which renders equation (2.29) different from its deterministic counterpart equation (2.11). Since the projection matrix $\hat{\mathrm{P}}_k$ is Hermitian, $\hat{y}_1$ is always real. The mean value of $\hat{y}_1$ is

$$E[\hat{y}_1] = E[\mathbf{X}_s^H \hat{\boldsymbol{P}} \mathbf{X}_s] = LN - \frac{1}{N} E[\mathbf{X}_s^H \hat{\mathbf{U}}\hat{\mathbf{U}}^H \mathbf{X}_s] \tag{2.30}$$

Define

$$\alpha = \frac{\mathbf{h}^H \mathbf{a}}{N} \tag{2.31}$$

as the spatial cross-correlation coefficient between the signal and the jammer, and

$$\beta = \frac{\mathbf{p}^T \mathbf{u}}{\sqrt{L}}, \quad \hat{\beta} = \frac{\mathbf{p}^T \hat{\mathbf{u}}}{\sqrt{L}} \tag{2.32}$$

as the exact and estimated temporal cross-correlation coefficient between the PN sequence and the jammer vector, respectively. Therefore,

$$\mathbf{X}_s^H \hat{\mathbf{U}} = (\mathbf{p} \otimes \mathbf{h})^H (\hat{\mathbf{u}} \otimes \mathbf{a}) = (\mathbf{p}^H \hat{\mathbf{u}})(\mathbf{h}^H \mathbf{a}) = \sqrt{L} N \alpha \hat{\beta} \tag{2.33}$$

It can be readily shown that

$$E[\hat{\mathbf{u}}\hat{\mathbf{u}}^H] = e^{-\sigma_\varepsilon^2}\mathbf{u}\,\mathbf{u}^H + \frac{1}{L}(1-e^{-\sigma_\varepsilon^2})\mathbf{I}_P \tag{2.34}$$

Hence,

$$\begin{aligned} E[y_1] &= LN(1-|\alpha|^2 E[|\hat{\beta}|^2]) = LN(1-|\alpha|^2 E[\frac{\mathbf{p}^T\hat{\mathbf{u}}\hat{\mathbf{u}}^H\mathbf{p}}{L}]) \\ &= LN\left[1-|\alpha|^2\left(e^{-\sigma_\varepsilon^2}|\beta|^2 + \frac{1-e^{-\sigma_\varepsilon^2}}{L}\right)\right] \end{aligned} \tag{2.35}$$

With the noise assumption,

$$E[\hat{y}_2] = 0 \tag{2.36}$$

Similar to $\hat{y}_1$, the mean value of $\hat{y}_3$ is obtained as

$$\begin{aligned} E[\hat{y}_3] &= E[\mathbf{X}_s^H\hat{\boldsymbol{P}}\mathbf{X}_j] = A\sqrt{L}\left(\mathbf{X}_s^H\mathbf{U} - \frac{1}{N}E[\mathbf{X}_s^H\hat{\mathbf{U}}\hat{\mathbf{U}}^H\mathbf{U}]\right) \\ &= A\sqrt{L}\left(\mathbf{X}_s^H\mathbf{U} - \frac{1}{N}N^2\alpha E[\mathbf{p}^T\hat{\mathbf{u}}\hat{\mathbf{u}}^H\mathbf{u}]\right) \\ &= AN\alpha\beta(1-e^{-\sigma_\varepsilon^2})(L-1) \end{aligned} \tag{2.37}$$

From (2.35) - (2.37), the mean value of $\hat{y}$ can be calculated by the sum

$$E[\hat{y}] = E[\hat{y}_1] + E[\hat{y}_2] + E[\hat{y}_3] \tag{2.38}$$

The mean square value due to the signal is

$$\begin{aligned} &E[|\hat{y}_1|^2] = E[\mathbf{X}_s^H\hat{\boldsymbol{P}}\mathbf{X}_s\mathbf{X}_s^H\hat{\boldsymbol{P}}\mathbf{X}_s] \\ &= E[L^2N^2 - 2L\mathbf{X}_s^H\hat{\mathbf{U}}\hat{\mathbf{U}}^H\mathbf{X}_s + \frac{1}{N^2}\mathbf{X}_s^H\hat{\mathbf{U}}\hat{\mathbf{U}}^H\mathbf{X}_s\mathbf{X}_s^H\hat{\mathbf{U}}\hat{\mathbf{U}}^H\mathbf{X}_s] \\ &= L^2N^2 - 2N^2L|\alpha|^2 E[\mathbf{p}^T\hat{\mathbf{u}}\hat{\mathbf{u}}^H\mathbf{p}] + N^2|\alpha|^4 E[\mathbf{p}^T\hat{\mathbf{u}}\hat{\mathbf{u}}^H\mathbf{p}\mathbf{p}^T\hat{\mathbf{u}}\hat{\mathbf{u}}^H\mathbf{p}] \\ &= L^2N^2 - 2N^2L|\alpha|^2(e^{-\sigma_\varepsilon^2}L|\beta|^2 + 1 - e^{-\sigma_\varepsilon^2}) + \\ &\quad N^2|\alpha|^4\left[(2+4L|\beta|^2 e^{-\sigma_\varepsilon^2})(1-e^{-\sigma_\varepsilon^2}) + L^2|\beta|^4 e^{-2\sigma_\varepsilon^2}\right] \end{aligned} \tag{2.39}$$

In deriving the above expression, $\mathbf{p}^T\hat{\mathbf{u}}$ is approximated by a complex Gaussian random variable, invoking the Central Limit Theorem. From (2.35) and (2.39), the variance of y_1 can be computed as

$$\sigma_{y_1}^2 = E[\hat{y}_1^2] - E^2[\hat{y}_1] \tag{2.40}$$

The mean square values of y_2 and y_3 are given by

$$
\begin{aligned}
E[\left|\hat{y}_2\right|^2] = \sigma_{y_2}^2 &= E[\mathbf{X}_s^H \hat{\boldsymbol{P}}\mathbf{W}\mathbf{W}^H \hat{\boldsymbol{P}}\mathbf{X}_s] \\
&= E[E[\mathbf{X}_s^H \hat{\boldsymbol{P}}\mathbf{W}\mathbf{W}^H \hat{\boldsymbol{P}}\mathbf{X}_s \mid \hat{\boldsymbol{P}}]] \\
&= \sigma^2 E[\mathbf{X}_s^H \hat{\boldsymbol{P}}\hat{\boldsymbol{P}}\mathbf{X}_s] \\
&= \sigma^2 E[\mathbf{X}_s^H \hat{\boldsymbol{P}}\mathbf{X}_s] = \sigma^2 E[y_1] \\
&= \sigma^2 LN\left[1-|\alpha|^2\left(e^{-\sigma_\varepsilon^2}|\beta|^2 + \frac{1-e^{-\sigma_\varepsilon^2}}{L}\right)\right]
\end{aligned}
\tag{2.41}
$$

$$
\begin{aligned}
&E[\left|\hat{y}_3\right|^2] = E[\mathbf{X}_u^H \hat{\boldsymbol{P}}\mathbf{X}_s\mathbf{X}_s^H \hat{\boldsymbol{P}}\mathbf{X}_u] = A^2 LE[\mathbf{U}^H \hat{\boldsymbol{P}}\mathbf{X}_s\mathbf{X}_s^H \hat{\boldsymbol{P}}\mathbf{U}] \\
&= A^2 LE[\mathbf{U}^H\mathbf{X}_s\mathbf{X}_s^H\mathbf{U} - \frac{1}{N}\mathbf{U}^H\hat{\mathbf{U}}\hat{\mathbf{U}}^H\mathbf{X}_s\mathbf{X}_s^H\mathbf{U} \\
&\quad - \frac{1}{N}\mathbf{U}^H\mathbf{X}_s\mathbf{X}_s^H\hat{\mathbf{U}}\hat{\mathbf{U}}^H\mathbf{U} + \frac{1}{N^2}\mathbf{U}^H\hat{\mathbf{U}}\hat{\mathbf{U}}^H\mathbf{X}_s\mathbf{X}_s^H\hat{\mathbf{U}}\hat{\mathbf{U}}^H\mathbf{U}] \\
&= A^2 L\{N^2 L|\alpha|^2|\beta|^2 - N^2|\alpha|^2\sqrt{L}\beta E[\mathbf{u}^H\hat{\mathbf{u}}\hat{\mathbf{u}}^H\mathbf{p}] \\
&\quad - N^2|\alpha|^2\sqrt{P}\beta^* E[\mathbf{p}^H\hat{\mathbf{u}}\hat{\mathbf{u}}^H\mathbf{u}] + N^2|\alpha|^2 E[\mathbf{u}^H\hat{\mathbf{u}}\hat{\mathbf{u}}^H\mathbf{p}\mathbf{p}^H\hat{\mathbf{u}}\hat{\mathbf{u}}^H\mathbf{u}]\} \\
&= A^2N^2L|\alpha|^2\{L|\beta|^2 - 2L|\beta|^2[e^{-\sigma_\varepsilon^2} + (1-e^{-\sigma_\varepsilon^2})/L] \\
&\quad + [e^{-\sigma_\varepsilon^2} + (1-e^{-\sigma_\varepsilon^2})/L](L|\beta|^2 e^{-\sigma_\varepsilon^2} + 1 - e^{-\sigma_\varepsilon^2})\}
\end{aligned}
\tag{2.42}
$$

Therefore, the variance of y_3 is given by

$$
\sigma_{y_3}^2 = E[\left|\hat{y}_3\right|^2] - \left|E[\hat{y}_3]\right|^2 \tag{2.43}
$$

The expression of the covariance and cross-correlation between the three components of the decision variable has no closed-form expression. Extensive numerical computations show that the covariance between $\hat{y}_i$ and $\hat{y}_j$ ($i \neq j$), i, j =1,2,3) assume small values relative to the respective variance values, and as such their contributions to the overall variance expression below can be ignored. The variance of the decision variable can be approximated by

$$
\sigma_{y_r}^2 = \sigma_{y_1}^2 + \frac{1}{2}(\sigma_{y_2}^2 + \sigma_{y_3}^2) \tag{2.44}
$$

The above equations are derived for only one block of the signal symbol. Below, the subscript m is added to identify $\hat{y}$ with block m (m=1, 2, …, Q), and should not be confused with those used in (2.29). The decision variable $\hat{y}_r$ can be expressed as

$$
\hat{y}_r = \mathrm{Re}[\sum_{m=1}^{Q}\hat{y}_m] \tag{2.45}
$$

Since the white Gaussian noise sequences and estimation errors are independent for different blocks, the expected value and variance of $\hat{y}_r$ become

$$E[\hat{y}_r] = \sum_{m=1}^{Q} \mathrm{Re}[E[\hat{y}_m]], \;\; Var[\hat{y}_r] = \sum_{m=1}^{Q} \mathrm{var}[\hat{y}_{rm}] \tag{2.46}$$

The above expressions can now be used to generate the desired receiver SINR,

$$SINR = \frac{E^2[\hat{y}_r]}{Var[\hat{y}_r]} \tag{2.47}$$

5. Simulation Results

In this section, we present simulation results illustrating the performance properties of the proposed projection technique.

Figure 5 depicts the receiver SINR, given by equation (2.24), as a function of the input SNR. We consider two chirp jammers, each of a sweeping time equals to the GPS C/A symbol duration. The angle-of-arrival (AOA) of the satellite signal and the jammers are 5^0, 40^0, and 60^0, respectively. A simple two-element array is considered with half-wavelength spacing (A longer array, or a higher dimensional array could be used, but would not draw a different conclusion). The satellite PN sequence is the Gold code of satellite SV#1, and the normalized frequency of the jammers are from 0.01 to 0.2 and from 0.5 to 0.3, respectively, and assumed to be perfectly estimated. (In all analysis and simulations, the jammer waveforms are assumed to occupy part or the full band of the GPS signal and it is properly sampled.) The SINR of the single sensor case is also plotted for comparison. The array gain is evident in Figure 5. In this example, $|\alpha_1|$=0.643, $|\alpha_2|$=0.340. Over the 20 blocks of the GPS signal symbol, the temporal cross-correlation is computed for each jammer. It is found that $|\beta_1|$ is in the range [0.0049- 0.0604], whereas $|\beta_2|$ is in the range [0.0067- 0.0839]. These different values of the temporal correlation coefficient are due to the fact that different blocks of the GPS symbol capture different segments of the chirp jammer. With the above values, the term (2.25) is far less than *2LNQ*, which allows SINR (2.24) to be very close to its upper bound, representing a jammer-free environment.

Next, we examine the effect of phase errors on the receiver performance. We consider a periodic chirp jammer whose period is equal to one block length of the GPS C/A symbol. The angle of arrival (AOA) of the satellite signal is 5^0. A two-element array is considered with half-wavelength spacing. The Jammer-to-Signal-Ratio (JSR) is set to 50 dB and SNR equal to –20 dB. Figure 6 depicts the simulated values of the receiver SINR vs. the phase error variance σ_ε^2, which changes in the narrow range [0, 0.01] for all blocks. Small errors in the phase estimates will only allow a small portion of the jammer to escape the excision process. However, with high jammer-to-signal ratio, this portion can significantly compromise the receiver performance. The above error range is selected to demonstrate such an effect, and it is also typical when using reliable IF estimators. The AOA of the jammer signals are set to 5^0, 35^0, and 65^0, respectively. It is clear from the figure that, as the error variance increases, the output SINR decreases. The SINR of the single sensor case is also plotted for comparison. Unlike the result of exact IF estimation, where antenna arrays bring a constant 3 dB array gain, the receiver SINR in the presence of those errors is dependent on the spatial signatures of the signal and jammer. For small spatial cross-correlation coefficients, the use of antenna array allows the receiver to be more robust to the IF estimation errors. The relation between the receiver SINR and the jammer AOA is shown in Figure 7. In this case, phase error variance σ_ε^2 in Figure 6 was kept constant at 0.01. It is important to observe that the peak and the null in Figure 6 correspond, respectively, to the lowest and highest values of the spatial correlation parameter between the GPS signal and jammer. This parameter behavior is shown in the same Figure 8.

In the next simulation, we consider multiple jammers. The angle of arrival (AOA) of the satellite signal is 50 degrees. The same satellite code and array of the previous example are used. The SNR is set to –20 dB. Figure 9 depicts the simulated values of the receiver SINR vs. the phase error variance σ_ε^2, which changes in the range [0, 0.01] for all blocks. JSR is equal to 50 dB. Both single jammer and multiple jammer cases are depicted. The AOA of the jammer signals are set to be 35^0 and 65^0 respectively. When two jammers are present, the jammer with AOA 35^0 has a frequency range [0, π], and the one with AOA 65^0 [0.6π, 0.8π]. It is clear from the figure that, as the error variance increases, the

output SINR decreases. The 35 degree jammer yields worse performance, since it possesses higher correlation with the desired signal. With the two jammers present, the performance is close to the worst single jammer performance. The receiver acts on removing the jammer that is least correlated with the desired signal using the spatial degrees of freedom, not counting much on the t-f signature distinction between its respective waveform and the GPS signal. The other jammer escapes the spatial filtering; in which case, the receiver seeks t-f signature distinctions for its removal. The errors in IF prevent complete suppression.

Conclusions

Subspace projection is a pre-correlation technique that can effectively reject the wideband interference effectively when the jammer has instantaneous narrowband t-f profile. In this chapter, suppression of frequency modulation interferers in GPS using antenna arrays and subspace projection techniques is proposed. It is shown that both the spatial and temporal signatures of the signals impinging on the multi-sensor receiver assume similar roles in the receiver performance. The spatial and temporal signatures' respective correlation coefficients appear as square multiplicative products in the SINR expression. However, due to the Gold code structure and the length of the PN, the differences in the temporal characteristics of the FM jammer and the C/A code yield negligible temporal correlation coefficients. These small values allow the receiver to perform very close to the no-jamming case, irrespective of the satellites and the jammers' angles of arrival. The fundamental offering of the array in the underlying interference suppression problem is through its gain, which is determined by the number of antennas employed at the receiver.

Since the subspace projection matrix is solely dependent on the IF estimation, IF estimation errors will perturb the projection matrix and allow part of the jammer power to escape the projection operation. The effects of the IF estimation errors on SINR performance of GPS receiver using array subspace projection in the presence has been analyzed. The phase errors are modeled as zero-mean white Gaussian, and independent over different chips. The spatial signature is assumed to be accurately estimated. The

analysis and simulation shows that, although the IF estimation errors can affect the receiver SINR significantly, the combination of temporal and spatial signature can provide more robustness in the presence of IF estimation errors, and as such, render better performance than the single antenna scheme.

Appendix A

For a single jammer and a single antenna receiver, the projected satellite signal, upon correlation with the receiver C/A code of the same satellite provides

$$y = \boldsymbol{p}^H \left[\boldsymbol{I} - \boldsymbol{u}\boldsymbol{u}^H \right] \boldsymbol{p} = \boldsymbol{p}^H \boldsymbol{p} - \left(\boldsymbol{p}^H \boldsymbol{u} \right)\left(\boldsymbol{u}^H \boldsymbol{p} \right) \tag{A.1}$$

Using the definition of the cross-correlation given by (2.15),

$$y = L - L\beta\beta^* = L\left(1 - |\beta|^2\right) \tag{A.2}$$

The above equation assumes the alignment of the received C/A code with the receiver C/A code. In general, this is not the case. Define $\boldsymbol{p}_\Delta$ as the vector containing the shifted C/A code such that the vector elements

$$\boldsymbol{p}_\Delta(n) = \boldsymbol{p}(\boldsymbol{n} - \Delta) \tag{A.3}$$

In this case, the correlation between the two non-aligned codes is

$$y_\Delta = \boldsymbol{p}_\Delta^H \boldsymbol{p} - \left(\boldsymbol{p}_\Delta^H \boldsymbol{u} \right)\left(\boldsymbol{u}^H \boldsymbol{p} \right) \tag{A.4}$$

Using the Gold code property,

$$\boldsymbol{p}_\Delta^H \boldsymbol{p} = \gamma \qquad \gamma = \pm 1, 0$$

and

$$\begin{aligned} y_\Delta &= \gamma - L\beta_\Delta\beta^* \\ &= -L\left(\frac{-\gamma}{L} + \beta_\Delta\beta^* \right) \end{aligned} \tag{A.5}$$

For unbiased peak location, we require

$$\left| L\left(1 - |\beta|^2\right) \right| > \left| L\left(\frac{\gamma}{L} - \beta_\Delta\beta^* \right) \right|$$

That is,

$$\left(1-\left|\beta\right|^2\right) > \left|\frac{\gamma}{L} - \beta_\Delta \beta^*\right|$$

Since $\left|\beta\right|$ □ 1, then

$$1 > \left|\frac{\gamma}{L} - \beta_\Delta \beta^*\right|$$

A tighter bound is

$$1 > \left|\frac{\gamma}{L}\right| + \left|\beta_\Delta\right|\left|\beta\right|, \qquad \frac{L-\left|\gamma\right|}{L} > \left|\beta_\Delta\right|\left|\beta\right|, \qquad \left|\beta_\Delta\right| < \frac{L-\left|\gamma\right|}{L}\frac{1}{\left|\beta\right|} \tag{A.6}$$

Since the maximum value of the cross-correlation is 1, and $\frac{L-\left|\gamma\right|}{L} \approx 1$ for $L = 1023$, then (A.6) is readily satisfied.

Appendix B

With presence of multiple jammers, the parameters in (2.31) and (2.32) will assume different values. For the *i*-th jammer, the spatial cross-correlation coefficient, exact and estimated temporal cross-correlation coefficients are given by

$$\alpha_i = \frac{\mathbf{h}^H \mathbf{a}_i}{N}, \qquad \beta_i = \frac{\mathbf{p}^T \mathbf{u}_i}{\sqrt{L}}, \quad \hat{\beta}_i = \frac{\mathbf{p}^T \hat{\mathbf{u}}_i}{\sqrt{L}} \tag{B.1}$$

Accordingly,

$$\mathbf{X}_s^H \hat{\mathbf{U}}_i = (\mathbf{p} \otimes \mathbf{h})^H (\mathbf{u}_i \otimes \mathbf{a}_i) = (\mathbf{p}^T \mathbf{u}_i)(\mathbf{h}^H \mathbf{a}_i) = \sqrt{L} N \alpha_i \hat{\beta}_i$$

It is straight forward to show that for *M*, (*M = D*), jammers, the mean values of three terms constituting the decision variable are give as follows:

$$\begin{aligned} E[\hat{y}_1] &= LN(1 - \sum_{i=i}^{M} |\alpha_i|^2 \, E[|\hat{\beta}_i|^2]) \\ &= LN[1 - \sum_{i=i}^{M} |\alpha_i|^2 \, (e^{-\sigma_i^2} |\hat{\beta}_i|^2 + \frac{1 - e^{-\sigma_i^2}}{L})] \end{aligned} \tag{B.2}$$

$$E[\hat{y}_2] = 0 \tag{B.3}$$

$$\begin{aligned} E[\hat{y}_3] &= E[\mathbf{X}_s^H \hat{\mathbf{V}} \mathbf{X}_u] = \sum_{i=1}^{M} A_i \sqrt{L} E[\mathbf{X}_s^H \hat{\mathbf{V}} \mathbf{U}_i] \\ &= \sum_{i=1}^{M} A_i \sqrt{L} E[\mathbf{X}_s^H \mathbf{U}_i - \frac{1}{N} \sum_{m=1}^{M} \mathbf{X}_s^H \hat{\mathbf{U}}_m \hat{\mathbf{U}}_m^H \mathbf{U}_i] \\ &= \sum_{i=1}^{M} A_i \sqrt{L} (N \sqrt{L} \alpha_i \beta_i - \frac{1}{N} \sum_{m=1}^{M} N^2 \alpha_m \alpha_{mi} E[\mathbf{p}^H \hat{\mathbf{u}}_m \hat{\mathbf{u}}_m^H \mathbf{u}_i]) \\ &= \sum_{i=1}^{M} A_i LN(\alpha_i \beta_i - \alpha_i \beta_i e^{-\sigma_i^2} - \sum_{m=1}^{M} \alpha_m \alpha_{mi} \frac{1 - e^{-\sigma_i^2}}{L} \beta_i) \end{aligned} \tag{B-4}$$

where

$$\alpha_{mi} = \frac{\mathbf{a}_m^H \mathbf{a}_i}{N} \tag{B.5}$$

is the spatial cross-correlation coefficient between the m^{th} and the i^{th} jammer components. The mean square value of $\hat{y}_1$ give by

$$\begin{aligned} E[\left|\hat{y}_1\right|^2] &= E[\mathbf{X}_s^H \hat{\mathrm{P}} \mathbf{X}_s \mathbf{X}_s^H \hat{\mathrm{P}} \mathbf{X}_s] \\ &= L^2N^2 - E[2L\mathbf{X}_s^H \hat{\mathbf{U}}\hat{\mathbf{U}}^H \mathbf{X}_s] + \frac{1}{N^2} E[\mathbf{X}_s^H \hat{\mathbf{U}}\hat{\mathbf{U}}^H \mathbf{X}_s \mathbf{X}_s^H \hat{\mathbf{U}}\hat{\mathbf{U}}^H \mathbf{X}_s] \\ &= L^2N^2 - y_{12} + y_{13} \end{aligned} \tag{B.6}$$

$$\hat{y}_{12} = \sum_{i=1}^{M} 2LN^2 \left|\alpha_i\right|^2 \mathbf{p}^H E[\hat{\mathbf{u}}_i \hat{\mathbf{u}}_i^H]\mathbf{p} = \sum_{i=1}^{M} 2LN^2 \left|\alpha_i\right|^2 (e^{-\sigma_i^2} L\left|\beta_i\right|^2 + 1 - e^{-\sigma_i^2})$$

The mean square values of the other two terms are given by

$$\begin{aligned} \sigma_{y_2}^2 &= E[\left|\hat{y}_2\right|^2] = E[\mathbf{X}_s^H \hat{\mathrm{P}} \mathbf{W}\mathbf{W}^H \hat{\mathrm{P}} \mathbf{X}_s] \\ &= E[E[\mathbf{X}_s^H \hat{\mathrm{P}} \mathbf{W}\mathbf{W}^H \hat{\mathrm{P}} \mathbf{X}_s \mid \hat{\mathrm{P}}]] = \sigma^2 E[\mathbf{X}_s^H \hat{\mathrm{P}}\hat{\mathrm{P}} \mathbf{X}_s] \\ &= \sigma^2 E[\mathbf{X}_s^H \hat{\mathrm{P}} \mathbf{X}_s] = \sigma^2 E[y_1] \\ &= \sigma^2 LN[1 - \sum_{i=i}^{M} \left|\alpha_i\right|^2 (e^{-\sigma_i^2} \left|\hat{\beta}_i\right|^2 + \frac{1 - e^{-\sigma_i^2}}{L})] \end{aligned} \tag{B.7}$$

$$E[\left|\hat{y}_3\right|^2] = E[\mathbf{X}_u^H \hat{\mathrm{P}} \mathbf{X}_s \mathbf{X}_s^H \hat{\mathrm{P}} \mathbf{X}_u] = \sum_{m=1}^{M}\sum_{n=1}^{M} A_m A_n L E[\mathbf{U}_m^H \hat{\mathrm{P}} \mathbf{X}_s \mathbf{X}_s^H \hat{\mathrm{P}} \mathbf{U}_n]$$

$$= \sum_{m=1}^{M}\sum_{n=1}^{M} A_m A_n L\{\mathbf{U}_m^H \mathbf{X}_s \mathbf{X}_s^H \mathbf{U}_n - \frac{1}{N} E[\sum_{s=1}^{M} \mathbf{U}_m^H \hat{\mathbf{U}}_s \hat{\mathbf{U}}_s^H \mathbf{X}_s \mathbf{X}_s^H \mathbf{U}_n] - \frac{1}{N} E[\sum_{t=1}^{M} \mathbf{U}_m^H \mathbf{X}_s \mathbf{X}_s^H \hat{\mathbf{U}}_t \hat{\mathbf{U}}_t^H \mathbf{U}_n]$$

$$+ \frac{1}{N^2} E[\sum_{s=1}^{M}\sum_{t=1}^{M} \mathbf{U}_m^H \hat{\mathbf{U}}_s \hat{\mathbf{U}}_s^H \mathbf{X}_s \mathbf{X}_s^H \hat{\mathbf{U}}_t \hat{\mathbf{U}}_t^H \mathbf{U}_n]\} = L^2N^2 \left|\sum_{m=1}^{M} A_m \alpha_m \beta_m\right|^2 - \hat{y}_{32} - \hat{y}_{33} + \hat{y}_{34} \tag{B.8}$$

where $\hat{y}_{32}$, $\hat{y}_{33}$ and $\hat{y}_{34}$ can be shown to be:

$$\hat{y}_{32} = \sum_{m=1}^{M}\sum_{n=1}^{M} A_m A_n L^2 N^2 \alpha_n \beta_m^* \beta_n (\alpha_m^* e^{-\sigma_m^2} + \sum_{s=1}^{M} \alpha_{ms} \alpha_s^* \frac{1 - e^{-\sigma_s^2}}{L}) \tag{B.9}$$

$$\hat{y}_{33} = \sum_{m=1}^{M}\sum_{n=1}^{M} A_m A_n L^2 N^2 \alpha_m^* \beta_m^* \beta_n (\alpha_n e^{-\sigma_n^2} + \sum_{t=1}^{M} \alpha_{tn} \alpha_t \frac{1 - e^{-\sigma_t^2}}{L}) \tag{B.10}$$

$$\hat{y}_{34} = LN^2 \sum_{m=1}^{M}\sum_{n=1}^{M} A_m A_n [L\beta_m^* \beta_n (e^{-\sigma_m^2}\alpha_m^* + \sum_{s=1}^{M}\alpha_{ms}\alpha_s^* \frac{1-e^{-\sigma_s^2}}{L})(e^{-\sigma_n^2}\alpha_n + \sum_{s=1}^{M}\alpha_s\alpha_{sn}\frac{1-e^{-\sigma_s^2}}{L}) + \sum_{m}^{M}|\alpha_m|^2 e^{-\sigma_m^2}(1-e^{-\sigma_m^2})$$
$$+\sum_{m=1}^{M}\sum_{s=1}^{M}|\alpha_{ms}|^2|\alpha_s|^2(e^{-\sigma_s^2}|\beta_n|^2 + \frac{1-e^{-\sigma_s^2}}{L})(1-e^{-\sigma_s^2}) - \sum_{m=1}^{M}\sum_{n=1}^{M}|\alpha_m|^2\alpha_{mn}\beta_m^*\beta_n e^{-\sigma_m^2}(1-e^{-\sigma_s^2}) \quad \text{(B.11)}$$
$$-\sum_{m=1}^{M}\sum_{n=1}^{M}|\alpha_n|^2\alpha_{mn}\beta_m^*\beta_n e^{-\sigma_n^2}(1-e^{-\sigma_n^2}) - \sum_{m=1}^{M}\sum_{n=1}^{M}\sum_{s=1}^{M}|\alpha_s|^2\alpha_{ms}\alpha_{sn}\beta_m^*\beta_n\frac{(1-e^{-\sigma_n^2})^2}{L}]$$

Therefore, the variance of $\hat{y}_3$ is given by

$$\sigma_{y_3}^2 = E[|\hat{y}_3|^2] - |E[\hat{y}_3]|^2 \quad \text{(B.12)}$$

It can be shown that the covariance between $\hat{y}_i$ and $\hat{y}_j$ ($i \neq j$), i, j =1,2,3) assume small values relative to the respective variance values. The variance of the decision variable can then be approximated by

$$\sigma_{y_r}^2 = \sigma_{y_1}^2 + \frac{1}{2}(\sigma_{y_2}^2 + \sigma_{y_3}^2) \quad \text{(B.13)}$$

Similar to the single-jammer case, the overall values of the mean and the variance should be averaged over *Q* blocks.

References

[1] O. Akay, F.G. Boudreaux-Bartels, "Broadband interference excision in spread spectrum communication systems via fractional Fourier transform," Proc. of 32th Asilomar Conf. on Sig., Sys. and Comp., pp. 823-827, Nov. 1998.

[2] M. G.Amin, "Interference mitigation in spread-spectrum communication systems using time-frequency distributions," IEEE Trans. Signal Processing, vol. 45, no. 1, pp. 90-102, Jan. 1997.

[3] M. G. Amin and A. Akansu, "Time-frequency for interference excision in spread-spectrum communications," Highlights of Signal Processing for Communications, Celebrating a Half Century of Signal Processing, editor: G. Giannakis, IEEE SP Magazine, vol. 16, no. 2, March 1999.

[4] M. Amin, S. Ramineni and A. Lindsey “Suppression of FM interference in DSSS communications using projection techniques,” Proceedings of Asilomar Conference on Signal, Systems, and Computers, vol .2, pp. 1063-1066, Pacific Grove, CA, October 1999.

[5] M. Amin, C. Wang, and A. Lindsey, "Optimum interference excision in spread spectrum communications using open loop adaptive filters, " IEEE Trans. Signal Processing, vol. 47, no. 7, pp. 1966-1976, July 1999.

[6] B. Badke and A. Spanias, "Partial band interference excisions for GPS using frequency-domain exponents," Proceedings of the IEEE International Conference on Acoustics, Speech, and Signal Processing, Orlando, FL, May 1-17, 2002.

[7] A. Belouchrani and M. Amin, “Blind source separation using time-frequency distributions,” IEEE Transactions on Signal Processing, vol. 46, no.11, pp. 2888-2898, November 1999.

[8] A. Belouchrani and M. Amin, “Time-frequency MUSIC,” IEEE Signal Processing Letters, vol. 6, no. 5, pp. 109-110, May 1999.

[9] B. Boashash, "Estimating and interpreting the instantaneous frequency of a signal Part 1," IEEE Proceedings, vol. 80, no. 4, pp. 519-539, April 1992.

[10] M. S. Braasch and A. J. Van Dierendonck, “GPS receiver architectures and measurements,” Proceedings of the IEEE, Jan. 1999.

[11] P. T. Capozza, B. J. Holland, T. M. Hopkinson, R. L. Landrau, “A single-chip narrow-band frequency-domain excisor for a global positioning system (GPS) receiver,” IEEE Journal of Solid State Circuits, vol. 35, No 3, March 2000.

[12] V. Chen and H. Ling, Time-Frequency Transforms for Radar Imaging and Signal Analysis, Boston, MA: Artech House, 2002.

[13] L. Cohen, Time-Frequency Analysis, Prentice Hall, Englewood Cliffs, New Jersey, 1995.

[14] R. Fante and J.J. Vaccaro, "Wideband cancellation of interference in a GPS receive array," IEEE Transactions on Aerospace and Electronic Systems, vol. 36, no.2, pp. 549-564, April 2000.

[15] S. C. Jang and P. J. Loughlin, "AM-FM interference excision in spread spectrum communications via projection filtering," J. Applied Signal Processing, 2001.

[16] E. Kaplan, (Ed.) Understanding GPS: Principles and Applications. Boston: Artech House, 1996.

[17] J. W. Ketchum and J. G. Proakis, “Adaptive algorithms for estimating and suppressing narrow-band interference in PN spread-spectrum systems," IEEE Trans. Communications., vol. COM-30, pp. 913-924, May 1982.

[18] S. Lach, M. G.Amin, and A. R. Lindsey, "Broadband nonstationary interference excision in spread-spectrum communications using time-frequency synthesis techniques," IEEE J. Select Areas Communications, vol. 17, no. 4, pp. 704-714, April 1999.

[19] R. Jr. Landry, P. Mouyon and D. Lekaim, “Interference mitigation in spread spectrum systems by wavelet coefficients thresholding,” European Trans. on Telecommunications, vol. 9, pp. 191-202, Mar-Apr 1998.

[20] B. C. Lovell and R. C. Willianson, “The statistical performance of some instantaneous frequency estimators,” IEEE Transactions on Signal Processing, vol. 40, no. 7, pp. 1708-1723, July 1992.

[21] L. B. Milstein, “Interference rejection techniques in spread spectrum communications,” Proceedings IEEE, vol. 76, No 6, June 1988.

[22] W. Mu, M. G. Amin, and Y. Zhang, “Bilinear signal synthesis in array processing,” Accepted, IEEE Transactions on Signal Processing.

[23] W. L. Myrick, J. S. Goldstein, and M. D. Zoltowski, " Low complexity anti-jam space-time processing for GPS," Proceedings of the IEEE International Conference on Acoustics, Speech, and Signal Processing, Salt Lake City, Utah, May 2001.

[24] B. Parkinson, and J. Spilker, (Eds.) (1996) Global Positioning System: Theory and Applications. Washington, DC: American Institute of Aeronautics and Astronautics, 1996.

[25] S. Qian and D. Chen, Joint Time-Frequency Analysis - Methods and Applications, Prentice-Hall, Englewood Cliffs, New Jersey, 1996.

[26] S. Ramineni, M. G. Amin, and A. R. Lindsey, “Performance analysis of subspace projection techniques in DSSS communications,” Proceedings of the International Conference on Acoustics, Speech, and Signal Processing, Istanbul, Turkey, May 2000.

[27] R. Suleesathira and L. Chaparro “Jammer excision in spread spectrum using discrete evolutionary-Hough transform and singular value decomposition,” Proc. of 10th IEEE Workshop on Stat. Sig. and Arraay Proc., pp. 519-524, Aug. 2000.

[28] M. V. Tazebay and A. Akansu, “Adaptive subband transforms in time-frequency excisers for DSSS Communications Systems,” IEEE Trans. on Sig. Process., Vol. 43, pp. 2776-2782, 1995.

[29] Y. Zhang and M. G. Amin, "Blind beamforming for suppression of instantaneously narrowband signals in DS/SS communications using subspace projection techniques," Proc. SPIE: Digital Wireless Communication II, vol. 4045, Orlando, FL, April 2000.

[30] Y. Zhang, W. Mu, and M. Amin, “Time-frequency maximum likelihood methods for direction finding,” Journal of Franklin Institute, vol. 337, no. 4, pp 483-497, July 1999.

[31] L. Zhao, M. G. Amin, and A. R. Lindsey, “Subspace projection techniques for anti-FM jamming GPS receivers,” Proceedings of the 10th IEEE Workshop on Statistical Signal and Array Processing, Pocono Manor, Pa, Aug. 2000.

[32] L. Zhao, M. G. Amin, and A. R. Lindsey, “Performance analysis of subspace projection techniques for FM interference rejection in GPS receivers,” Proceedings of SPIE, Digital Wireless Communications, Orlando, FL, Apr. 2001.

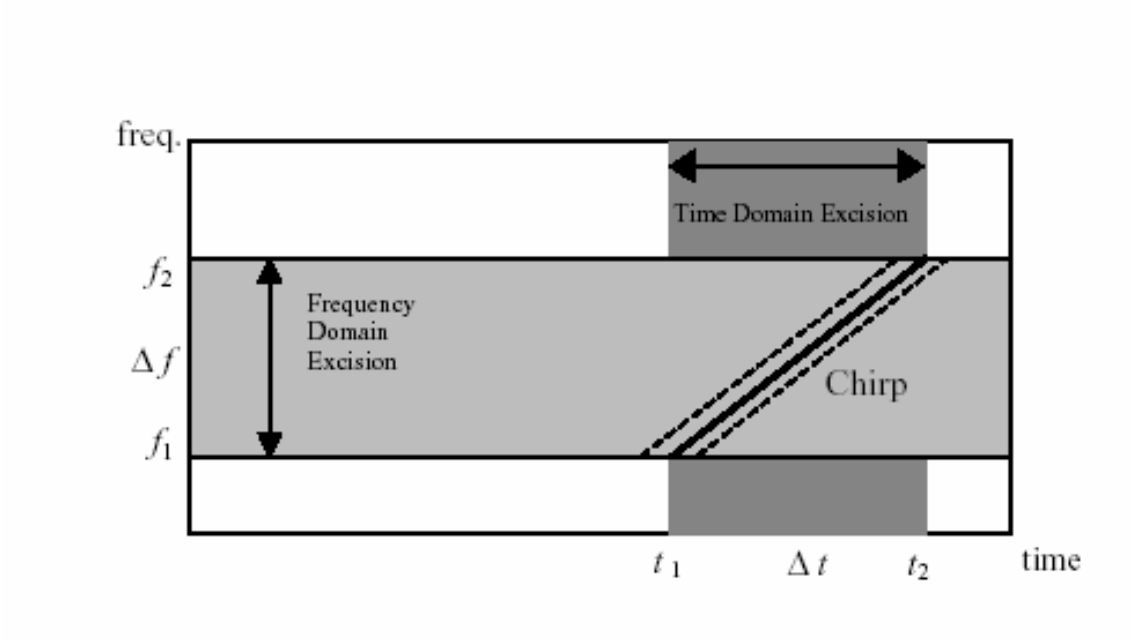

Figure 1. Pictorial representation of interference excision techniques

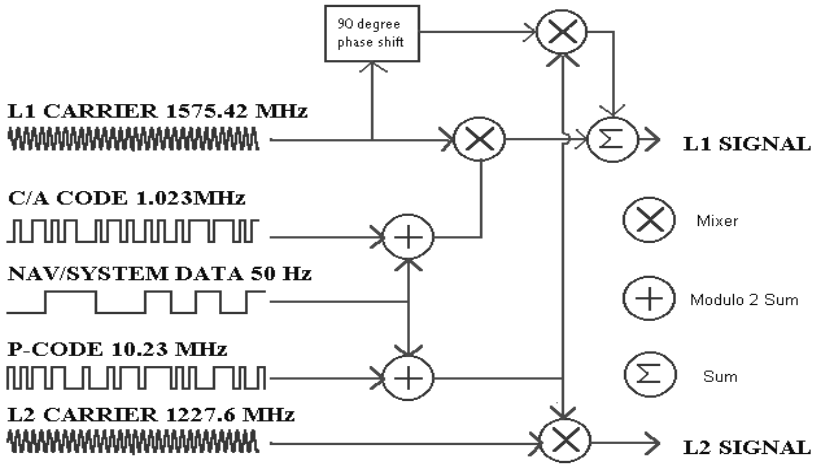

Figure 2. The GPS signal structure.

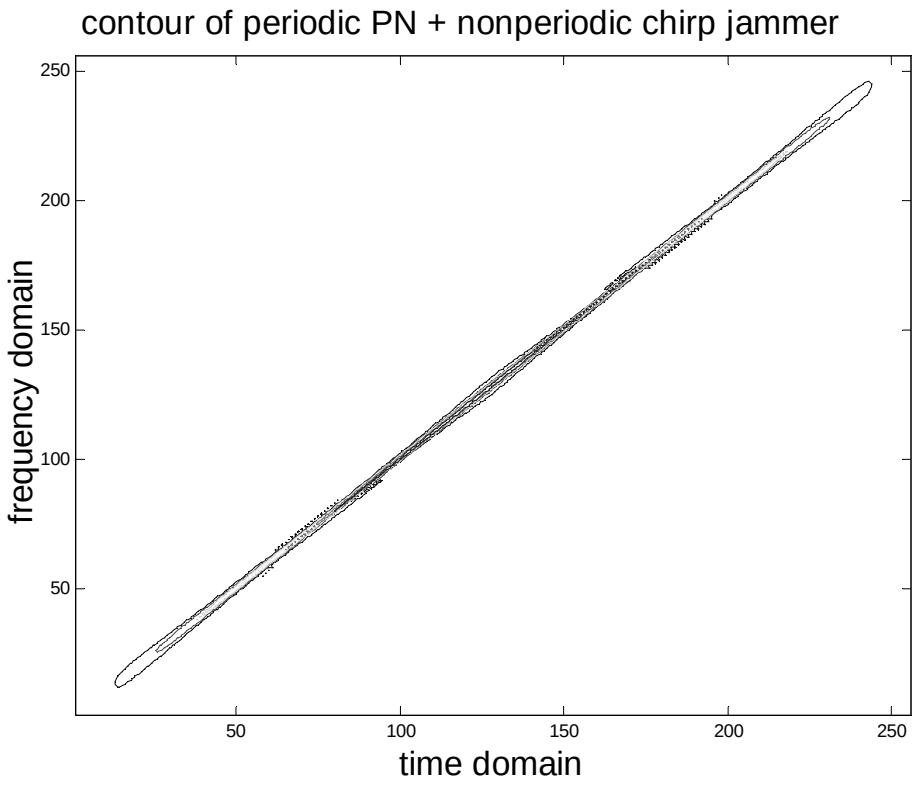

Figure 3. Wigner distribution for a periodic PN sequence and chirp jammer in noise (JSR=40dB, SNR=20dB).

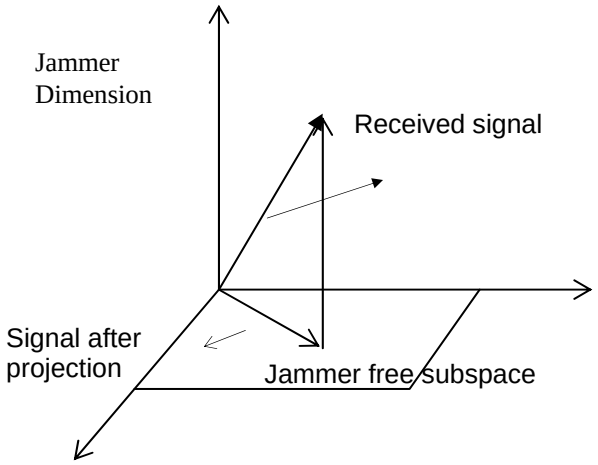

Figure 4. Jammer suppression by subspace projection.

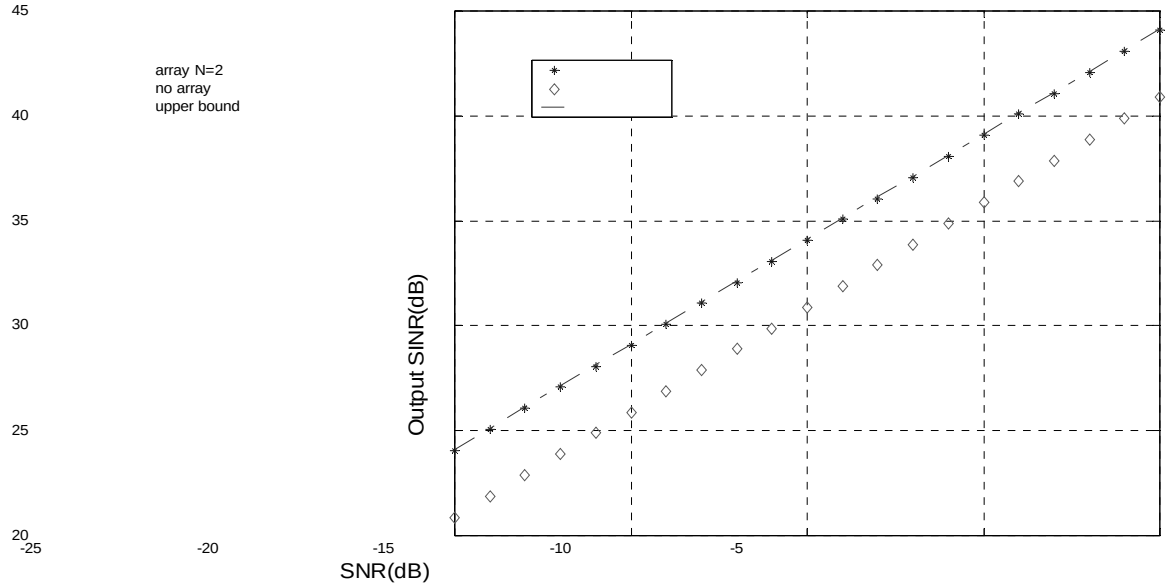

Figure 5: Output SINR vs. SNR.

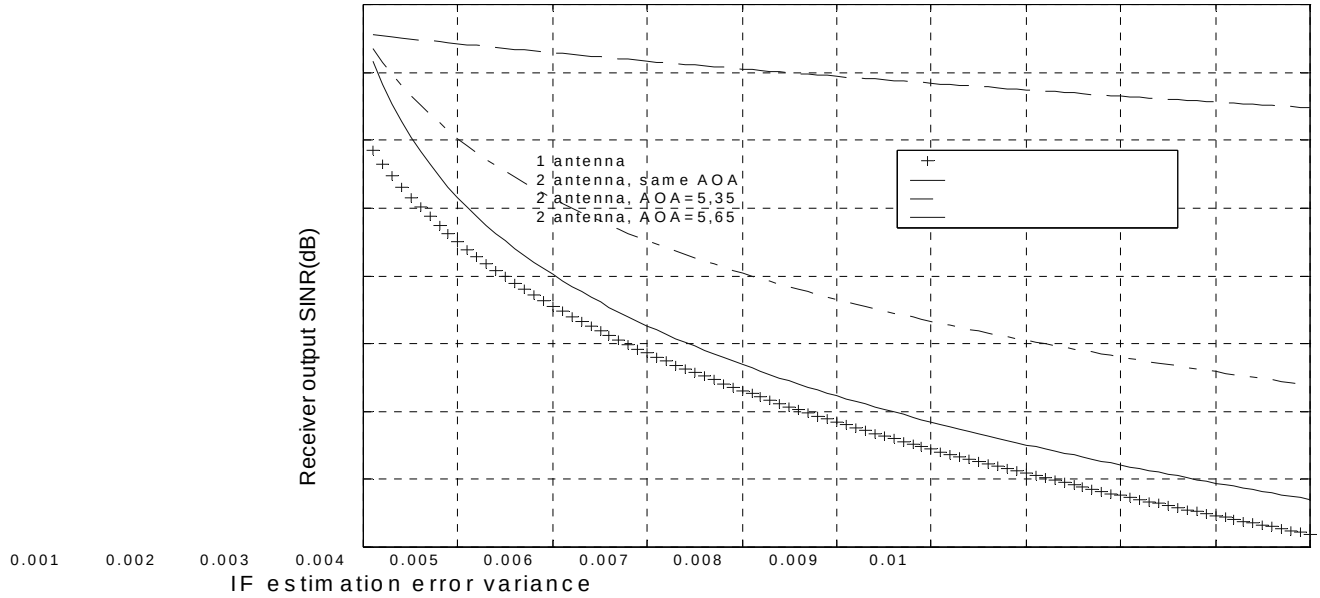

Figure 6. Receiver SINR v. error variance

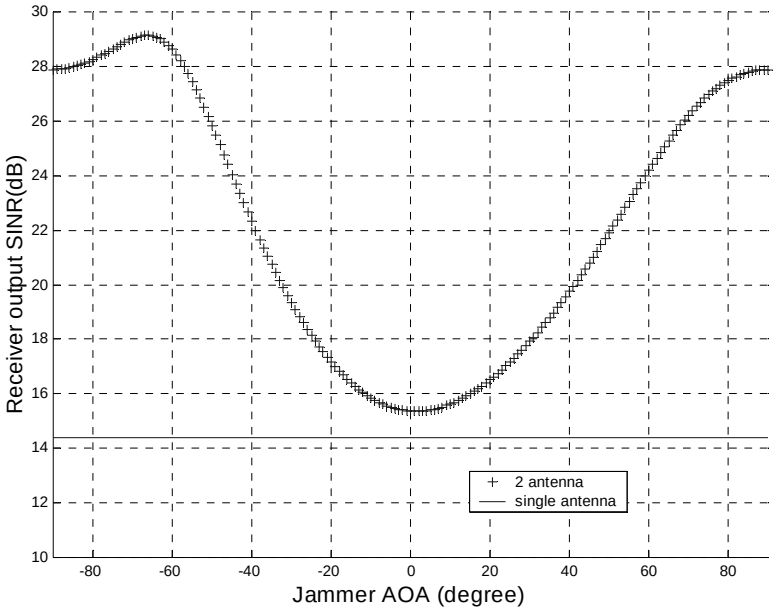

Figure 7. Receiver SINR vs. jammer AOA

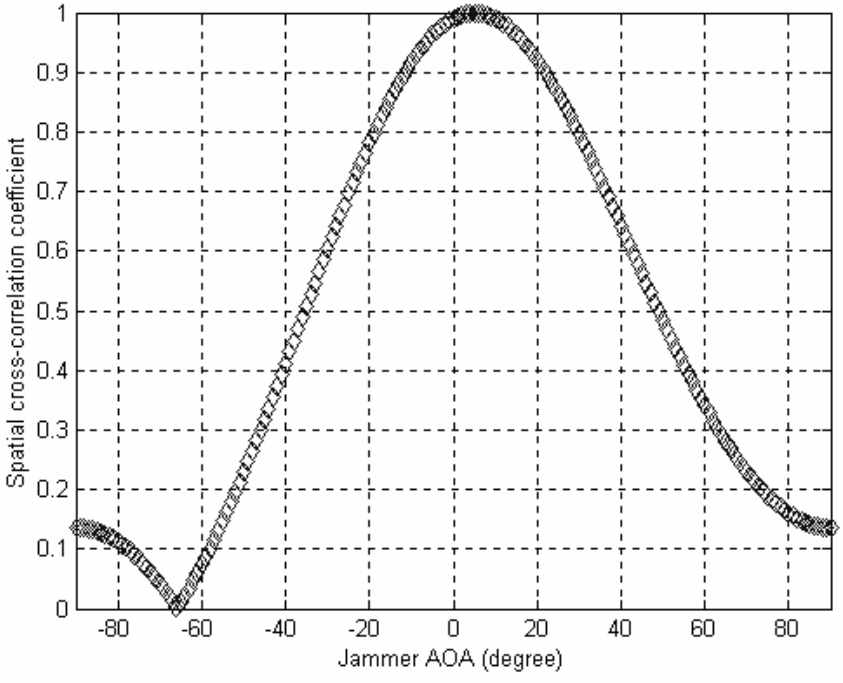

Figure 8. Spatial cross-correlation vs. jammer AOA

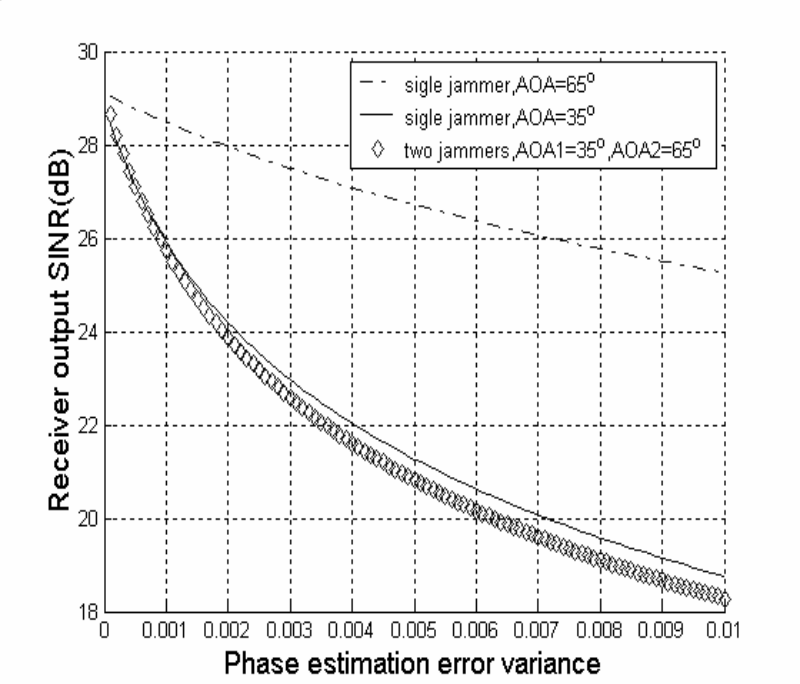

Figure 9. Receiver SINR vs. phase estimation error variance for multiple jammers.

Chapter 3
Array Processing for Nonstationary Interference Suppression in DS/SS Communications Using Subspace Projection Techniques

1. Introduction

There are several methods that have been proposed for interference suppression in DS/SS communications, most have been related to one domain of operation [1], [2]. These methods include the narrowband interference waveform estimation [3], [4], frequency domain interference excision [5], zero-forcing techniques [6], adaptive subspace-based techniques [7], [8], and minimum-mean-square error (MMSE) interference mitigation techniques [9].

Nonstationary interferers, which have model parameters that change with time, are particularly troublesome due to the inability of a single domain mitigation algorithm to adequately remove their effects. The recent development of the quadratic time-frequency distributions (TFDs) for improved signal power localization in the time-frequency plane has motivated several new approaches for excision of interference with rapidly time-varying frequency characteristics in the DS/SS communication systems. Comprehensive summary of TFD-based interference excision is given in reference [10]. The two basic methods for time-frequency excision are based on notch filtering and subspace projections. Utilization of the interference instantaneous frequency (IF), as obtained via TFDs, to design an open loop adaptive notch filter in the temporal domain, has been thoroughly discussed in [11], [12]. Subspace projection methods, commonly used for mitigating narrowband interference [13], [14], have been recently introduced for suppression of frequency modulated (FM) interference and shown to

properly handle multi-component interference, reduce the self-noise, and improve the receiver performance beyond that offered by other time-frequency based techniques [15], [16], [17].

The main purpose of this chapter is to integrate spatial and temporal processing for suppression of nonstationary interferers in DS/SS systems. Specifically, we extend the projection-based interference mitigation techniques in [15], [16], [17] to multi-sensor array receivers. The proposed multi-sensor interference excision technique builds on the offerings of quadratic time-frequency distributions for estimation of 1) the time-frequency subspace and time-frequency signature of nonstationary signals, and 2) the spatial signature of nonstationary sources using direction finding and blind source separations. With the knowledge of the time-frequency and spatial signatures, the objective is to effectively suppress strong nonstationary interferers with few array sensors. The proposed technique does not require the knowledge of the array response or channel estimation of the DS/SS signal, but it utilizes the distinction in both of its spatial- and time-frequency signatures from those of the interferers that impinge on the array. With the combined spatial-time-frequency signatures, the projection of the data vector onto the subspace orthogonal to that of the interferers leads to improved receiver performance over that obtained using the subspace projection in the single-sensor case.

The rest of the chapter is organized as follows. In Section 2, the signal model is described. Section 3 briefly reviews the subspace projection technique. We present in Section 4 blind beamforming based on subspace projection and derive the receiver output signal-to-interference-plus-noise ratio (SINR). Several numerical results are given in Section 5. Section 6 concludes this chapter.

2. Signal Model

In DS/SS communications, each symbol is spread into $L=T/T_c$ chips, where T and T_c are, respectively, the symbol duration and chip duration. We use discrete-time form, where all signal arrivals are sampled at the chip-rate of the DS/SS signal. The symbol-rate source signal is denoted as $s(n)$, and the aperiodic binary spreading sequence of the nth symbol period is represented by $c(n,l)\in\pm 1$, $l=0,1,\cdots,L-1$. The chip-rate sequence of the DS/SS signal can be expressed as

$$d(k) = s(n)c(n,l) \quad \text{with} \quad k = nL + l \tag{3.1}$$

For notation simplicity, we use $c(l)$ instead of $c(n,l)$ for the spreading sequence.

We consider an antenna array of N sensors. The propagation delay between antenna elements is assumed to be small relative to the inverse of the transmission bandwidth, so that the received signal at the N sensors are identical to within complex constants. The received signal vector of the DS/SS signal at the array is expressed by the product of the chip-rate sequence $d(k)$ and its spatial signature $\underline{\mathrm{h}}$,

$$\underline{\mathrm{x}}_s(k) = d(k)\underline{\mathrm{h}} \tag{3.2}$$

The channel is restricted to flat-fading, and is assumed fixed over the symbol length, and as such $\underline{\mathrm{h}}$ in the above equation is not a function of k.

The array vector associated with a total of U interference signals is given by

$$\underline{\mathrm{x}}_u(k) = \sum_{i=1}^{U} \underline{\mathrm{a}}_i u_i(k) \tag{3.3}$$

where $\underline{a}_i$ is the array response to the ith interferer, $u_i(k)$. Without loss of generality, we set $\|\underline{h}\|_F^2 = N$ and $\|\underline{a}_i\|_F^2 = N$, i=1,2,···,U, where $\|\square\|_F$ is the Frobenius norm of a vector. The input data vector is the sum of three components,

$$\underline{x}(k) = \underline{x}_s(k) + \underline{x}_u(k) + \underline{b}(k) = d(k)\underline{h} + \sum_{i=1}^{U} \underline{a}_i u_i(k) + \underline{b}(k) \tag{3.4}$$

where $\underline{b}(k)$ is the additive noise vector. In regards to the above equation, we make the following assumptions.

A1) The information symbols $s(n)$ is a wide-sense stationary process with $E\left[s(n)s^*(n)\right] = 1$, where the superscript * denotes complex conjugation. The spreading sequence $c(k)$ is a binary random sequence with $E[c(k)c(k+l)] = \delta(l)$, where $\delta(l)$ is the delta function.[1]

A2) The noise vector $\underline{b}(k)$ is zero-mean, temporally and spatially white with

$$E\left[\underline{b}(k)\underline{b}^T(k+l)\right] = 0, \quad \text{for all } l$$

and

$$E\left[\underline{b}(k)\underline{b}^H(k+l)\right] = \sigma\delta(l)\mathbf{I}_N$$

where σ is the noise power, the superscripts ^{T} and ^{H} denote transpose and conjugate transpose, respectively, and $\mathbf{I}_N$ is the $N\times N$ identity matrix.

A3) The signal and noise are statistically uncorrelated.

[1]This assumption is most suitable for military applications and P-code GPS.

3. Subspace Projection

The aim of subspace projection techniques is to remove the interference components before despreading by projecting the input data on the subspace orthogonal to the interference subspace, as illustrated in Figure 1. The receiver block diagram is shown in Figure 2.

A nonstationary interference, such as an FM signal, often shares the same bandwidth with the DS/SS signal and noise. As such, for a chirp signal or a signal with high-order frequency laws, the signal spectrum may span the entire frequency band, and the sample data matrix loses its complex exponential structure responsible for its singularity. Therefore, the interference subspace can no longer be obtained from the eigendecomposition of the sample data matrix [13], [15] or the data covariance matrix [14], as it is typically the case in stationary environments. The nonstationary interference subspace, however, may be constructed using the interference time-frequency signature. Methods for estimating the instantaneous frequency, instantaneous bandwidth, and more generally, a time-frequency subspace, based on the signal time-frequency localization properties are, respectively, discussed in references [18], [19], [15].

For the general class of FM signals, and providing that interference suppression is performed separately over the different data symbols, the interference subspace is one-dimensional in an L-dimensional space. We note that since an FM interference has a constant amplitude, its respective data vector can be determined from the IF up to a complex multiplication factor. The unit norm normalization of this vector represents the one-dimensional interference subspace basis vector. Among candidate methods of IF estimation is the one based on the time-frequency distributions. For example, the discrete form of Cohen's class of TFD of a signal $x(t)$ is given by [20]

$$D_{xx}(t, f) = \sum_{m=-\infty}^{\infty} \sum_{\tau=-\infty}^{\infty} \phi(m,\tau) x(t+m+\tau) x^*(t+m-\tau) e^{-j4\pi f\tau} \tag{3.5}$$

where $\phi(m,\tau)$ is a time-frequency kernel that could be signal-dependent. The TFD concentrates the interference signal power around the IF and makes it visible in the noise and PN sequence background [18], [21]. It has been shown that, for linear FM signals, Radon-Wigner transform provides improved IF estimates over the TFD [22]. Parametric methods using autoregressive model have also been proposed [23].

Other nonstationary interference with instantaneous bandwidth or spread in the time-frequency domain are captured in a higher-dimension subspace. In this case, the interference subspace can be constructed from the interference localization region Ω in the time-frequency domain (see, for example, [15]). The subspace of interest becomes that which fills out the interference time-frequency region Ω energetically, but has little or no energy outside Ω.

Interference-free DS/SS signals are obtained by projecting the received data vector (in the temporal domain processing, the vector consists of data samples at different snapshots) on the subspace orthogonal to the interference subspace.

3.1. Temporal Processing

In the single-sensor receiver, the input data is expressed as

$$x(k) = x_s(k) + x_u(k) + b(k) = d(k) + \sum_{i=1}^{U} u_i(k) + b(k) \tag{3.6}$$

Using L sequential chip-rate samples of one symbol of the received signals at time index k, we obtain the following input vector

$$\begin{aligned}&\left[x(k) \quad x(k-1) \quad \cdots \quad x(k+L+1)\right]^T \\ &=\left[x_s(k) \quad x_s(k-1) \quad \cdots \quad x_s(K-L+1)\right]^T \\ &+\left[x_u(k) \quad x_u(k-1) \quad \cdots \quad x_u(K-L+1)\right]^T \\ &+\left[b(k) \quad b(k-1) \quad \cdots \quad b(k+L+1)\right]^T\end{aligned} \tag{3.7}$$

or simply

$$X(k) = X_s(k) + X_u(k) + B(k) \tag{3.8}$$

We drop the variable *k* for simplicity, with the understanding that processing is performed over the *n*th symbol that starts at the *k*th chip. Then, equation (3.8) becomes

$$X = X_s + X_u + B \tag{3.9}$$

Below, we relax the FM condition used in [13], [16] that translates to a single dimension interference. The general case of an interference occupying higher dimension subspace is considered. We assume that the *i*th interferer spans M_i dimensional subspace, defined by the orthonormal basis vectors $V_{i,1}$, $V_{i,2}$, $\cdots$, V_{i,M_i} , and the different interference subspaces are disjoint. Define

$$V_i = \left[V_{i,1} \quad V_{i,2} \quad \cdots \quad V_{i,M_i}\right] \tag{3.10}$$

and let $M = \sum_{i=1}^{U} M_i$ as the number of total dimensions of the interferers. With $L>M$, the $L\times M$ matrix

$$V = \left[V_1 \quad V_2 \quad \cdots \quad V_U\right],\ V_i \cap V_i = \Phi \ \text{ for } i \neq j \tag{3.11}$$

is full rank and its columns span the combined interference subspace *J*. The respective projection matrix is

$$\overline{P} = V(V^H V)^{-1} V^H \tag{3.12}$$

The projection matrix associated with the interference orthogonal subspace, G, is then given by

$$P = \mathbf{I}_L - V(V^H V)^{-1} V^H \tag{3.13}$$

When applied to X, matrix P projects the input data vector onto G, and results in

$$X_\perp = PX = PX_s + PB \tag{3.14}$$

which no longer includes any interference component.

The single-sensor receiver implementing subspace projection for excision of a single instantaneously narrowband FM interferer (i.e., $U = 1$, $M_1 = 1$) in DS/SS communications is derived in [24]. The receiver SINR is shown to be

$$\text{SINR} = \frac{(L-1)^2}{\left(1 - \frac{2}{L}\right) + \sigma(L-1)} = \frac{L-1}{\frac{L-2}{L(L-1)} + \sigma} \tag{3.15}$$

For typical values of L, $(L\text{-}2)/(L\text{-}1) \approx 1$, and equation (3.15) can be simplified as

$$\text{SINR} \approx \frac{N(L-1)}{\sigma + N/L} \tag{3.16}$$

Compared to the interference-free environment, where the receiver SINR is L/σ, nonstationary interference (3.16) is achieved by reducing the processing gain by 1 and increasing the noise power by the self-noise factor of $1/L$.

4. Subspace Projection in Multi-Sensor Receiver

In this section, we consider nonstationary interference excision in multi-sensor receivers using subspace projections. We note that if the subspace projection method discussed in Section III is extended to an N-element array by suppressing the interference independently in each sensor data and then combining the results by maximum ratio combining (see Figure 3), then it is straightforward to show that the receiver SINR is given by

$$\text{SINR} \approx \frac{N(L-1)}{\sigma + N/L} \tag{3.17}$$

The above extension, although clearly improves over (3.16), does not utilize the potential difference in the spatial signatures of signal arrivals, and, therefore, is inferior to the receiver proposed in this Section.

4.1. Spatio-Temporal Signal Subspace Estimation

To construct the spatio-temporal signal subspace of the interference signals, it is important to estimate both the time-frequency signature (or subspace) and the spatial signature of each interferer. The IF estimation of an FM interference signal based on time-frequency distribution is addressed in Section III. It is noteworthy that when multiple antennas are available, the TFD may be computed at each sensor data separately and then averaged over the array. This method has been shown in [25] to improve the IF estimation, as it reduces noise and cross terms that often obscure the source true power localization in the time-frequency domain.

On the other hand, the estimation of source spatial signature can be achieved, for example, by using direction finding and source separation techniques. When the interference signals have clear bearings, methods like MUSIC [26] and maximum likelihood (ML) [27] can be used to estimate the steering matrix of the interference signals. These methods can be revised to incorporate the TFD of the signal arrivals for improved performance [28], [29], [30]. On the other hand, in fading channels where the steering vector loses its known structure due to multipath, blind source separation methods should be used [31], [32], [33]. Since the interferers in DS/SS communications often have relatively high power, good spatial signature estimation is expected.

More conveniently, the spatial signatures can be simply estimated by using matched filtering once the time-frequency signatures are provided. The maximum likelihood estimator for the vector $\underline{a}_i$ is obtained as

$$\hat{\underline{a}}_i = \sqrt{N}\sum_{k=0}^{L-1}\hat{u}_i^*(k)\underline{x}(k) \Big/ \left\|\sum_{k=0}^{L-1}\hat{u}_i^*(k)\underline{x}(k)\right\|_F \tag{3.18}$$

where $\hat{u}_i(k)$ is the estimated waveform of the *i*th interferer. It is noted that the possible phase ambiguity in the waveform estimation of $\hat{u}_i(k)$ does not affect the estimation of the spatial signature. For slowly varying channels, the above average can also be performed over multiple symbols to improve the estimation accuracy.

In the analysis presented herein, we assume knowledge of the interference subspace and its angle-of-arrival (AOA) to derive the receiver SINR.

4.2. Proposed Technique

The subspace projection problem for nonstationary interference suppression in DS/SS communications is now considered within the context of multi-sensor array using *N* array elements. We use one symbol DS/SS signal duration (i.e., *L* chip-rate temporal snapshots), and stack *L* discrete observations to construct an *NL*×1 vector of the received signal sequence in the joint spatio-temporal domain. In this case, the received signal vector in (3.4) becomes

$$\begin{aligned}
&\left[\underline{x}^T(k) \quad \underline{x}^T(k-1) \quad \cdots \quad \underline{x}^T(k+L+1)\right]^T \\
&= \left[\underline{x}_s^T(k) \quad \underline{x}_s^T(k-1) \quad \cdots \quad \underline{x}_s^T(K-L+1)\right]^T \\
&+ \left[\underline{x}_u^T(k) \quad \underline{x}_u^T(k-1) \quad \cdots \quad \underline{x}_u^T(K-L+1)\right]^T \\
&+ \left[\underline{b}^T(k) \quad \underline{b}^T(k-1) \quad \cdots \quad \underline{b}^T(k+L+1)\right]^T
\end{aligned} \tag{3.19}$$

or simply

$$\mathbf{X} = \mathbf{X}_s + \mathbf{X}_u + \mathbf{B} \tag{3.20}$$

where again the variable *k* is dropped for simplicity.

In (3.19), the interference vector in the single-sensor problem, given by (3.7), is extended to a higher dimension. With the inclusion of both temporal and spatial samples, the *m*th basis of the *i*th interference becomes

$$\mathrm{V}_{i,m} = \mathrm{V}_{i,m} \otimes \underline{\mathrm{a}}_i \tag{3.21}$$

and

$$\mathrm{V}_i = \begin{bmatrix} \mathrm{V}_{i,1} & \mathrm{V}_{i,2} & \cdots & \mathrm{V}_{i,M_i} \end{bmatrix} \tag{3.22}$$

where $\otimes$ denotes the Kronecker product. The columns of the $LN \times M$ matrix

$$\mathrm{V} = \begin{bmatrix} \mathrm{V}_1 & \mathrm{V}_2 & \cdots & \mathrm{V}_U \end{bmatrix} \tag{3.23}$$

spans the overall interference signal subspace. For independent spatial signatures, the matrix rank is M. The orthogonal projection matrix is given by

$$\mathrm{P} = \mathbf{I}_{LN} - \mathrm{V}(\mathrm{V}^H \mathrm{V})^{-1} \mathrm{V}^H \tag{3.24}$$

The projection of the signal vector on the orthogonal subspace of the interferers' yields

$$\mathbf{X}_\perp = \mathbf{PX} = \mathbf{PX}_\mathrm{s} + \mathbf{PB} \tag{3.25}$$

The block diagram of the proposed method is presented in Figure 4. As shown in the next section, effective interference suppression can be achieved solely based on the spatial signatures or the time-frequency signatures, or it may require both information.

4.3. Performance Analysis

Below we consider the performance of the multi-sensor receiver system implementing subspace projections. Recall that

$$V_{i,m}^H V = 0 \quad \text{for any} \quad i, m \neq j, n. \tag{3.26}$$

and

$$\mathbf{V}^H \mathbf{V} = N \mathbf{I}_\mathrm{M} \tag{3.27}$$

the projection matrix **P** becomes

$$\mathbf{P} = \mathbf{I}_{LN} - \frac{1}{N}\mathbf{V}\mathbf{V}^H \tag{3.28}$$

The signal vector $\mathbf{X}_s$ can be rewritten as

$$\begin{aligned}\mathbf{X}_s &= \left[\underline{\mathrm{x}}_s^T(k) \quad \underline{\mathrm{x}}_s^T(k-1) \quad \cdots \quad \underline{\mathrm{x}}_s^T(k+L+1)\right]^T \\ &= \left[d(k)\underline{\mathrm{h}}^T \quad d(k-1)\underline{\mathrm{h}}^T \quad \cdots \quad d(k-L+1)\underline{\mathrm{h}}^T\right]^T \\ &= s(n)\left[c(L-1) \quad c(L-2) \quad \cdots \quad c(0)\right]^T \otimes \mathrm{h} \\ &\square\ s(n)\mathbf{q}\end{aligned} \tag{3.29}$$

where the $LN\times 1$ vector

$$\mathbf{q} = \left[c(L-1) \quad c(L-2) \quad \cdots \quad c(0)\right]^T \otimes \underline{\mathrm{h}} \square\ \underline{\mathrm{c}} \otimes \underline{\mathrm{h}} \tag{3.30}$$

defines the spatio-temporal signature of the desired DS/SS signal. **q** is the extension of the DS/SS code by replicating it with weights defined by the signal spatial signature.

By performing despreading and beamforming, the symbol-rate decision variable is given by

$$y(n) = \mathbf{q}^H\mathbf{X}_\perp(k) = s(n)\mathbf{q}^H\mathbf{P}\mathbf{q} + \mathbf{q}^H\mathbf{P}\mathbf{B}(k) \square\ y_1(n) + y_2(n) \tag{3.31}$$

where $y_1(n)$ is the contribution of the desired DS/SS signal to the decision variable, and $y_2(n)$ is the respective contribution from the noise.

The SINR of the array output becomes (see Appendix A)

$$\mathrm{SINR} = \frac{E^2\left[y(k)\right]}{\mathrm{var}\left[y(k)\right]} = \frac{\left(L - \sum_{i=1}^{U} M_i\left|\beta_i\right|^2\right)^2}{\left(\left(\sum_{i=1}^{U} M_i\left|\beta_i\right|^2\right)^2 - 2\sum_{i=1}^{U}\xi_i\left|\beta_i\right|^4\right) + \frac{\sigma}{N}\left(L - \sum_{i=1}^{U} M_i\left|\beta_i\right|^2\right)} \tag{3.32}$$

where ξ_i is defined in (A.9), and β_i is the spatial correlation coefficient between the spatial signatures $\underline{h}$ and $\underline{a}_i, i = 1, 2, \cdots U$, and is given by

$$\beta_i = \frac{1}{N} \underline{h}^H \underline{a}_i \tag{3.33}$$

Note that when the noise power is small, i.e., $\sigma << 1$, the variance of y_1 becomes dominant, and the output SINR reaches the following upper bound

$$\text{SINR}_{\text{high SNR}} \approx \frac{\left(L - \sum_{i=1}^{U} M_i |\beta_i|^2 \right)^2}{\left(\sum_{i=1}^{U} M_i |\beta_i|^2 \right)^2 - 2 \sum_{i=1}^{U} \xi_i |\beta_i|^4} \tag{3.34}$$

This result is affected by the factors L, M_i, $|\beta_i|$, and $\xi_i, i = 1, \cdots, U$. On the other hand, when the noise level is very high, i.e., $\sigma >> 1$, the noise variance plays a key role in determining var[$y(k)$], and the output SINR becomes

$$\text{SINR}_{\text{low SNR}} \approx \frac{\left(L - \sum_{i=1}^{U} M_i |\beta_i|^2 \right)^2}{\frac{\sigma}{N} \left(L - \sum_{i=1}^{U} M_i |\beta_i|^2 \right)} = \frac{N}{\sigma} \left(L - \sum_{i=1}^{U} M_i |\beta_i|^2 \right) \tag{3.35}$$

Unlike the high input SNR case, the output SINR in (3.36) also depends on both N and σ. Comparing (3.34) and (3.35), it is clear that the improvement in the receiver SINR becomes more significant when the spatial signatures produce small spatial correlation coefficients and under high SNR.

Next, we consider some specific important cases. When $\beta_i = 0, i = 1, \cdots U$, $\text{var}\left[y_1(n) \right] = 0$ the receiver SINR in (3.32) becomes $SINR = LN/\sigma$. This is to say, the output SINR is improved by a factor of LN over the input signal-to-noise ratio (SNR) (not the input SINR!). This implies that

the interferers are suppressed by spatial selectivity of the array and their suppression does not cause any distortion of the temporal characteristics of the DS/SS signal. The DS/SS signal in this case enjoys the array gain that contributes the factor *N* to the SINR.

For a single FM interferer (U=1, M_1=1), equation (3.32) becomes

$$\text{SINR} \approx \frac{\left(L-|\beta_1|^2\right)^2}{\left(1-\frac{2}{L}\right)|\beta_1|^4+\frac{\sigma}{N}\left(L-|\beta_1|^2\right)} \tag{3.37}$$

It is easy to show that SINR in (3.37) monotonously decreases as $|\beta_1|$ increases, and the lower bound of the SINR is reached for β_1=1, which is the case of the desired DS/SS signal and the interference signal arriving from the same direction. With a unit value of β_1,

$$\text{SINR} \approx \frac{\left(L-1\right)^2}{\left(1-\frac{2}{L}\right)+\frac{\sigma}{N}\left(L-1\right)} \approx \frac{N(L-1)}{\frac{N}{L}+\sigma} \tag{3.38}$$

This result is the same as that of the single-sensor case developed in [16], except for the appearance of the array gain, *N*, for the desired DS/SS signal over the noise. This equation also coincides with (3.17). That is, the independent multi-sensor subspace projection, illustrated in Figure 3, results in the same output SINR with the proposed multi-sensor subspace projection method when $|\beta_1|$=0.

On the other hand, the maximum value in (3.36) corresponds to $\beta = 0$, and is equal to $SINR = LN/\sigma$, as discussed above. For the illustration of the SINR behavior, we plot in Figure 5 the SINR in (3.36) versus $|\beta_1|$ for a two-sensor array, where L=64, and one FM jammer is considered with $M = 7$. The input SNR is 0dB.

4.4. Remarks

Given the temporal and spatial signatures, the proposed technique simplifies to two consecutive tasks. The first is to estimate the spatio-temporal signature. When using multiple antenna receivers, a basis vector of the orthogonal projection matrix is obtained by the Kronecker product of a jammer's temporal signature and its spatial signature that results in the $LN \times LN$ orthogonal project matrix instead of $L \times L$ in the single antenna case. The second task is jammer suppression via subspace projection. This involves the multiplication of an $LN \times LN$ matrix and an $LN \times 1$ vector.

Note such increase in computations is natural due to increase of dimensionality. It is noteworthy that array processing expands overall space dimensionality but maintains the jammer subspace dimension. As a result, it yields improved SINR performance over temporal processing or spatial processing only methods.

5. Numerical Results

A two-element array is considered with half-wavelength spacing. The DS/SS signal uses random spreading sequence with L=64. The AOA of the DS/SS signal is 0 degree from broadside ($\theta_D = 0^\circ$).

We consider two interference signals. Each interference signal is assumed to be made up of uncorrelated FM component with $M_i = 7, i = 1, 2$. The overall interference subspace is M = 14. The AOAs of the two interferers are θ_J=[40^o,60^o]. The respective spatial correlations in this example are $|\beta_1|$=0.53 and $|\beta_2|$=0.21. Note that, in the subspace projection method, the output SINR is independent of the input jammer-to-signal ratio (JSR), since the interferers are entirely suppressed, regardless of their power. Figure 6 shows the receiver SINR versus the input SNR.

The upper bounds correspond to interference-free data. For high input SNR, the receiver SINR is decided by the induced signal distortion, described by the variance given in (A.10). It is evident from Figure 6 that the two-antenna receiver outperforms the single-antenna receiver case by a factor much larger than the array gain. Since the output SINR in the two-antenna receiver highly depends on the spatial correlation coefficients, the curves corresponding to a two-sensor array in Figure 6 will assume different values upon changing β_1, or/and β_2. The best performance is achieved at $\beta_1=\beta_2=0$.

Figure 7 shows the receiver SINR versus the number of chips per symbol (L). We let L vary from 8 to 4096, whereas the input SNR is fixed at 0 dB. The two interference signals are incident on the array with angles $\theta_J=[40^o,60^o]$. They are assumed to maintain their time-frequency spread with increased value of L. As such, the respective dimensions of their subspaces grow proportional to the number of chips per symbol. In this example, the dimension of each interference signal is assumed to be 10 percent of L (round to the nearest integer). The ouput SINR improvement by performing array processing at different L is evident from this figure. It is seen that, unlike the case of the instantaneously narrowband FM interference, where the output SINR increases rapidly as L increases, the output SINR in the underlying scenario ceases to increase as L assumes large values. This is because the rank of the interference signal subspace increases with L.

In Figure 8 we investigate the receiver SINR performance versus the number of array sensors. In this figure, L is set at 64, and the input SNR is 0 dB. Two interference signals composed of uncorrelated FM components are considered, and $M_i = 7, i = 1, 2,$ are assumed. Two examples are used to examine the effect of different AOAs. In the first example, $\theta_J=[40^o,60^o]$. The output

SINR improves sharply as the number of array sensors increases from one to three, beyond which the improvement becomes insignificant. The differences in the above AOAs of the desired DS/SS signal and the interference signals are relatively large, and a small number of array sensors leads to negligible spatial correlation coefficients. We also show a case with closely spaced interference signals where θ_J=[5^o,15^o]. In this case, the output SINR slowly improves as the number of array sensors increases.

It is noted that, when we consider a specific case, the output SINR does not increase monotonously with the number of array sensors. This is because the relationship between the spatial correlation coefficient and the AOAs is by itself not monotonous. Nevertheless, when we consider the general case with different AOA combinations, high number of array sensors often reduce the spatial correlation coefficients.

6. Conclusions

In this chapter, subspace projection techniques were employed to suppress nonstationary interferers in direct sequence spread spectrum (DS/SS) communication systems. Interference suppression is based on the knowledge of both the interference time-frequency and spatial signatures. While the former is based on instantaneous frequency information that can be gained using several methods, including time-frequency distributions, the later can be provided from applying higher resolution methods or blind source separation techniques to the signal arrivals.

The differences between the DS/SS signal and interference signatures both in the time-frequency and spatial domains equip the projection techniques with the ability to remove the interference with a minimum distortion of the desired signal.

The receiver performance based on subspace projections was analyzed. It was shown that the lower performance bound is obtained when the sources have the same angular position. In this case, the problem becomes equivalent to a single-antenna receiver with only the presence of the array gain. On the other hand, the upper bound on performance is reached in the interference-free environment and also corresponds to the case in which the spatial signature of the interference is orthogonal to that of the DS/SS signal.

Numerical results were presented to illustrate the receiver SINR dependency on spatial correlation coefficient, input SNR, and the PN sequence length.

Appendix A

To derive the output SINR expression, we use $s(n) = +1$ (the output SINR is independent of $s(n)$ and same result follows when $s(n) = -1$). Then,

$$\begin{aligned} E\left[y_1(n)\right] &= E\left[\mathrm{q}^H \mathrm{P} \mathrm{q}\right] \\ &= E\left[\mathrm{q}^H \left(\mathrm{I} - \frac{1}{N}\mathrm{V}\mathrm{V}^H\right)\mathrm{q}\right] \\ &= E\left[\mathrm{q}^H \mathrm{q}\right] - \frac{1}{N} E\left[\mathrm{q}^H \mathrm{V}\mathrm{V}^H \mathrm{q}\right] \\ &= LN - \frac{1}{N} E\left[\mathrm{q}^H \sum_{i_1=1}^{U}\sum_{M_1=1}^{M_i} \mathrm{V}_{i_1,M_1} \sum_{i_2=1}^{U}\sum_{M_2=1}^{M_i} \mathrm{V}^H_{i_2,M_2} \mathrm{q}\right] \end{aligned} \tag{A.1}$$

It is straightforward to show that

$$\mathrm{q}^H \mathrm{V}_{i,m} = \left(\underline{\mathrm{c}} \otimes \underline{\mathrm{h}}\right)^H \left(V_{i,m} \otimes \underline{\mathrm{a}}_i\right) = \left(\underline{\mathrm{c}}^T V_{i,m}\right) \otimes \left(\underline{\mathrm{h}}^H \underline{\mathrm{a}}_i\right) = N\beta i \sum_{l=0}^{L-1} V_{i,m}(l) c(l) \tag{A.2}$$

Using the orthogonal property of the spreading sequence A1), (A.1) becomes

$$\begin{aligned} E\left[y_1(n)\right] &= LN - NE\left[\sum_{i_1=1}^{U} \beta_{i_1} \sum_{m_1=1}^{M_{i_1}}\sum_{l_1=0}^{L-1} V_{i_1,m_1}(l_1) c(l_1) \sum_{i_2=1}^{U} \beta^*_{i_2} \sum_{m_2=1}^{M_{i_2}}\sum_{l_2=0}^{L-1} V_{i_2,m_2}(l_2) c(l_2)\right] \\ &= LN - N\sum_{i=1}^{U} \left|\beta_i\right|^2 \sum_{m=1}^{M_{i_1}}\sum_{l=0}^{L-1} \left|V_{i,m}(l)\right|^2 c^2(l) \\ &= N\left(L - \sum_{i=1}^{U} M_i \left|\beta_i\right|^2\right) \end{aligned} \tag{A.3}$$

Due to the zero-mean property of noise (assumption A2) $E\left[y_2(n)\right] = 0$. Accordingly,

$$E\left[y(n)\right] = E\left[y_1(n)\right] = N\left(L - \sum_{i=1}^{U} M_i \left|\beta_i\right|^2\right) \tag{A.4}$$

It is clear from (A.4) that the increase in the space dimensionality from L to NL does not simply translate into a corresponding increase in the desired mean value, or subsequently in the

processing gain. Also, from assumption A3), the cross-correlation between $y_1(n)$ and $y_2(n)$ is zero, i.e.,

$$E\left[y_1^*(n) y_2(n) \right] = E\left[y_1(n) y_2^*(n) \right] = 0 \tag{A.5}$$

Therefore, the mean square value of the decision variable is made up of only two terms,

$$E\left[\left| y(n) \right|^2 \right] = E\left[\left| y_1(n) \right|^2 \right] + E\left[\left| y_2(n) \right|^2 \right] \tag{A.6}$$

The first term is the mean square value of $y_1(n)$. From (3.26), we have

$$\begin{aligned} E\left[\left| y_1(n) \right|^2 \right] &= E\left[\mathrm{q}^H \mathrm{P} \mathrm{q} \mathrm{q}^H \mathrm{P}^{\mathrm{H}} \mathrm{q} \right] \\ &= E\left[\mathrm{q}^H \left(\mathrm{I}_N - \frac{1}{N} \mathrm{V}\mathrm{V}^H \right) \mathrm{q} \mathrm{q}^H \left(\mathrm{I}_{LN} - \frac{1}{LN} \mathrm{V}\mathrm{V}^H \right) \mathrm{q} \right] \\ &= E\left[\mathrm{q}^H \mathrm{q} \mathrm{q}^H \mathrm{q} \right] - \frac{2}{N} E\left[\mathrm{q}^H \mathrm{q} \mathrm{q}^H \mathrm{V}\mathrm{V}^H \mathrm{q} \right] + \frac{1}{N^2} E\left[\mathrm{q}^H \mathrm{V}\mathrm{V}^H \mathrm{q} \mathrm{q}^H \mathrm{V}\mathrm{V}^H \mathrm{q} \right] \\ &= (LN)^2 - 2LN^2 \sum_{i=1}^{U} M_i \left| \beta_i \right|^2 + N^2 \left(2\left(\sum_{i=1}^{U} M_i \left| \beta_i \right|^2 \right)^2 + \left| \sum_{i=1}^{U} \beta_i^2 \gamma_i \right| - 2\sum_{i=1}^{U} \xi_i \left| \beta_i \right|^4 \right) \end{aligned} \tag{A.7}$$

where

$$\gamma_i = \sum_{m_1=1}^{M_i} \sum_{m_2=1}^{M_i} \sum_{l_2=0}^{L-1} V_{i,m_1}(l) V_{i,m_2}(l) \tag{A.8}$$

and

$$\xi_i = \sum_{m=1}^{M_i} \sum_{l=1}^{L-1} \left| V_{i,m}(l) \right|^4 \tag{A.9}$$

In practice, γ_i takes negligible values, and equation (A.7) can be simplified to

$$E\left[\left| y_1(n) \right|^2 \right] = \left(LN \right)^2 - 2LN^2 \sum_{i=1}^{U} M_i \left| \beta_i \right|^2 + N^2 \left(2\left(\sum_{i=1}^{U} M_i \left| \beta_i \right|^2 \right)^2 - 2\sum_{i=1}^{U} \xi_i \left| \beta_i \right|^4 \right) \tag{A.10}$$

The value of ξ_i depends on the type of interference signals. Specifically, when the *i*th interference signal is made up of a single FM or a number of uncorrelated FM signal components, then the basis vectors are of constant modulus, and

$$\xi_i = \frac{M_i}{L} \tag{A.11}$$

The second term of (A.6) is the mean-square value of $y_2(n)$,

$$\begin{aligned} E\left[\left|y_2(n)\right|^2\right] &= E\left[\mathrm{q}^H \mathrm{PB}(k)\mathrm{B}^H(k)\mathrm{P}^H\mathrm{q}\right] \\ &= \sigma E\left[\mathrm{q}^H \mathrm{PP}^H\mathrm{q}\right] = \sigma E\left[\mathrm{q}^H \mathrm{Pq}\right] = \sigma N\left(L - \sum_{i=1}^{U} M_i \left|\beta_i\right|^2\right) \end{aligned} \tag{A.12}$$

The variance of *y*(*n*) is given by

$$\begin{aligned} \mathrm{var}\left[y(n)\right] &= E\left[\left|y(n)\right|^2\right] - E^2\left[y(n)\right] \\ &= E\left[\left|y_1(n)\right|^2\right] + E\left[\left|y_2(n)\right|^2\right] - E^2\left[y_1(n)\right] \\ &= N^2\left(\left(\sum_{i=1}^{U} M_i \left|\beta_i\right|^2\right)^2 - 2\sum_{i=1}^{U} \xi_i \left|\beta_i\right|^4\right) + \sigma\left(L - \sum_{i=1}^{U} M_i \left|\beta_i\right|^2\right) \end{aligned} \tag{A.13}$$

Equation (3.32) follows by using the results of (A.4) and (A.13).

References

[1] H. V. Poor and L. A. Rusch, “Narrowband interference suppression in spread-spectrum CDMA," *IEEE Personal Comm. Mag.*, vol. 1, no. 8, pp. 14–27, Aug. 1994.

[2] J. D. Laster and J. H. Reed, “Interference rejection in digital wireless communications," *IEEE Signal Processing Mag.*, vol. 14, no. 3, pp. 37–62, May 1997.

[3] L. B. Milstein, “Interference rejection techniques in spread spectrum communications," *Proc. IEEE*, vol. 76, pp.657–C671, June 1988.

[4] J. Wang and L. B. Milstein, Adaptive LMS filters for cellular CDMA overlay," *IEEE J. Select. Areas Commun.*, vol. 14, no. 8, pp. 1548–1559, Oct. 1996.

[5] S. Sandberg, Adapted demodulation for spread-spectrum receivers which employ transform-domain interference excision," *IEEE Trans. Commun.*, vol. 43, pp. 2502–2510, Sept. 1995.

[6] L. A. Rusch and H. Poor, Multiuser detection techniques for narrow-band interference suppression in spread spectrum communications," *IEEE Trans. Commun.*, vol. 43, no. 2/3/4, pp. 1725–1737, Feb./Mar./Apr. 1995.

[7] H. Fathallah and L. A. Rusch, A subspace approach to adaptive narrow-band interference suppression in DSSS," *IEEE Trans. Commun.*, vol. 45, no. 12, pp. 1575–1585, Dec. 1997.

[8] M. Lops, G. Ricci, and A. T. Tulino, “Narrow-band-interference suppression in multiuser CDMA systems," *IEEE Trans. Signal Processing*, vol. 46, no. 9, pp. 1163–1175, Sept. 1998.

[9] L. A. Rusch, MMSE detector for narrow-band interference suppression in DS spread spectrum," in *Proc. Interference Rejection and Signal Separation in Wireless Commun. Symp.*, Newark, NJ, March 1996.

[10] M. G. Amin and A. Akansu, “Time-frequency for interference excision in spread-spectrum communications," in “Highlights of signal processing for communications: celebrating a half century of signal processing," *IEEE Signal Processing Mag.*, vol. 16, no. 2, March 1999.

[11] M. G. Amin, Interference mitigation in spread spectrum communication systems using time-frequency distribution," *IEEE Trans. Signal Processing*, vol. 45, no. 1, pp.90–102, Jan. 1997.

[12] M. G. Amin, C. Wang, and A. Lindsey, Optimum interference excision in spread spectrum communications using open loop adaptive filters," *IEEE Trans. Signal Processing*, vol. 47, no. 7, pp.1966–1976, July 1999.

[13] B. K. Poh, T. S. Quek, C. M. S. See, and A. C. Kot, “Suppression of strong narrowband interference using eigen-structure-based algorithm," in *Proc. Milcom*, pp. 1205–1208, July 1995.

[14] A. Haimovich and A. Vadhri, “Rejection of narrowband interferences in PN spread spectrum systems using an eigenanalysis approach," in *Proc. IEEE Signal Processing Workshop on Statistical Signal and Array Processing*, Quebec, Canada, pp. 1002–1006, June 1994.

[15] F. Hlawatsch and W. Kozek, “Time-frequency projection filters and time-frequency signal expansions," *IEEE Trans. Signal Processing*, vol. 42, no. 12, pp. 3321–3334, Dec. 1994.

[16] M. G. Amin and G. R. Mandapati, Nonstationary interference excision in spread spectrum communications using projection filtering methods," in *Proc. 32nd Annual Asilomar Conf. on Signals, Systems, and Computers*, Pacific Grove, CA, Nov. 1998.

[17] S. Barbarossa and A. Scaglione, Adaptive time-varying cancellation of wideband interferences in spread-spectrum communications based on time-frequency distributions," *IEEE Trans. Signal Processing*, vol. 47, no. 4, pp. 957–965, April 1999.

[18] B. Boashash, “Estimating and interpreting the instantaneous frequency of a signal," *Proc. IEEE*, vol. 80, no. 12, Dec. 1990.

[19] P. Loughlin and K. Davidson, “Instantaneous bandwidth of multicomponent signals," in *Proc. SPIE: Advanced Signal Processing Algorithms, Architectures, and Implementations IX*, vol. 3807, pp. 546–551, July 1999.

[20] L. Cohen, *Time-Frequency Analysis*, Prentice Hall, 1995.

[21] P. Rao and F. J. Taylor, “Estimation of the instantaneous frequency using the discrete Wigner distribution," *Electronics Lett.*, vol. 26, no. 4, pp. 246–248, Feb. 1990.

[22] M. Wang, A. Chan, and C. Chui, “Linear frequency-modulated signal detection using Radon-ambiguity transform," *IEEE Trans. Signal Processing*, vol. 46, no. 3, pp. 571–586, March 1998.

[23] P. Shan abd A. A. Beex, “FM interference suppression in spread spectrum communications using time-varying autoregressive model based instantaneous frequency estimation," in *Proc. IEEE Int. Conf. Acoust., Speech, Signal Process.*, Phoenix, AZ, pp.2559–2562, March 1999.

[24] R. S. Ramineni, M. G. Amin, and A. R. Lindsey, “Performance analysis of subspace projection techniques for interference excision in DSSS communications," in *Proc. IEEE Int. Conf.Acoust., Speech, Signal Process.*, Istanbul, Turkey, June 2000.

[25] W. Mu, Y. Zhang, and M. G. Amin, “Bilinear signal synthesis in array processing,” in *Proc. IEEE Int. Conf. Acoust., Speech, Signal Process.*, Salt Lake City, UT, May 2001.

[26] R. O. Schmidt, “Multiple emitter location and signal parameter estimation," *IEEE Trans. Antennas Propagat.*, vol. 34, no. 3, pp. 276–280, March 1986.

[27] I. Ziskind and M. Wax, “Maximum likelihood localization of multiple sources by alternating projection," *IEEE Trans. Acoust., Speech, Signal Processing*, vol. ASSP-36, no. 10, pp. 1553–1560, Oct. 1988.

[28] A. Belouchrani and M. Amin, “Time-frequency MUSIC," *IEEE Signal Processing Lett.*, vol. 6, no. 5, pp. 109–110, May 1999.

[29] Y. Zhang, W. Mu, and M. G. Amin, “Time-frequency maximum likelihood methods for direction finding," *J. Franklin Inst.*, vol. 337, no. 4, pp. 483–497, July 2000.

[30] —, “Subspace analysis of spatial time-frequency distribution matrices," *IEEE Trans. Signal Processing*, vol. 49, pp.747–C759, Apr. 2001.

[31] J. F. Cardoso, A. Belouchrani, K. Abed Maraim, and E. Moulines, “A blind source separation technique using second order statistics," *IEEE Trans. Signal Processing*, vol. 45, no. 2, pp. 434–444, Feb. 1997.

[32] A. Belouchrani and M. Amin, Blind source separation based on time-frequency signal representation," *IEEE Trans. Signal Processing*, vol. 46, no. 11, pp. 2888–2898, Nov. 1998.

[33] Y. Zhang and M. G. Amin, “Blind separation of sources based on their time-frequency signatures," in *Proc. IEEE Int. Conf.Acous. Speech, Signal Process.*, Istanbul, Turkey, pp.3132–3135, June 2000.

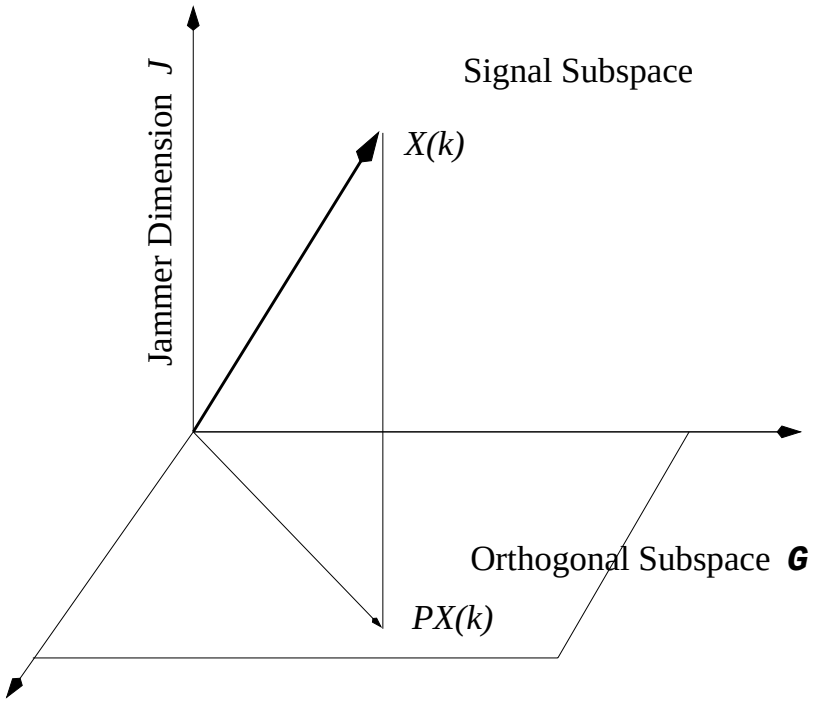

Figure 1. Jammer suppression by subspace projection.

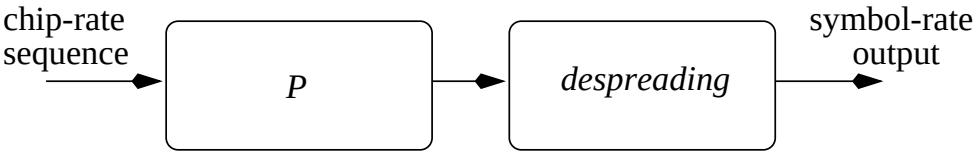

Figure 2. Block diagram of single-sensor subspace projection.

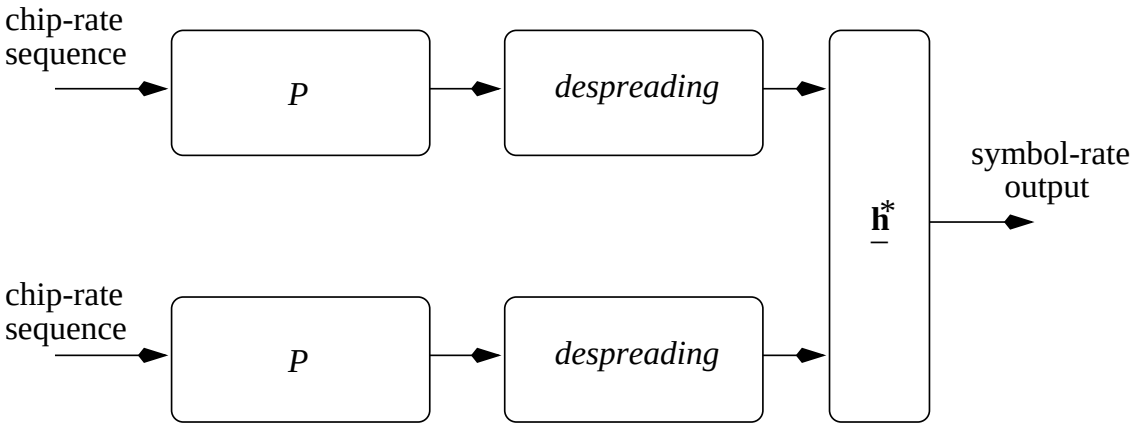

Figure 3. Block diagram of independent multi-sensor subspace projection.

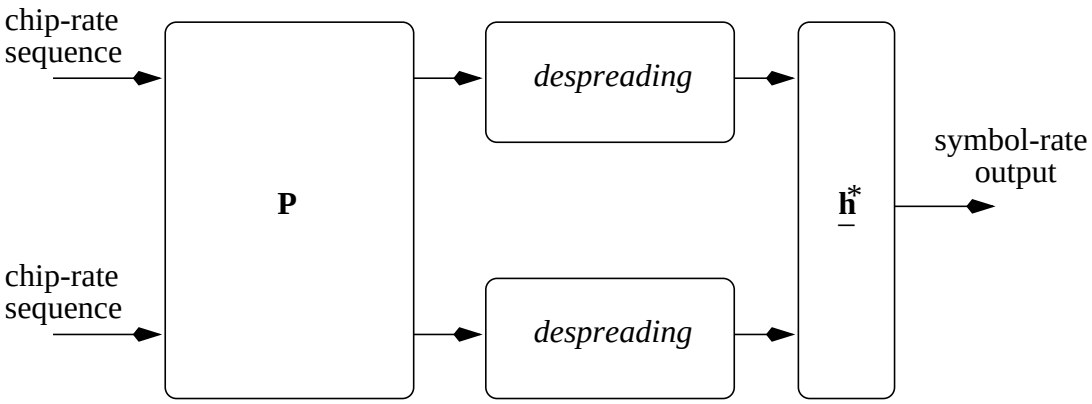

Figure 4. Block diagram of proposed multi-sensor subspace projection.

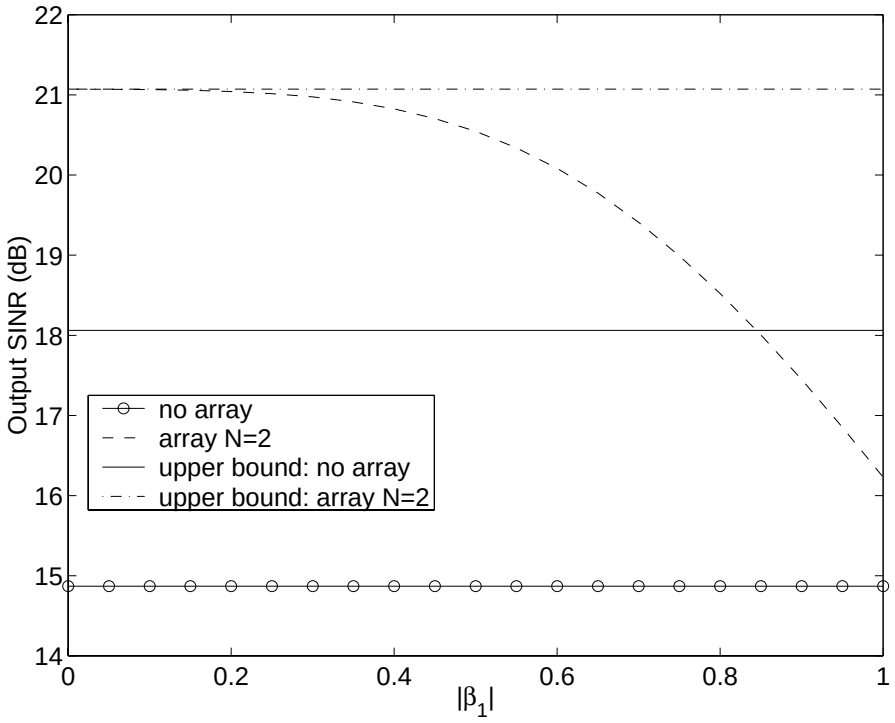

Figure 5. Output SINR versus $|\beta_1|$ (input SNR=0dB, *L*=64, *U*=1, *M*=7).

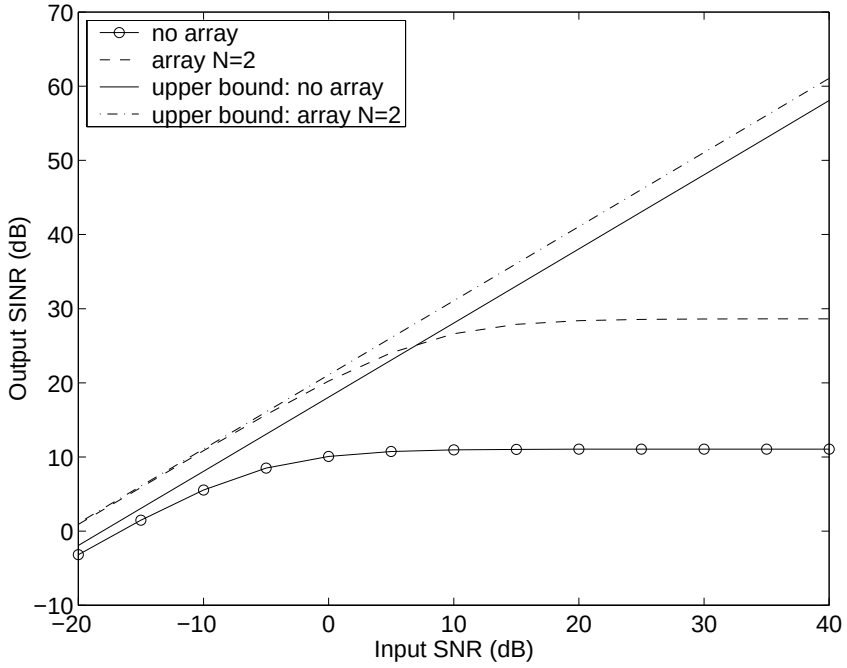

Figure 6. Output SINR versus input SNR (L=64, U=2, M1=M2=7, qD=0^o, qJ=[40^o,60^o]).

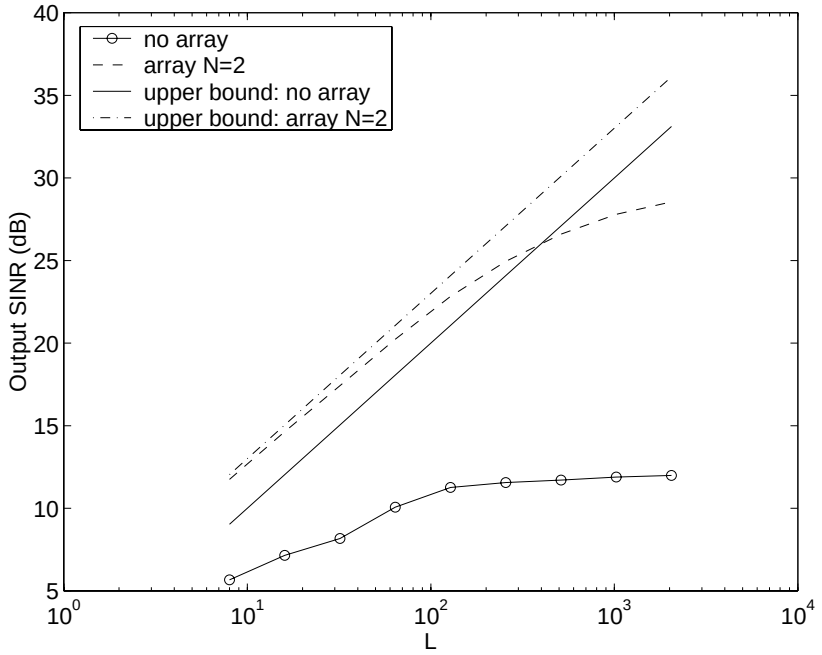

Figure 7. Output SINR versus the number of chips per symbol (*L*) (input SNR=0dB, *U*=2, M_1=M_2=7, θ_D=0^o, θ_J=[40^o,60^o]).

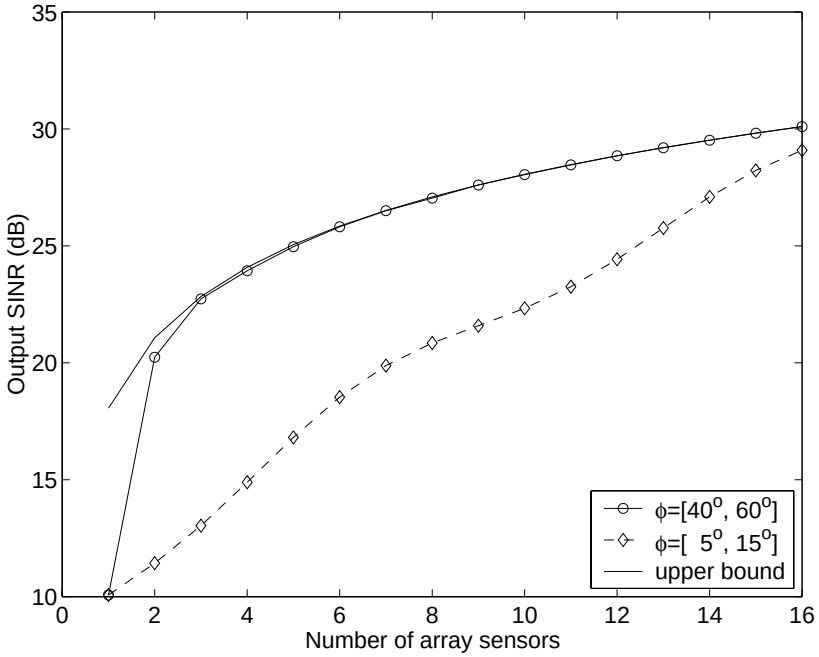

Figure 8. Output SINR versus the number of array sensors (input SNR=0dB, *L*=64, *U*=2, M_1=M_2=7).

Chapter 4
Performance Analysis of GPS Receivers in Impulsive Noise

1. Introduction

Impulsive noise is encountered in many environments. It has been shown that this type of noise has a significant effect on satellite-mobile radio systems [1]. One major source of impulsive noise is the automotive ignition systems. The frequency range of automotive ignition noise is 100 MHz ~ 10 GHz [2], which extends over the GPS carrier frequency of 1.58 GHz and its 1 MHz bandwidth. The impulsive noise from the ignition systems shows a random nature of the amplitudes, inter-arrival times, and durations of noise bursts. This noise might be a hidden menace to GPS receivers since the ignition wire and the body of the automobile act as a radiation antenna. Another source of impulsive signals is ultrawideband (UWB) signals that cover the GPS operating band and find increasing number of applications in outdoor and indoor environments.

This chapter considers the effect of impulsive noise on the GPS receiver performance, specifically, its delay lock loop (DLL). We use Middleton noise [3] and generalized Cauchy noise [4], which are two of the canonical models that are widely used to describe the statistics of the impulsive noise. We also examine the impact on the GPS receiver by automotive ignition noise and UWB noise models based on experiment data provided in [5], [6]. The central limit theorem (CLT) is applied to characterize the noise components resulting from the correlation with the early, late, and punctual C/A reference code. It is shown that the correlator noise is also Gaussian. The variance of the discriminator is derived and shown to be highly dependent on the signal-to-noise ratio (SNR), sample rate, and precorrelation bandwidth. Computer simulations are performed and compared with theoretical results.

2. The Impulsive Noise Models

2.1. Middleton noise model

Middleton impulsive noise model [3] is composed of both Gaussian and impulsive noise components. The probability density function (PDF) is defined by two parameters *A* and Γ. The term *A* represents the product of the average duration of the pulse and the average number of pulses occurring in unit time. Small values of *A* increases the impulsiveness of the noise, whereas large values of *A* move the model closer to a Gaussian distribution. The parameter, $\Gamma = \sigma_G^2 / \sigma_I^2$, is defined as the Gaussian-to-impulsive power ratio, where σ_G^2 represents the Gaussian noise power and σ_I^2 is the impulsive noise power. The total noise power is

$$\sigma^2 = \sigma_G^2 + \sigma_I^2 \tag{4.1}$$

The PDF is given by

$$p(z) = \sum_{m=0}^{\infty} \frac{e^{-A} A^m}{m!} \cdot \frac{1}{\sqrt{2\pi\sigma_m^2}} \exp\left(-\frac{|z|^2}{2\sigma_m^2}\right) \tag{4.2}$$

where

$$\sigma_m^2 = \frac{(m/A) + \Gamma}{1 + \Gamma} \tag{4.3}$$

If *A* is sufficiently small, then we can simplify the model by only keeping the dominant terms in (4.2) corresponding to m = 0, 1, 2 [7]. In this case, the noise PDF function, shown in Figure 1(a), can be approximated by

$$p_Z(z) = \sum_{m=0}^{2} \frac{e^{-A} A^m}{m!} \cdot \frac{1}{\sqrt{2\pi\sigma_m^2}} \exp\left(-\frac{|z|^2}{2\sigma_m^2}\right) \tag{4.4}$$

A sample of Middleton noise sequence is shown in Figure 1(b).

2.2. Generalized Cauchy noise model

A generalized Cauchy probability density function is defined in terms of three parameters, σ^2, $k > 0$ and $\upsilon > 0$ [4],

$$p(z) = \frac{B}{\{1+\frac{1}{\upsilon}[\frac{|z|}{A}]^k\}^{\upsilon+1/k}} \quad , \quad A = [\sigma^2 \frac{\Gamma(1/k)}{\Gamma(3/k)}]^{1/2}, \quad B = \frac{k\upsilon^{-1/k}\Gamma(\upsilon+1/k)}{2A\Gamma(\upsilon)\Gamma(1/k)} \tag{4.5}$$

In the above equation, $\Gamma(\cdot)$ is the Gamma function, given by

$$\Gamma(a) = \int_0^\infty x^{a-1}e^{-x}dx \tag{4.6}$$

The parameter *k* controls the impulsiveness of the noise, whereas υ controls the noise variance and σ^2 is a scale parameter. In the example shown in Figure 2, we set $k = 0.2$, $\upsilon = 40$, and $\sigma^2 = 4.7$.

2.3 Ignition noise model

The motor ignition noise based on the experiment data [5] is a statistical process consisting of two distributions: a Weibull distribution, due to the high power peaks, and a Gaussian distribution, due to other low power values. These distributions are thown in Figures 3(a) and 3(b), respectively. The Weibull distribution PDF is given by

$$p(z) = ab^{-a}z^{a-1}e^{-(z/b)^2} \tag{4.7}$$

where $a = 1.14$ and $b = 4.00$. The inter-arrival times between successive noise peaks are shown to be exponentially distributed, as depicted in Figure 3(c). The sample noise sequence is provided in Figure 3(d).

2.4. UWB noise model

The UWB type of noise generated using multiple UWB signal sources is reported in [6] based on several data measurements. It was concluded that the amplitude of the aggregate UWB signals approximates a Rayleigh distribution, which is shown in Figure 4(a). Figure 4(b) gives the sample sequence of the noise with unit variance.

3. DLL Performance Under Impulsive Noise

The major operations for code synchronization in the DLL are the cross-correlations performed of the incoming data and the receiver reference code. Figure 5 shows three pairs of correlators required to produce three in-phase components, I_E , I_P , I_L and three quadraphase components Q_E , Q_P , Q_L , respectively corresponding to the early (E), punctual (P) and late (L) reference C/A codes. With the above six components, the receiver could construct at least three different DLL discriminators [8], namely

Coherent

$$D = (I_E - I_L)\text{sign}(I_P) \tag{4.8}$$

Early-minus-late power (noncoherent)

$$D = (I_E^2 + Q_E^2) - (I_L^2 + Q_L^2) \tag{4.9}$$

Dot-product (noncoherent)

$$D = (I_E - I_L)I_P + (Q_E - Q_L)Q_P \tag{4.10}$$

where $\text{sign}(I_P)$ is the sign of the navigation message data bit. Ideal synchronization is reached by finding the location of the correlation peak. Commonly, the discriminator determines the peak correlation location by reaching zero output value. The output of correlator *j*, corresponding to the Figure 5: GPS DLL cross-correlation process early, punctual or late stage, when the summation is performed over T (usually 0.001) seconds, can be written as [9]:

$$I_j = i_j + \eta_{Ij} = \sqrt{2S}MR(\tau_j)\cos\varphi + \eta_{Ij}, \quad Q_j = q_j + \eta_{Qj} = \sqrt{2S}MR(\tau_j)\sin\varphi + \eta_{Qj} \tag{4.11}$$

where S is the signal power, M is the number of samples used in cross-correlation computations (usually it is an integer multiple of 1023), φ is the residual phase tracking error at the time, $R(\tau_j)$ is the cross-correlation function between the incoming C/A code and the reference code corresponding to stage j for a delay τ_j, and η_{Ij} and η_{Qj} are the in-phase and quadraphase noise components of the correlator outputs. Clearly, if $g_{j,i}$ represents the reference code samples, and $n_{Ij,i}$ and $n_{Qj,i}$ represent the input noise samples, then the noise components can be expressed as

$$\eta_{Ij} = \sum_{i=1}^{M} g_{j,i} n_{Ij,i} \quad , \qquad \eta_{Qj} = \sum_{i=1}^{M} g_{j,i} n_{Qj,i} \tag{4.12}$$

3.1. Sample rate

The C/A code consists of 1023 chips. In order to generate the proper early and late correlation functions for the discriminator, the sample rate, i.e. the number of samples per chip, becomes dependent on the early and late correlator spacing d. For d = m/n chips, where m and n are integers, forming an irreducible fraction, then the number of samples per chip should be no less than 2n, if m is not a multiple of 2, or no less than n, if m is a multiple of 2. In Figure 6, we choose the coherent discriminator and set the early-late correlator spacing to 1 chip. Accordingly, the number of samples per chip should be 2. Without multipath and noise, the discriminator output, which is the difference between the early and late correlators, assumes zero value at synchronization.

3.2. Precorrelation filtering

The precorrelation filter in GPS receiver is used to suppress out-of-band noise and interference. However, filtering may cause correlation changes and removes the sidelobes of C/A code spectrum. Figure 7 shows the GPS frequency spectrum transformation due to the application of Butterworth filter.

The effect of the filter on the C/A code autocorrelation function is broadening its peak [10], as shown in Figure 8. Therefore, the early-late correlator spacing has to be selected sufficiently large to keep the discriminator properly functioning over a linear range. As evident from Figure 8, the correlation function is not absolutely symmetric, which leads to slight deflection of zero-delay error point. The ideal band limited filtered noise has a sinc autocorrelation function, rather than a delta function. In baseband,

$$R_{fn}(\tau) = \frac{\sin(\pi B_f \tau)}{\pi B_f \tau} \tag{4.13}$$

where B_f is the precorrelation filter bandwidth of 2 MHz. Noise samples spaced by 0.5 microseconds are uncorrelated. Oversampling will generate correlated noise samples which will adversely affect the discriminator performance. Correlated and uncorrelated noise samples distort the early and late

correlation functions, causing the discriminator output to assume non-zero values at the correct signal propagation delay. Figure 9 shows the distorted correlation and discriminator function in -10 dB impulsive noise.

To evaluate the discriminator error, we use the dot-product discriminator as an example. From (4.10) and (4.11), the discriminator output is:

$$D = (I_E - I_L)I_P + (Q_E - Q_L)Q_P = (i_E - i_L + \eta_{IE} - \eta_{IL})(i_P + \eta_{IP}) + (q_E - q_L + \eta_{QE} - \eta_{QL})(q_P + \eta_{QP}) \tag{4.14}$$

Thus, the discriminator variance is

$$\mathrm{Var}(D) = E[\, i_P{}^2(\eta_{IE} - \eta_{IL})^2 + \eta_{IP}{}^2(\eta_{IE} - \eta_{IL})^2 + q_P{}^2(\eta_{QE} - \eta_{QL})^2 + \eta_{QP}{}^2(\eta_{QE} - \eta_{QL})^2\,] \tag{4.15}$$

where

$$\begin{aligned} &E[(\eta_{IE} - \eta_{IL})^2] = E[(\eta_{QE} - \eta_{QL})^2] = 2(E[\eta_{IE}{}^2] - E[\eta_{IE}\eta_{IL}]) \\ &2P_n[dM + \sum_{i=1}^{k-kd-1}(M-i)(1+d-i/k)\frac{\sin(i\pi B_f/B_s)}{i\pi B_f/B_s} + 2\sum_{k-kd}^{k-1}(M-i)(1-i/k)\frac{\sin(i\pi B_f/B_s)}{i\pi B_f/B_s} \\ &- \sum_{i=1}^{k+kd-1}(M-i)(1-|kd-i|/k)\frac{\sin(i\pi B_f/B_s)}{i\pi B_f/B_s}] \end{aligned} \tag{4.16}$$

$$\begin{aligned} &E[\eta_{IP}{}^2(\eta_{IE} - \eta_{IL})^2] = E[\eta_{QP}{}^2(\eta_{QE} - \eta_{QL})^2] \\ &= 2P_n{}^2[M + 2\sum_{i=1}^{k-1}(M-i)(1-i/k)\frac{\sin(i\pi B_f/B_s)}{i\pi B_f/B_s}][dM + \sum_{i=1}^{k-kd-1}(M-i)(1+d-i/k)\frac{\sin(i\pi B_f/B_s)}{i\pi B_f/B_s} \\ &+ 2\sum_{k-kd}^{k-1}(M-i)(1-i/k)\frac{\sin(i\pi B_f/B_s)}{i\pi B_f/B_s} - \sum_{i=1}^{k+kd-1}(M-i)(1-|kd-i|/k)\frac{\sin(i\pi B_f/B_s)}{i\pi B_f/B_s}] \end{aligned} \tag{4.17}$$

The derivation of the above equations is lengthy and given in Appendix A.

4. Simulations

In this section, we present the results obtained from 20,000 Monte Carlo trials, generated based on the noise models described before. The purpose is to evaluate the effects of the precorrelation bandwidth and sample rate on the early-late discriminator error variance. We compare the analytical results with the simulations results. The first set of simulation provides the details of how the discriminator error variance

changes according to the precorrelation bandwidth. The second set of simulations shows the discriminator statistics in terms of the sample rate.

In the first set of simulations, we compute the values of discriminator error variance over different precorrelation bandwidths of 2, 4, 6, 8, and 10 MHz. The sample rate is fixed to 30 samples per chip, and the early-late correlator spacing is set to 0.4 chips. Both UWB noise and Middleton's impulsive noise are considered. The signal-to-noise ratio (SNR) is set to -30 dB. Figure 10 shows that the discriminator error variance decreases as the precorrelation bandwidth increases. It is evident that the analytical and the simulation results are similar. The result demonstrates that a narrow precorrelation bandwidth compromises the discriminator performance. For a clear view, we divide the discriminator error variance based on (4.15) into four components, (a) $E[i_P^2(\eta_{IE}-\eta_{IL})^2]$, (b) $E[q_P^2(\eta_{QE}-\eta_{QL})^2]$, (c) $E[\eta_{IP}^2(\eta_{IE}-\eta_{IL})^2]$, and (d) $E[\eta_{QP}^2(\eta_{QE}-\eta_{QL})^2]$. Figure 11 shows the simulation and the analytical behaviors of those components, which are clearly similar.

The second set of simulations also applies UWB noise and Middleton's noise. Figure 12 shows the different values of discriminator error variance with different sample rates of 5, 10, 15, 20, and 30 samples per chip, under SNR of -30 dB. The precorrelation bandwidth is fixed as 2 MHz and the early-late correlator spacing is set to 0.4 chips. We find that the discriminator error variance increases as the sample rate increases. This simulation results agree with the corresponding analytical results. Figure 13 depicts the close simulation and analytical values of the four components, which sum up to the discriminator error variance of Figure 12.

By examining the contributions of the four components (a), (b), (c) and (d) to the discriminator error, we find that both (a) and (b) have the signal power terms i_P^2 and q_P^2, whereas (c) and (d) only include the noise power terms. This means that (a) and (b) dominate the discriminator error variance at high SNRs, whereas (c) and (d) play a more important role at low SNRs. Figure 14 shows the values of the aforementioned components at different SNR of -90, -70, -50, -30 and -10 dB, with the sample rate of 10 samples per chip and an early-late correlator spacing of 0.4 chips.

5. Conclusions

Several impulsive noise models were adopted to evaluate their effect on the delay lock loop of the GPS receiver. We defined the required sample rate for the early-late discriminator and performed statistical analyses of discriminator error variance induced by the impulsive noise, the precorrelation bandwidth, and the sample rate. The required sample rate is dependent on the early-late correlator spacing. A narrower spacing requires more samples per chip. The use of the precorrelation filter may change the correlation between noise samples, which subsequently affects the discriminator error. Narrower precorrelation bandwidth and higher sample rate lead to increased discriminator errors. With reasonable and careful selections of the sample rate and the precorrelation bandwidth, the GPS synchronization error can be limited.

Appendix A

We begin with the variance expression (4.15)

$$E[\,(\eta_{IE}-\eta_{IL})^2\,] = E[\,\eta_{IE}{}^2\,] + E[\,\eta_{IL}{}^2\,] - 2E[\,\eta_{IE}\eta_{IL}\,] \tag{A.1}$$

We note that,

$$E[\,\eta_{IE}{}^2\,] = E[\,(\sum_{i=1}^{M} n(i)g(i))^2\,]$$

$$=E[\,\sum_{i=1}^{M}(n(i)g(i))^2 + \; 2n(1)g(1)\sum_{i=2}^{M} n(i)g(i) + 2n(2)g(2)\sum_{i=3}^{M} n(i)g(i) + \cdots + 2n(M-1)g(M-1)n(M)g(M)\,] \tag{A.2}$$

where n(i) represents the noise sample, $g(i)$ is the C/A code sample, and M is the total number of samples. For simplification, we use

$$R_f(i) = 1 - i/k \quad \text{for } i = 1, 2, \ldots, k-1; \qquad R_f(i) = 0 \quad \text{for } i = k, k+1, \ldots, M \tag{A.3}$$

where k is the number of samples per chip, to approximate the correlation function between the filtered and the reference C/A code, and

$$R_{fn}(i) = P_n \frac{\sin(i\pi B_f / B_s)}{i\pi B_f / B_s} \tag{A.4}$$

for the noise correlation function, in which P_n is the noise variance. Thus, (A2) becomes

$$E[\,\eta_{IE}{}^2\,] = P_n\,[M + 2\sum_{i=1}^{k-1}(M-i)(1-i/k)\frac{\sin(i\pi B_f / B_s)}{i\pi B_f / B_s}] \tag{A.5}$$

where the total number of samples M = 1023k. Similarly,

$$E[\,\eta_{IL}{}^2\,] = E[\,\eta_{IE}{}^2\,] = E[\,\eta_{IP}{}^2\,] \tag{A.6}$$

Moreover,

$$E[\,\eta_{IE}\eta_{IL}\,] = E[\,(\sum_{i=1}^{M} n(i)g(i))\;(\sum_{i=1}^{M} n(i)g(i+kd))\,]$$

$$= E[\,\sum_{i=1}^{M} n(i)g(i)n(i)g(i+kd)\,]$$

$$+ E[\,n(1)g(1)\sum_{i=2}^{M} n(i)g(i+kd) + n(2)g(2)\sum_{i=3}^{M} n(i)g(i+kd) \; + \cdots + n(M-1)g(M-1)n(M)g(M+kd)\,]$$

$$+ E[\, n(2)g(2)n(1)g(1+kd) + n(3)g(3)\sum_{i=1}^{2} n(i)g(i+kd) + \cdots + n(M)g(M)\sum_{i=1}^{M-1} n(i)g(i+kd)\,]$$

$$= P_n \{(1-d)M + \sum_{i=1}^{k-kd-1} (M-i)(1-d-i/k)\frac{\sin(i\pi B_f/B_s)}{i\pi B_f/B_s} + \sum_{i=1}^{k+kd-1} (M-i)(1-|kd-i|/k)\frac{\sin(i\pi B_f/B_s)}{i\pi B_f/B_s}\} \quad (A.7)$$

From (A.5), (A.6) and (A.7), (A.1) becomes

$$\begin{aligned} &E[(\eta_{IE}-\eta_{IL})^2] = E[(\eta_{QE}-\eta_{QL})^2] = 2(E[\eta_{IE}^2] - E[\eta_{IE}\eta_{IL}]) \\ &2P_n[dM + \sum_{i=1}^{k-kd-1}(M-i)(1+d-i/k)\frac{\sin(i\pi B_f/B_s)}{i\pi B_f/B_s} + 2\sum_{k-kd}^{k-1}(M-i)(1-i/k)\frac{\sin(i\pi B_f/B_s)}{i\pi B_f/B_s} \\ &- \sum_{i=1}^{k+kd-1}(M-i)(1-|kd-i|/k)\frac{\sin(i\pi B_f/B_s)}{i\pi B_f/B_s}] \end{aligned} \quad (A.8)$$

Based on Central Limit Theorem (CLT), it's obvious that all the noise components η_{Ij} and η_{Qj} are zero mean Gaussian random variables. It is known that, for zero mean Gaussian variables $\eta_1, \eta_2, \eta_3, \eta_4$,

$$E[\eta_1\eta_2\eta_3\eta_4] = E[\eta_1\eta_2]E[\eta_3\eta_4] + E[\eta_1\eta_3]E[\eta_2\eta_4] + E[\eta_1\eta_4]E[\eta_2\eta_3] \quad (A.9)$$

Therefore, we have

$$\begin{aligned} &E[\eta_{IP}^2(\eta_{IE}-\eta_{IL})^2] = E[\eta_{QP}^2(\eta_{QE}-\eta_{QL})^2] \\ &= 2(E[\eta_{IP}^2\eta_{IE}^2] - E[\eta_{IP}^2\eta_{IE}\eta_{IL}]) \\ &= 2(E[\eta_{IP}^2]E[\eta_{IE}^2] + 2E^2[\eta_{IP}\eta_{IE}] - E[\eta_{IP}^2]E[\eta_{IE}\eta_{IL}] - 2E[\eta_{IP}\eta_{IE}]E[\eta_{IP}\eta_{IL}]) \\ &= 2(E[\eta_{IP}^2]E[\eta_{IE}^2] - E[\eta_{IP}^2]E[\eta_{IE}\eta_{IL}]) \\ &= 2E[\eta_{IP}^2](E[\eta_{IE}^2] - E[\eta_{IE}\eta_{IL}]) \\ &= 2P_n^2[M + 2\sum_{i=1}^{k-1}(M-i)(1-i/k)\frac{\sin(i\pi B_f/B_s)}{i\pi B_f/B_s}][dM + \sum_{i=1}^{k-kd-1}(M-i)(1+d-i/k)\frac{\sin(i\pi B_f/B_s)}{i\pi B_f/B_s} \\ &+ 2\sum_{k-kd}^{k-1}(M-i)(1-i/k)\frac{\sin(i\pi B_f/B_s)}{i\pi B_f/B_s} - \sum_{i=1}^{k+kd-1}(M-i)(1-|kd-i|/k)\frac{\sin(i\pi B_f/B_s)}{i\pi B_f/B_s}] \end{aligned} \quad (A.10)$$

References

[1] M. Button and J. Gardiner, "Measurement of the impulsive noise environment for satellite-mobile radio systems at 1.5 GHz", IEEE Transactions on Vehicular Technology, vol. 51, No. 3, May 2002.

[2] D. Apostolakis and P. Constantinou, "Man made noise measurements and modeling", *'Personal Communications: Gateway to the 21st Century' Conference Record, 2nd International Conference,* vol. 2, pp. 585, Oct. 1993.

[3] S. M. Zabin and H. V. Poor, "Parameter estimation for Middleton Class A interference processes", *IEEE Transactions on Communications,* vol. 37, No. 10, Oct 1989.

[4] S. A. Kassam, *Signal Detection in Non-Gaussian Noise*, pp. 74-90, Dowden & Culver, Inc., New York, 1988.

[5] D. Apostolakis and P. Constantinou, "Man made noise measurements and modeling", *'Personal Communications: Gateway to the 21st Century' Conference Record, 2nd International Conference,* vol. 2, pp. 586-588, Oct. 1993.

[6] J. Hoffman and M. Cotton, "Measurements to determine potential interference to GPS ultrawideband transmission systems", *NTIA Report 01-384*, February 2001.

[7] K. Mizutani, D. Umehara, M. Kawai, and Y. Morihiro, "Noncoherent FSK optimum receiver over impulsive noise channels", *Proceedings of the 7th International Symposium on Power-Line Communications and Its Applications, Kyoto, Japan*, pp. 91, March 26-28, 2003.

[8] A. J. Van Dierendonck, P. Fenton, and T. Ford, "Theory and performance of narrow correlator spacing in a GPS receiver", Navigation: Journal of the Institute of Navigation, vol. 39, No. 3, pp. 281, Fall 1992.

[9] B. Parkinson and J. Spilker Jr., *Global Positioning System: Theory and Applications Volume I*, pp. 363-364, American Institute of Aeronautics and Astronautics, Inc., Washington, 1996.

[10] A. J. Van Dierendonck, "Novatel GPS receiver – the high performance OEM sensor of the future", *Institute of Navigation Satellite Division's 4th International Technical Meeting IONGPS-91, Albuquerque, NM*, Sept. 9-13, 1991

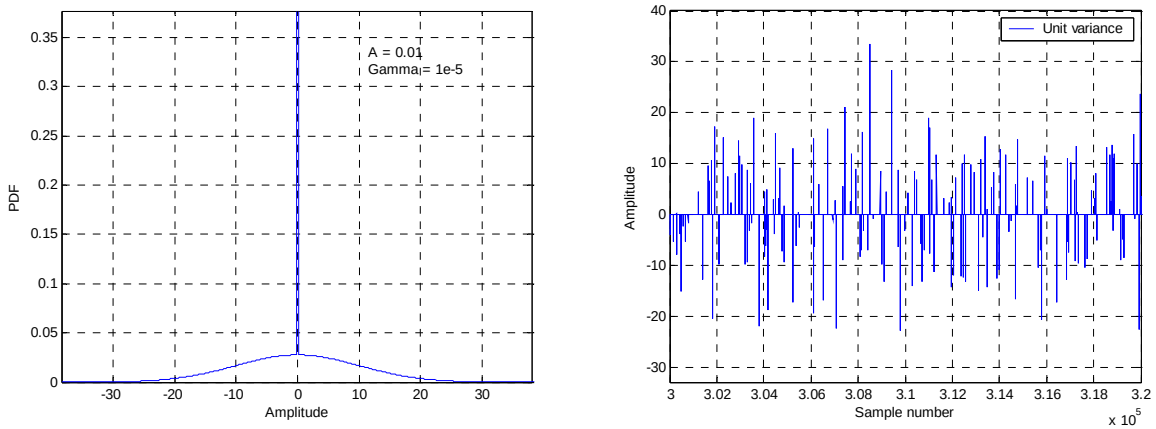

(a) (b)

Figure 1. (a) PDF of the simplified Middleton noise model, (b) Middleton noise sequence with unit variance

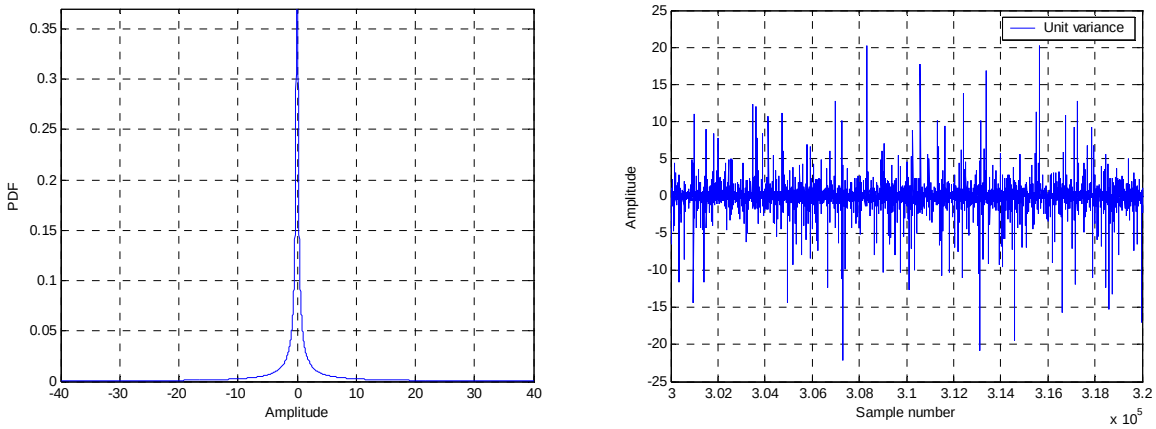

(a) (b)

Figure 2. (a) PDF of generalized Cauchy noise model, (b) Generalized Cauchy noise sequence with unit variance.

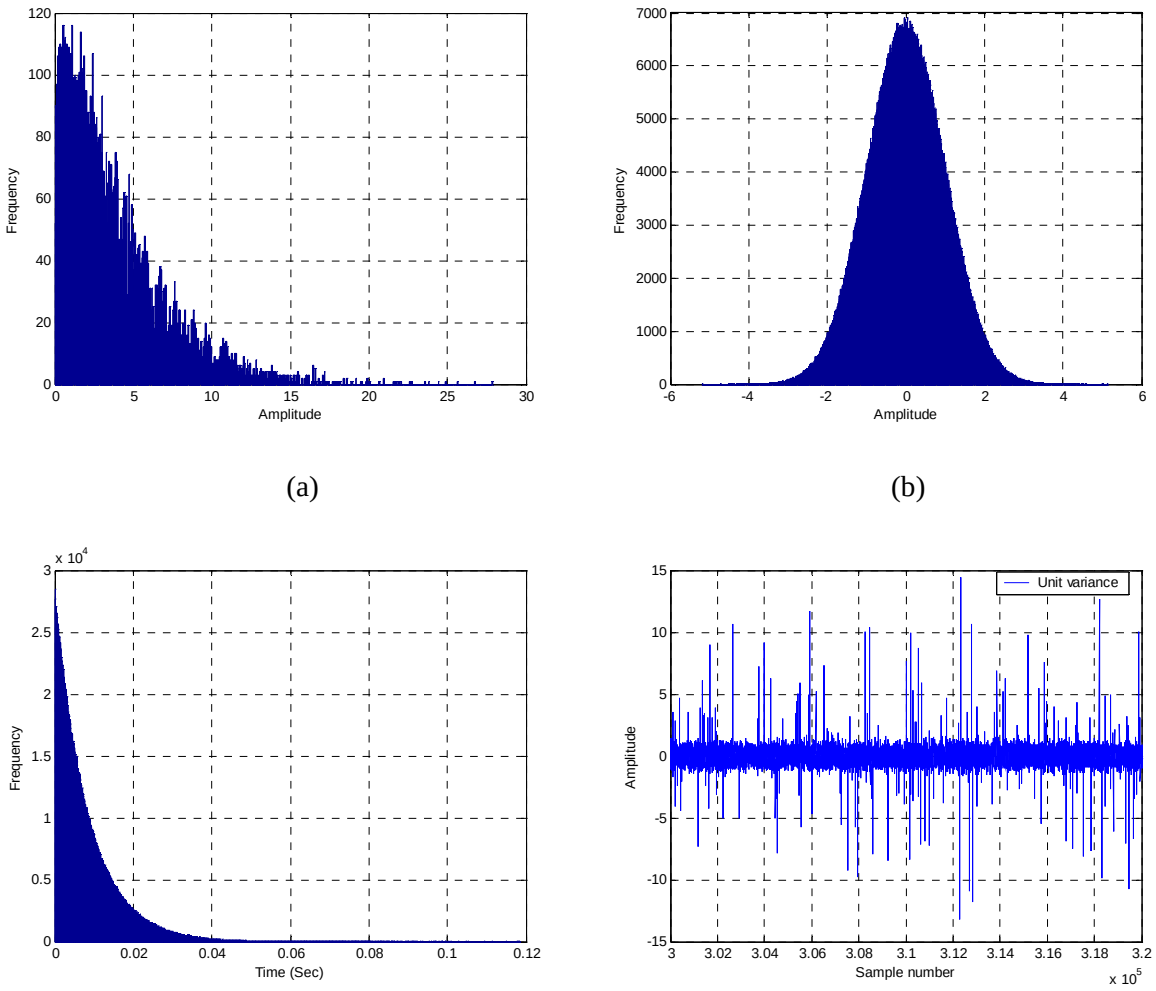

Figure 3. (a) PDF of the power peaks, (b) PDF of the low power values, (c) PDF of the inter-arrival times between successive peaks, (d) Sample sequence of ignition noise with unit variance

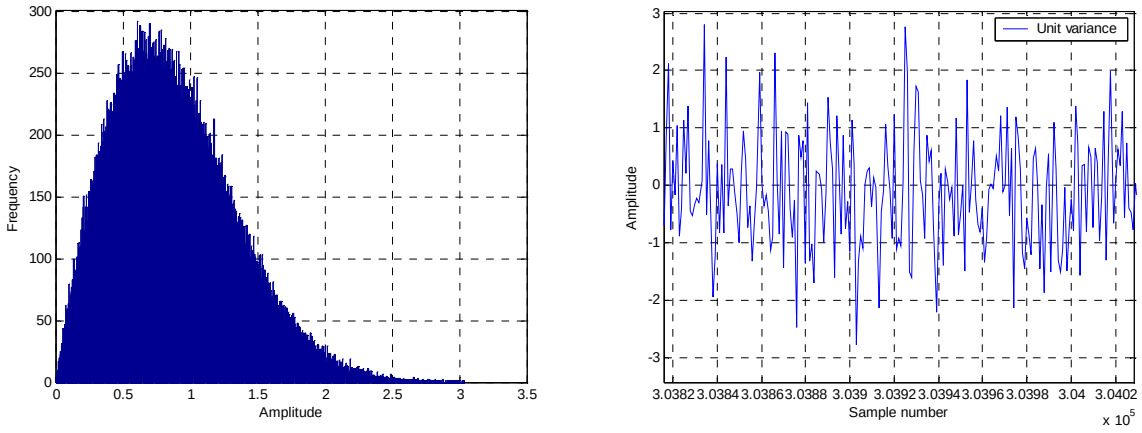

(a) (b)

Figure 4 (a). PDF of the amplitude of aggregate UWB signals, (b) Sample sequence of UWB noise with unit variance.

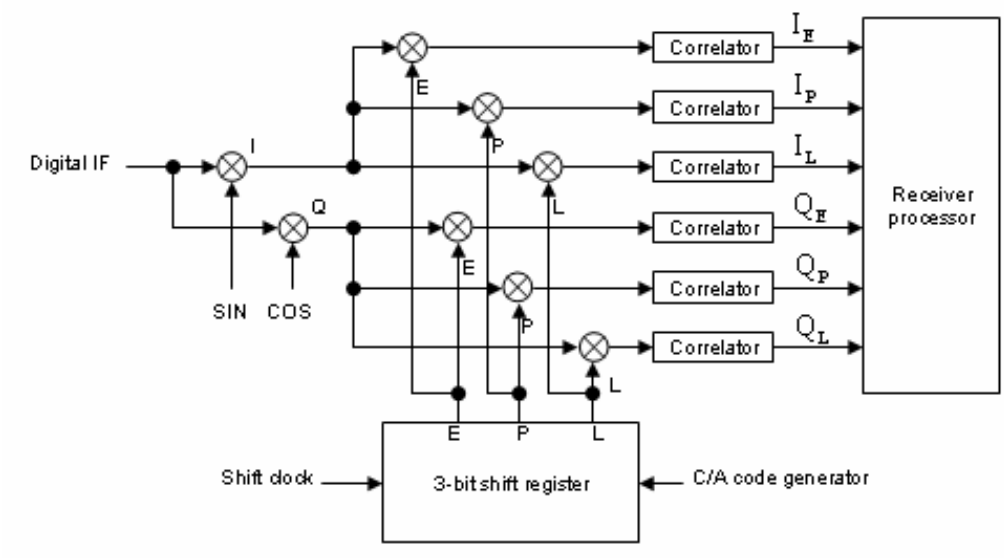

Figure 5. GPS DLL cross-correlation process

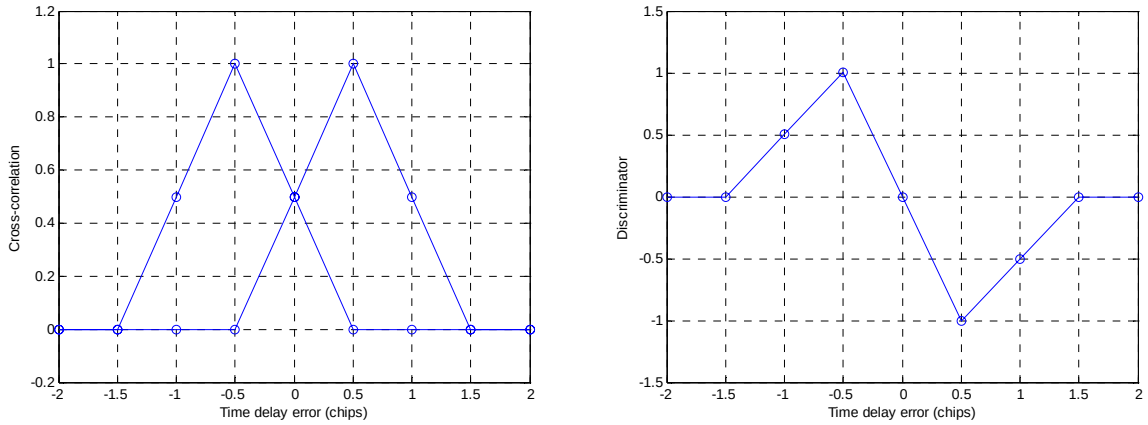

(a) (b)

Figure 6. (a) Early and late correlation functions, (b) Discriminator function with 1 chip spacing and 2 samples per chip

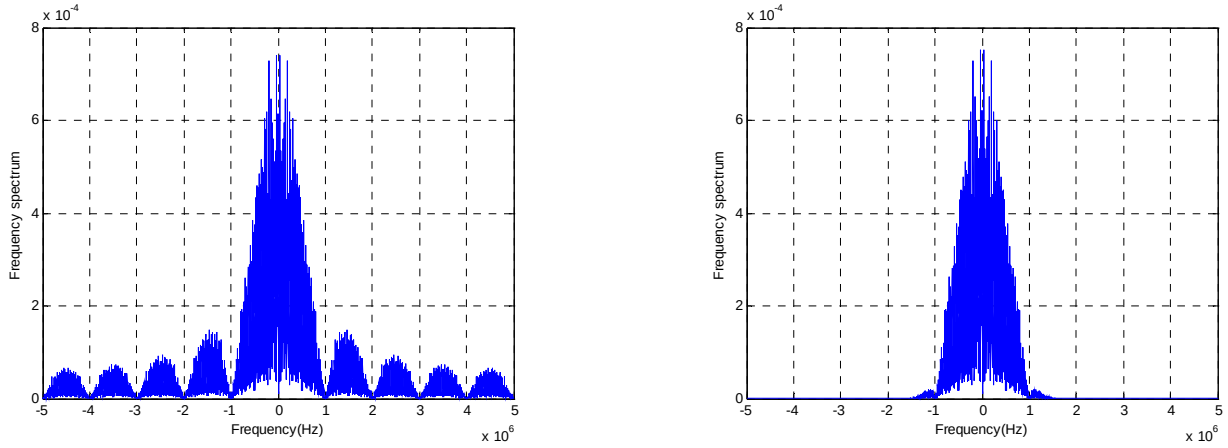

(a) (b)

Figure 7. The frequency spectrum of C/A code with 2 MHz bandwidth Butterworth precorrelation filtering (a) before filtered, (b) after filtered

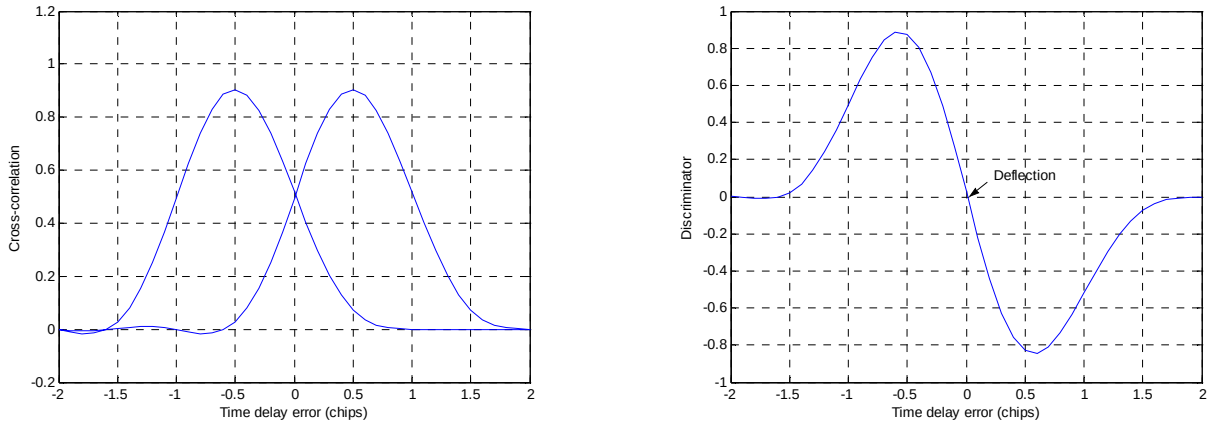

(a) (b)

Figure 8. (a) Early and late correlation functions, (b) Discriminator function with 1 chip spacing and 2 MHz precorrelation filtering

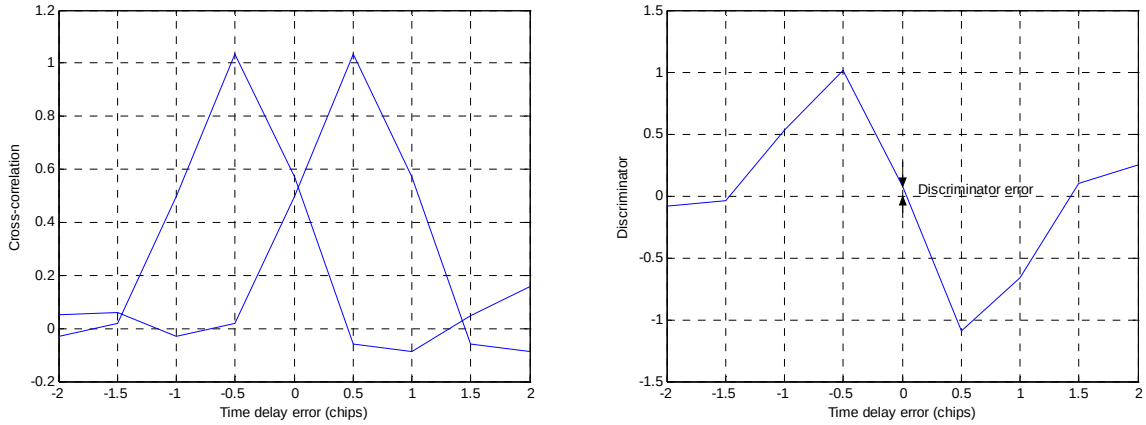

(a) (b)

Figure 9. (a) Early and late correlation functions, (b) Discriminator function with 1 chip spacing and 2 samples per chip under -10 dB impulsive noise

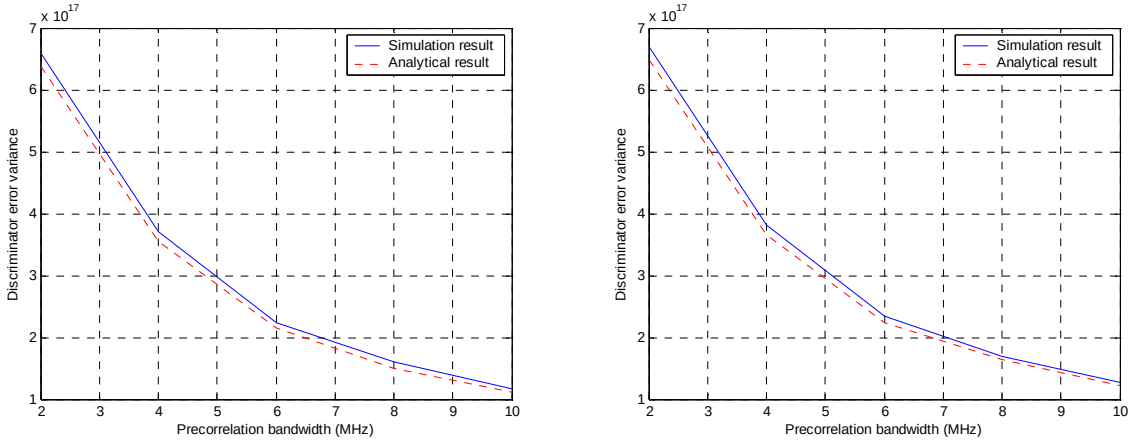

Figure 10. The discriminator error variance through different bandwidth precorrelation filter (a) under UWB noise, (b) under Middleton's impulsive noise

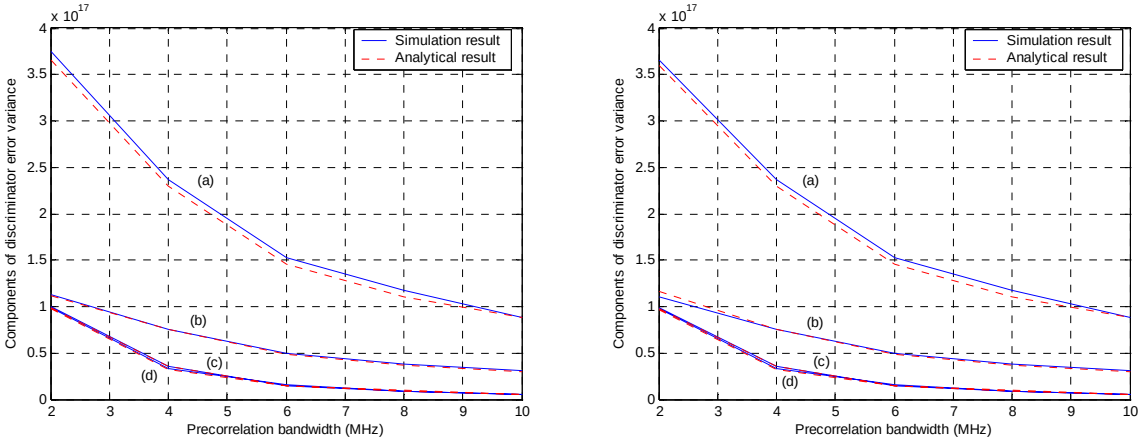

Figure 11. The components of discriminator error variance through different bandwidth precorrelation filter (a) under UWB noise, (b) under Middleton's impulsive noise

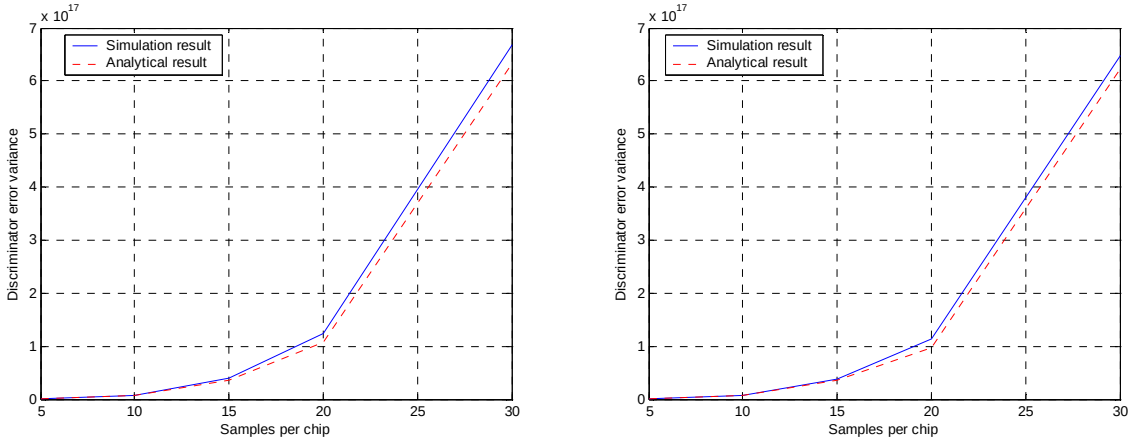

Figure 12. The discriminator error variance with different sample rate (a) under UWB noise, (b) under Middleton's impulsive noise

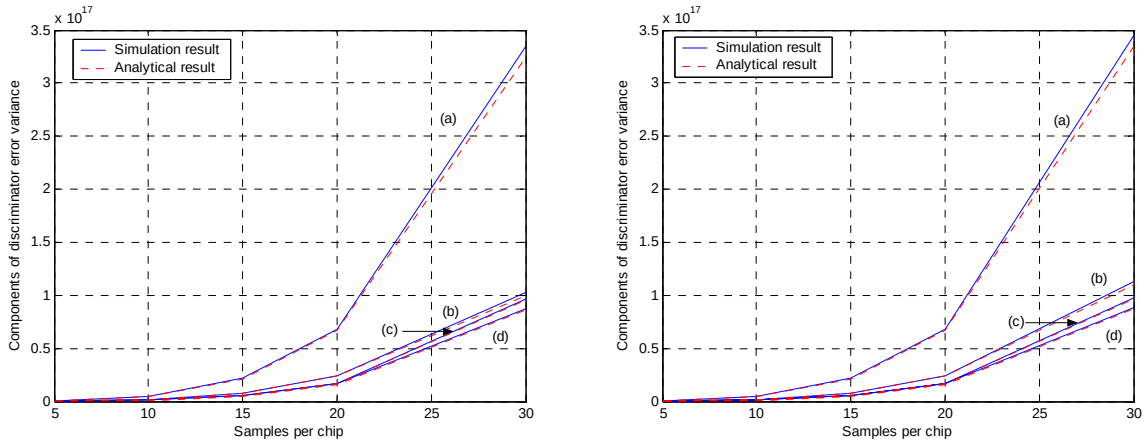

Figure 13. The components of discriminator error variance with different sample rate (a) under UWB noise, (b) under Middleton's impulsive noise

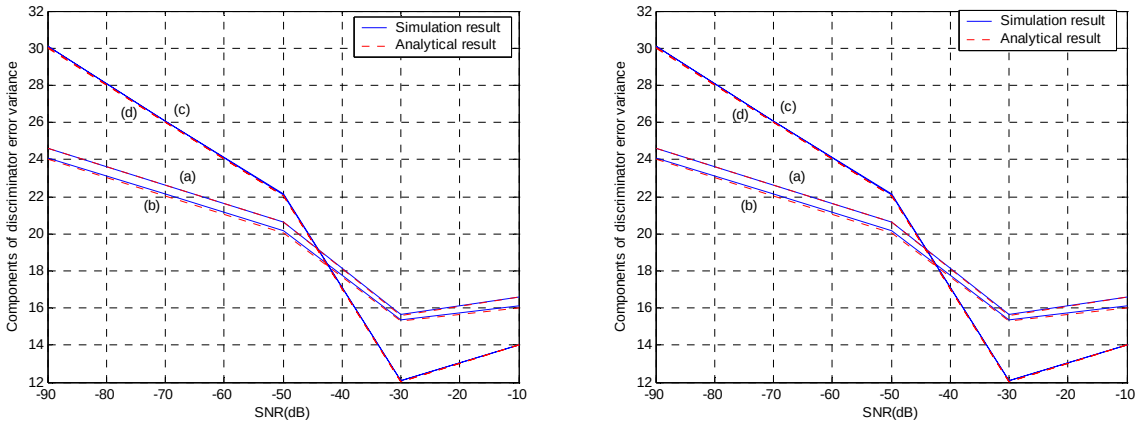

(a) (b)

Figure 14. The components of discriminator error variance at different SNR (a) under UWB noise, (b) under Middleton's impulsive noise

Chapter 5
Maximum Signal-to-Noise Ratio GPS Anti-Jam Receiver with Subspace Tracking

1. Introduction

Global Positioning System (GPS) is a tool to determine position, velocity, and precise time worldwide by measuring the time-of-arrival of signals emitted from satellites. In addition to its original military purpose, GPS has found a wide range of civilian applications such as navigation, land surveying and mapping, and timing and synchronization for telecommunication networks.

For GPS applications, the main challenges are the vulnerability of the GPS receivers to strong interference and the multipath effects on receiver synchronization. GPS employs spread-spectrum (SS) signaling, which provides a certain degree of protection against interference. However, if the interfering signal's power exceeds the 30 dB processing gain offered via the spreading/dispreading of the GPS C/A signal, the receiver is unable to recover the navigation information conveyed in GPS signal. Therefore, the design of GPS receivers must mitigate the interference and combat its effect on the receiver's ability to synchronize with different satellites. Multipath, on the other hand, is caused by signal reflections and diffractions between the satellite and the GPS receiver. In GPS, the desired signal is the direct path signal. All other signals distort the desired signal and lead to ranging measurement errors.

In this chapter, we propose an interference suppression scheme which combines subspace tracking and adaptive beamforming. Specifically, the received signal is first projected into its noise subspace. The resulting interference-free signal is then processed by a spatial filter, whose weights are determined by the maximum signal-to-noise ratio (MSNR) criterion. Computer simulations have shown that the proposed method is effective in combating strong interference and enhancing the GPS signal.

2. Subspace Tracking Interference Suppression

2.1. Signal Model

The GPS receiver is equipped with an *M*-element spatial array, as shown in Figure 1. The waveforms impinging on the array are those of the GPS signal and its multipath, interference, and noise. After down-conversion and chip-rate sampling, the received signal vector from the antenna array can be presented in discrete-time format as

$$\mathbf{x}(n) = \sum_{k=0}^{K} s_k(n) c_k(nT_s - \tau_k(n))\mathbf{a}_k + \sum_{l=1}^{L} u_l(n)\mathbf{d}_l + \mathbf{v}(n) \tag{5.1}$$

where

T_s Nyquist sampling interval;

K number of multipath components;

$s_k(n)$ *k*th signal component;

c_k *k*th C/A-code sample;

$\tau_k(n)$ time-delay of the *k*th component;

a_k spatial signature of the *k*th satellite multipath;

L number of interferers;

$u_l(n)$ waveform of the *l*th interferer;

$\mathbf{d}_l$ spatial signature of the *l*th interferer;

$\mathbf{v}(n)$ additive white Gaussian noise sample vector.

Due to the weak cross-correlation of the C/A-codes, only one satellite is considered in Eq. (5.1). The subscript 0 is designated to the direct-path signal. Let $\mathbf{s}(n) = s_0(n)c_0(nT_s - \tau_0(n))\mathbf{a}_0$ denote the data vector across the array due to the direct-path signal. Then, Eq. (5.1) can be rewritten as

$$\mathbf{x}(n) = \mathbf{s}(n) + \mathbf{s}_{\mathrm{m}}(n) + \mathbf{u}(n) + \mathbf{v}(n) \tag{5.2}$$

where $\mathbf{s}_{\mathrm{m}}(n)$ denotes the contributions from *K* multipath reflections,

$$\mathbf{s}_{\mathrm{m}}(n) = \sum_{k=1}^{K} s_k(n) c_k(nT_s - \tau_k(n)) \mathbf{a}_k \tag{5.3}$$

and $\mathbf{u}(n) = \sum_{l=1}^{L} u_l(n)\mathbf{d}_l$ is the compound interference vector.

2.2. Subspace Tracking Based Interference Suppression

Under the assumption that the GPS signals, interference, and noise are independent, the covariance matrix of the received signal becomes

$$\mathbf{R}_{xx} = E\left\{\mathbf{x}(n)\mathbf{x}^H(n)\right\} = \mathbf{R}_s + \mathbf{R}_u + \mathbf{R}_v \tag{5.4}$$

where $E\{\cdot\}$ represents the statistical expectation, $(\cdot)^H$ denotes conjugate transpose, and $\mathbf{R}_s$, $\mathbf{R}_u$, and $\mathbf{R}_v$ are the covariance matrices of the GPS signals, the interference, and the noise, which are defined, respectively, as:

$$\mathbf{R}_s = E\left\{\left[\mathbf{s}(n) + \mathbf{s}_{\mathrm{m}}(n)\right]\left[\mathbf{s}(n) + \mathbf{s}_{\mathrm{m}}(n)\right]^H\right\} \tag{5.5}$$

$$\mathbf{R}_u = E\left\{\mathbf{u}(n)\mathbf{u}^H(n)\right\} \tag{5.6}$$

$$\mathbf{R}_v = E\left\{\mathbf{v}(n)\mathbf{v}^H(n)\right\} = \sigma_v^2 \mathbf{I}_M \tag{5.7}$$

where $\mathbf{I}_M$ is an $M \times M$ identity matrix.

The subspace tracking based GPS anti-jam receiver is motivated by the fact that in GPS, the desired GPS signals are well below the noise floor (usually 20 to 30 dB below the noise floor). As such, the total received signal power is dominated by the jamming signals. In this case, the covariance matrix $\mathbf{R}_{xx}$ is approximated as [1]

$$\mathbf{R}_{xx} \approx \mathbf{R}_u + \mathbf{R}_v \tag{5.8}$$

By performing singular value decomposion (SVD) of $\mathbf{R}_{xx}$, we can effectively decompose the received signal into two subspaces:

$$\begin{aligned}\mathbf{R}_{xx} &= \sum_{i=1}^{M} \lambda_i \mathbf{e}_i \mathbf{e}_i^H \approx \sum_{i=1}^{L} \lambda_i \mathbf{e}_i \mathbf{e}_i^H + \sigma_v^2 \sum_{i=L+1}^{M} \mathbf{e}_i \mathbf{e}_i^H \\ &\square\ \mathbf{U}_{\mathrm{I}} \boldsymbol{\Sigma}_{\mathrm{I}} \mathbf{U}_{\mathrm{I}}^{\mathrm{H}} + \mathbf{U}_{\mathrm{V}} \boldsymbol{\Sigma}_{\mathrm{V}} \mathbf{U}_{\mathrm{V}}^{\mathrm{H}}\end{aligned} \tag{5.9}$$

where $\boldsymbol{\Sigma}_{\mathrm{I}} = \mathrm{diag}\{\lambda_1, \quad \cdots, \quad \lambda_L\}$ is an $L \times L$ diagonal matrix whose elements are the L largest eigenvalues. $\mathbf{U}_{\mathrm{I}}$ is an $M \times L$ matrix whose columns, eigenvectors $\mathbf{e}_1, \cdots \mathbf{e}_L$ associated with L largest eigenvalues, span the *interference subspace*. $\boldsymbol{\Sigma}_{\mathrm{V}} = \sigma_v^2 \mathbf{I}_{M-L}$ contains the rest M-L eigenvalues, which are assumed to be equivalent to σ_v^2, and the columns of the $M \times M$-L matrix $\mathbf{U}_{\mathrm{V}}$ are the associated M-L eigenvectors, which span the *noise subspace*. Note that vectors $\{\mathbf{d}_1, \quad \cdots \quad \mathbf{d}_L\}$ also span the interference subspace, i.e.,

$$\mathrm{span}\{\mathbf{e}_1, \quad \cdots, \quad \mathbf{e}_L\} = \mathrm{span}\{\mathbf{d}_1, \quad \cdots, \quad \mathbf{d}_L\} \tag{5.10}$$

Even though the spatial signatures $\mathbf{d}_l$, l=1,···,L of the interferers are usually unknown at the receiver, the interference subspace can be explicitly obtained by first computing an estimate of $\mathbf{R}_{xx}$, then performing SVD. For large arrays, however, the eigendecomposition imposes heavy computational burdens on the receiver. Therefore, such method may not be suitable for real time processing of GPS signals. An alternative approach is to use the so called *subspace tracking* techniques [2]. Such techniques are especially suitable for GPS because the power of the interferer is much stronger than that of the GPS signal, and the number of interferers is limited which, in turn, limits the dimension of the interference subspace. Subspace tracking estimates the interference subspace recursively on a sample-by-sample basis and, thus, avoids explicit calculation of the matrix $\mathbf{R}_{xx}$. For the anti-jam GPS receiver, we use the projection approximation subspace tracking with deflation (PASTd) method proposed in [3]. The PASTd algorithm first estimates the most dominant eigenvector and the projection of the received data onto this eigenvector is then removed from the received data. Now the second dominant eigenvector becomes the

most dominant one in the updated data vector and it can be extracted as well. Repeating this procedure, all desired eigencomponents can be estimated sequentially. The PASTd algorithm is summarized in Table 1.

Table 1: The PASTd Algorithm

Choose an initial **e**(0) properly

For n = 1,2,··· Do

$$\mathbf{x}_1(n) = \mathbf{x}(n)$$

For l = 1 to L Do

$$\alpha_l(n) = \mathbf{e}_l^H(n-1)\mathbf{x}_l(n)$$

$$\gamma_l(n) = \beta\gamma_l(n-1) + |\alpha_l(n)|^2$$

$$\mathbf{e}_l(n) = \mathbf{e}_l(n-1) + \frac{\left[\mathbf{x}_l(n) - \mathbf{e}_l(n-1)\alpha_l(n)\right]\alpha_l^*(n)}{\gamma_l(n)}$$

$$\mathbf{x}_{l+1}(n) = \mathbf{x}_l(n) - \mathbf{e}_l(n)\alpha_l(n)$$

Usually, the initial **e**(0) can be chosen from an identity matrix. In the above algorithm, $\boldsymbol{e_l}$ is an estimate of the lth eigenvector and γ_l is the corresponding eigenvalue, and $0 < \beta \leq 1$ is the forgetting factor.

Once the interference subspace is available, the noise subspace can be obtained from the orthogonal projection of the interference subspace, which is given by

$$\mathbf{U}_{\mathrm{I}}^{\perp} = \mathbf{I}_{\mathrm{M}} - \mathbf{U}_{\mathrm{I}}^{\perp}(\mathbf{U}_{\mathrm{I}}^H\mathbf{U}_{\mathrm{I}})^{-1}\mathbf{U}_{\mathrm{I}}^H \tag{5.11}$$

where $(\square)^{-1}$ denotes matrix inverse. Therefore, columns of $\mathbf{U}_{\mathrm{I}}^{\perp}$ span the noise subspace. The projection of $\mathbf{x}(n)$ onto $\mathbf{U}_{\mathrm{I}}^{\perp}$ yields

$$\mathbf{y}(n) = \mathbf{U}_{\mathrm{I}}^{\perp}\mathbf{x}(n) = \mathbf{U}_{\mathrm{I}}^{\perp}\left[s(n) + \mathbf{s_m}(n)\right] + \mathbf{U}_{\mathrm{I}}^{\perp}\mathbf{v}(n) \tag{5.12}$$

which only contains contributions from the GPS components and noise.

3. MSNR Beamformer

From the above discussion, we know that by projecting the received data onto the noise subspace, the interfering signals are completely suppressed. After the suppression of the interference, the GPS signal is still far below the noise floor. In order to synchronize the receiver with the satellite, which is usually achieved by cross-correlating the received data with a locally generated C/A-code and identifying the maximum value, the GPS signal must be enhanced. To this end, we design a filter such that the output of the filter achieves the maximum signal-to-noise ratio (MSNR).

Let $\mathbf{w}$ be the $M\times 1$ weight vector. Then, the output of the filter is given by

$$\begin{aligned} z(n) &= \mathbf{w}^H \mathbf{y}(n) \\ &= \mathbf{w}^H \mathbf{U}_{\mathrm{I}}^{\perp} \left[s(n) + \mathbf{s}_{\mathbf{m}}(n) \right] + \mathbf{w}^H \mathbf{U}_{\mathrm{I}}^{\perp} \mathbf{v}(n) \end{aligned} \tag{5.13}$$

and the filter $\mathbf{w}$ is determined from

$$\begin{aligned} \mathbf{w}_{\mathrm{MSNR}} &= \max_{\mathbf{w}} \frac{E\left\{ \left| \mathbf{w}^H \mathbf{U}_{\mathrm{I}}^{\perp} \left[s(n) + \mathbf{s}_{\mathbf{m}}(n) \right] \right|^2 \right\}}{E\left\{ \left| \mathbf{w}^H \mathbf{U}_{\mathrm{I}}^{\perp} \mathbf{v}(n) \right|^2 \right\}} \\ &= \max_{\mathbf{w}} \frac{\mathbf{w}^H \mathbf{U}_{\mathrm{I}}^{\perp} \mathbf{R}_s \mathbf{U}_{\mathrm{I}}^{\perp H} \mathbf{w}}{\mathbf{w}^H \mathbf{U}_{\mathrm{I}}^{\perp} \mathbf{U}_{\mathrm{I}}^{\perp H} \mathbf{w}} \end{aligned} \tag{5.14}$$

Equation (5.14) indicates that the determination of beamformer $\mathbf{w}$ requires the power of the GPS signal (contains both the power from the direct-path signal and the contributions from its multipath components) at the receiver. Generally, the calculation of the GPS signal power requires some *a priori* knowledge of the satellite. For example, as indicated in [4], if the location of the satellite is known, then the GPS signal power can be computed as follows. Assume that the satellite is located at the angle (θ, ψ). For GPS, the temporal autocorrelation of the transmitted signal, which is essentially the autocorrelation function of the Gold code denoted as $\mathbf{R}_c(\tau)$ is known. The $M\times M$ matrix $\mathbf{R}_s$ is calculated in the absence of interference and noise. Let $\eta(m)$ denote the phase shift for the GPS satellite at the angle (θ,ψ) to the mth antenna and let $\mathbf{r} \square \left[e^{j\eta(1)} \quad \cdots \quad e^{j\eta(M)} \right]^T$. Then, $\mathbf{R}_s$ is given by $\mathbf{R}_s = R_c(0)\mathbf{r}\mathbf{r}^H$.

On the other hand, if the satellite location information is not available at the receiver, we take an alternative approach to solve the above maximization problem. From Eq. (5.12) we know that $\mathbf{y}(n)$ only contains contributions from the GPS signals and noise. Due to the weakness of the GPS signals, the output of the projection is dominated by noise. Note that

$$\begin{aligned}\frac{E\left\{\left|\mathbf{w}^H\mathbf{y}(n)\right|^2\right\}}{E\left\{\left|\mathbf{w}^H\mathbf{U}_{\mathrm{I}}^{\perp}\mathbf{v}(n)\right|^2\right\}} &= \frac{\mathbf{w}^H\mathbf{U}_{\mathrm{I}}^{\perp}\mathbf{R}_{xx}\mathbf{U}_{\mathrm{I}}^{\perp H}\mathbf{w}}{\sigma_v^2\mathbf{w}^H\mathbf{U}_{\mathrm{I}}^{\perp}\mathbf{U}_{\mathrm{I}}^{\perp H}\mathbf{w}} \\ &= \frac{\mathbf{w}^H\mathbf{U}_{\mathrm{I}}^{\perp}\mathbf{R}_{s}\mathbf{U}_{\mathrm{I}}^{\perp H}\mathbf{w}}{\sigma_v^2\mathbf{w}^H\mathbf{U}_{\mathrm{I}}^{\perp}\mathbf{U}_{\mathrm{I}}^{\perp H}\mathbf{w}} + 1\end{aligned} \tag{5.15}$$

which shows that the beamformer $\mathbf{w}$ that maximizes

$$\frac{\mathbf{w}^H\mathbf{U}_{\mathrm{I}}^{\perp}\mathbf{R}_{s}\mathbf{U}_{\mathrm{I}}^{\perp H}\mathbf{w}}{\sigma_v^2\mathbf{w}^H\mathbf{U}_{\mathrm{I}}^{\perp}\mathbf{U}_{\mathrm{I}}^{\perp H}\mathbf{w}} \tag{5.16}$$

also maximizes

$$\frac{\mathbf{w}^H\mathbf{U}_{\mathrm{I}}^{\perp}\mathbf{R}_{xx}\mathbf{U}_{\mathrm{I}}^{\perp H}\mathbf{w}}{\sigma_v^2\mathbf{w}^H\mathbf{U}_{\mathrm{I}}^{\perp}\mathbf{U}_{\mathrm{I}}^{\perp H}\mathbf{w}} \tag{5.17}$$

Therefore, the filter $\mathbf{w}$ can be found by solving

$$\mathbf{w}_{\mathrm{MSNR}} = \max_{\mathbf{w}} \frac{\mathbf{w}^H\mathbf{U}_{\mathrm{I}}^{\perp}\mathbf{R}_{xx}\mathbf{U}_{\mathrm{I}}^{\perp H}\mathbf{w}}{\sigma_v^2\mathbf{w}^H\mathbf{U}_{\mathrm{I}}^{\perp}\mathbf{U}_{\mathrm{I}}^{\perp H}\mathbf{w}} \tag{5.18}$$

Thus, the optimum $\mathbf{w}$ is the eigenvector corresponding to the dominant eigenvalue of the following generalized eigenvalue problem:

$$\mathbf{U}_{\mathrm{I}}^{\perp}\mathbf{R}_{xx}\mathbf{U}_{\mathrm{I}}^{\perp H}\mathbf{w} = \mu\mathbf{U}_{\mathrm{I}}^{\perp}\mathbf{U}_{\mathrm{I}}^{\perp H}\mathbf{w} \tag{5.19}$$

where μ denotes the dominant eigenvalue, which is also the maximum SNR.

In practice, $\mathbf{R}_{xx}$ is replaced by its sample estimate, which can also be computed recursively [5].

4. Simulations

A linear uniform array consisting of M=7 sensors with half-wavelength spacing is used in the simulation.

In the first simulation, we investigate the convergence of the PASTd algorithm. In this experiment, there is one jammer added to the received signal and we set the signal-to-noise ratio (SNR) to -10 dB and signal-to-interference ratio (SIR) to -30 dB. This lead to the interference-to-noise ratio (INR) of 20 dB. Figure 2 shows that after 250 samples, the eigenvalue converges to the true INR of 20 dB.

In the next experiment, we examine the interference suppression performance of the proposed GPS receiver. There are two jammers located at 30° and 60°, and the satellite is at 10°. Figure 3 shows that the receiver can successfully generate high gain toward the satellite direction, while placing deep nulls at the jammer locations. By using the proposed GPS receiver, the desired GPS signal is enhanced, whereas the jammers are suppressed.

Finally, we investigate the proposed receiver's synchronization capability. Generally, the synchronization can be achieved by cross-correlating the received signal with the locally generated C/A-code [6]. When the receiver synchronizes with the satellite, there is a maximum correlation. In the simulation, we considered three different scenarios to illustrate the receiver's performance. We set SNR= -30 dB and SIR=-40 dB. In the first case, the received signal is directly correlated with the C/A-code and the resulting normalized cross-correlation is shown in Figure 4(a). It is noted that without any processing, the synchronization fails. If only the interference suppression is applied, the receiver is able to synchronize with the satellite after the cross-correlation, but the noise contribution remains significant, as shown in 4(b). With the proposed receiver, however, the noise can be drastically reduced. This is shown in 4(c).

5. Conclusions

In this chapter, we have considered the problem of interference cancellation in GPS. Specifically, a GPS receiver combining the subspace interference suppression and MSNR beamforming is proposed. Through computer simulations, we have shown that the proposed receiver is capable of providing high gains for the desired GPS signal while suppressing the strong interferers.

References

[1] B. Poh, T. Quek, C. See, and A. Kot, "Suppression of strong narrowband interference using an eigen-structurebased algorithm," in *Proceedings of the 1995 MilitaryCommunications Conference Proceedings (MILCOM'95)*, vol. 3, 1995, pp. 1205–1208.

[2] W. Utschick, "Tracking of signal subspace projectors," *IEEE Transactions on Signal Processing*, vol. 50, no. 4, pp. 769–778, April 2002.

[3] B. Yang, "Projection approximation subspace tracking," *IEEE Transactions on Signal Processing*, vol. 43, no. 1, pp. 95–107, January 1995.

[4] R. L. Fante and J. J. Vaccaro, "Wideband cancellation of interference in a GPS receive array," *IEEE Transactions on Aerospace and Electronic Systems*, vol. 36, no. 2, pp. 549–564, April 2000.

[5] S. Haykin, *Adaptive Filter Theory*, 4th ed. Upper Saddle River, NJ: Prentice Hall, 2002.

[6] E. D. Kaplan (eds.), *Understanding GPS: Principles and Applications*. Artech House Publisher, 1996.

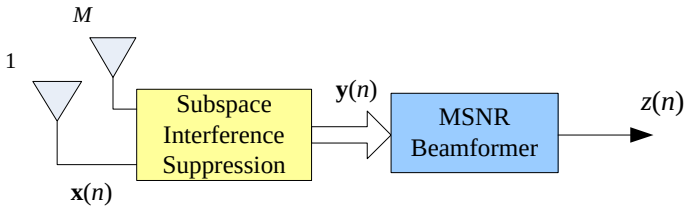

Figure 1. Block diagram of the proposed GPS receiver.

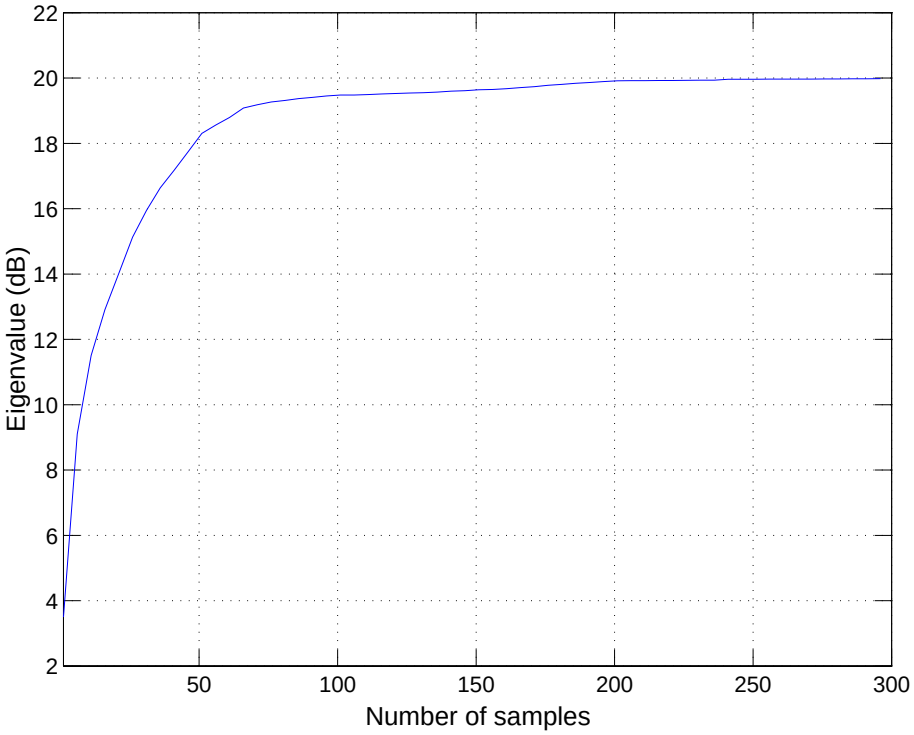

Figure 2. Convergence of the eigenvalue.

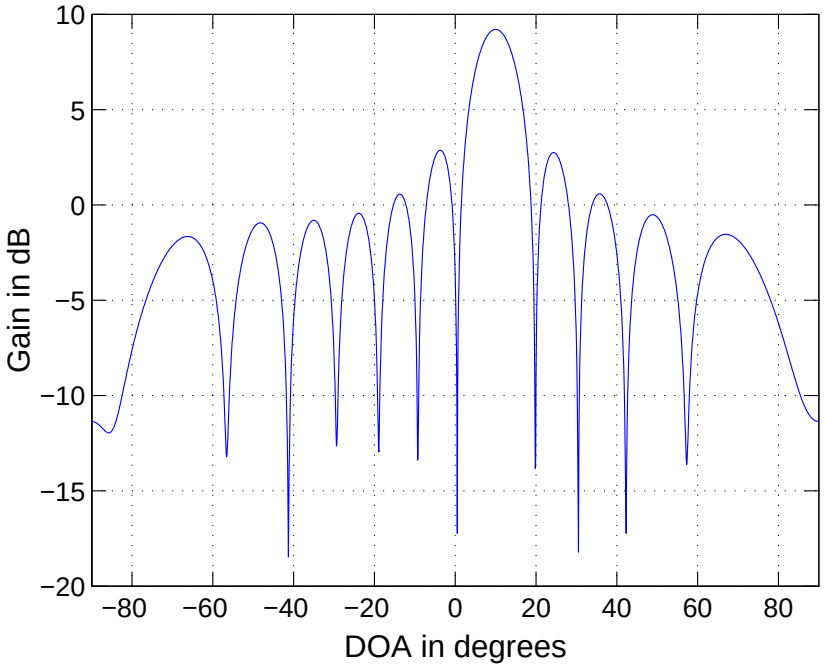

Figure 3. Beampattern of the proposed GPS receiver.

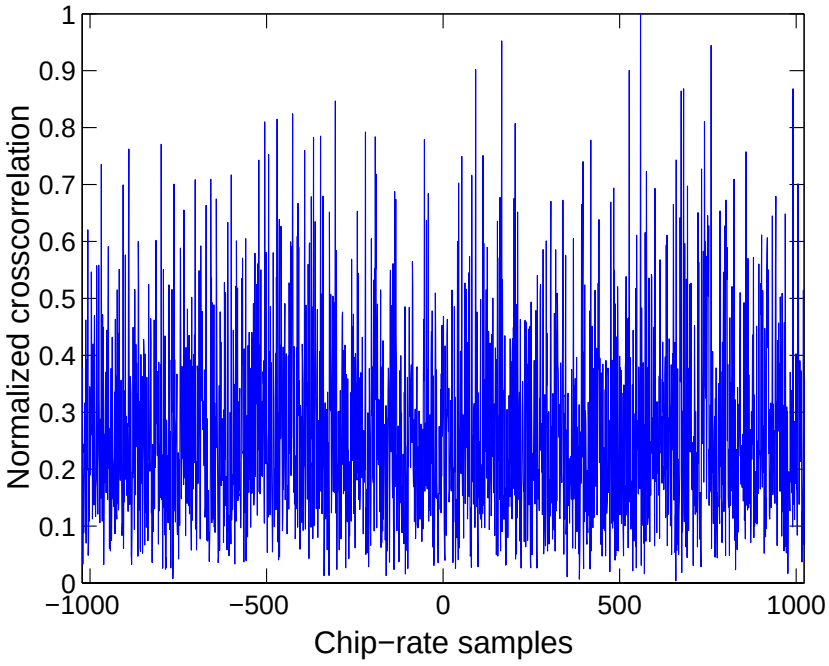

(a)

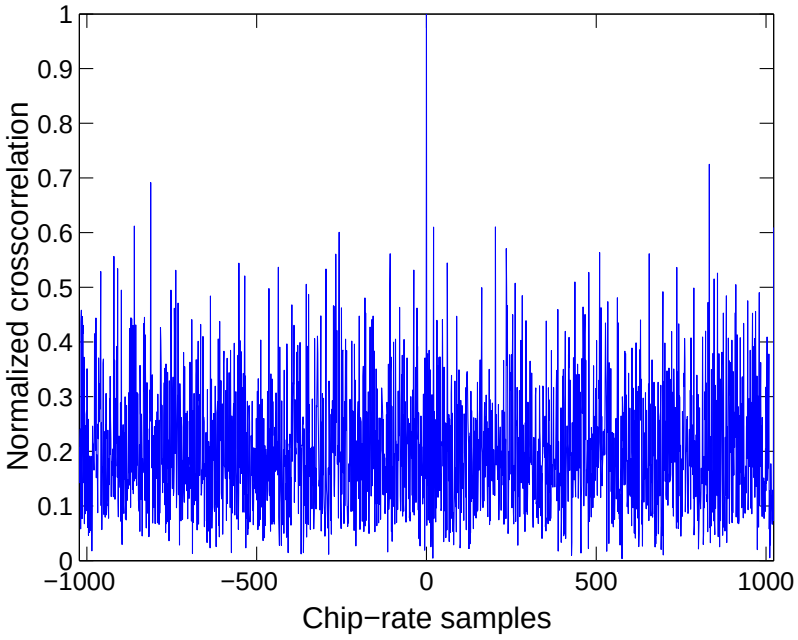

(b)

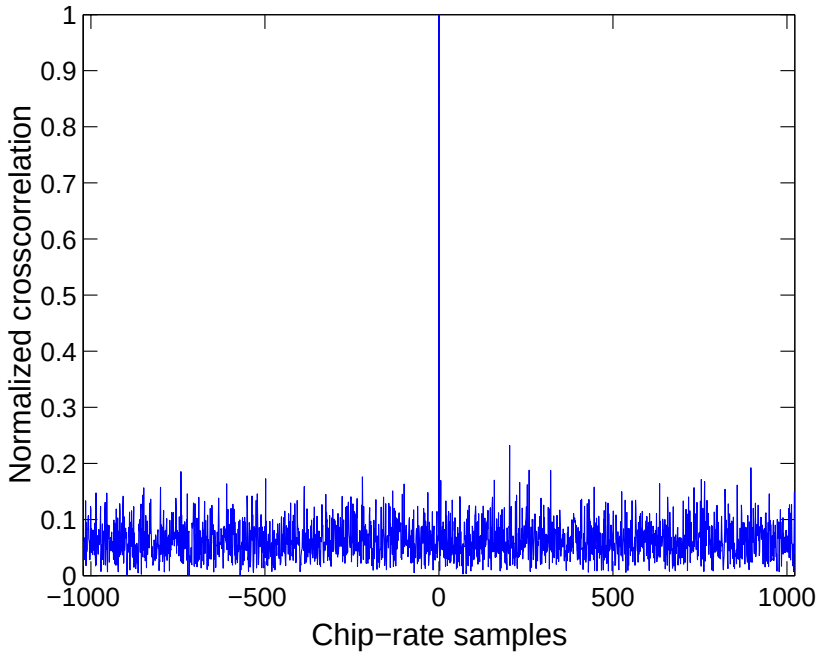

(c)

Figure 4. Normalized cross-correlation. (a) Without interference suppression and beamforming; (b) With interference suppression but without beamforming; (c) Proposed receiver.

Publication List

Book Chapters

1. Moeness Amin, Wei Sun, and Alan Lindsey, ``Adaptive Arrays for GPS Receivers," in M. Ibnkahla Ed., Signal Processing for Mobile Communications Handbook, CRC Press, 2004.
2. M. G. Amin, Y. Zhang, G. J. Frazer, and A. R. Lindsey, "Spatial time-frequency distributions: Theory and applications," in L. Debnath (ed.), Wavelets and Signal Processing, Boston, MA: Birkhauser, 2003.
3. M. G. Amin and Y. Zhang, "Interference suppression in spread spectrum communication systems," in J. G. Proakis (ed.), The Wiley Encyclopedia of Telecommunications, New York, NY: John Wiley, 2002.

Journal Papers

1. Wei Sun and Moeness Amin, “A Self-Coherence Based GPS Anti-Jamming Receiver,” IEEE Transaction on Signal Processing}, accepted for publication.
2. Moeness Amin and Wei Sun, “A Novel Interference Suppression Scheme For Global Navigation Satellite Systems Using Antenna Array,” IEEE Journal on Selected Areas in Communications, Special Issue on Advances in Military Wireless Communications, vol.23, no. 5, May 2005.
3. W. Mu, M. G. Amin, and Y. Zhang, "Bilinear signal synthesis in array processing," IEEE Transactions on Signal Processing, vol. 51, no. 1, Jan. 2003.
4. Y. Zhang and M. G. Amin, "Array processing for nonstationary interference suppression in DS/SS communications using subspace projection techniques," IEEE Transactions on Signal Processing, vol. 49, no. 12, Dec. 2001.

Conference Papers

1. Wei Sun and Moeness Amin, “Maximum Signal-to-Noise Ratio GPS Anti-Jam Receiver with Subspace Tracking,” The 2005 IEEE International Conference on Acoustics, Speech, and Signal Processing, Philadelphia, PA, USA, March 19 - 23, 2005.
2. Wei Sun and Moeness Amin, “Interference Suppression and Multipath Mitigation for Global Navigation Satellite Systems,” The Fourth IEEE Symposium on Signal Processing and Information Technology, Rome, Italy, December 18 - 21, 2004.
3. Jun Yang, Wei Sun and Moeness Amin, “Optimal Training Sequence for Space-Time Block Coded Systems in Frequency-Selective Fading Channels,” The 38th Annual Conference on Information Sciences and Systems, pp. 650 - 653, Princeton University, Princeton, NJ, March 17 - 19, 2004.
4. Wei Sun and Moeness Amin, “Interference Suppression for GPS Coarse/Acquisition Signal Using Antenna Array,” The 2004 IEEE International Conference on Acoustic, Speech, and Signal Processing, Vol. 4, pp. 929 - 932, Montreal, Quebec, Canada, May 17 - 21, 2004.
5. Wei Sun and Moeness Amin, “GPS Interference Suppression Using Self-Coherent Feature of GPS Signals,” The 3rd IEEE International Symposium on Signal Processing and Information Technology, Darmstadt, Germany, December 14 - 17, 2003.
6. Wei Sun and Moeness Amin, “Minimum Variance Receiver for Multicarrier CDMA Systems with Space-Time Coding,” The 37th Asilomar Conference on Signals, Systems and Computers, pp. 1152 - 1155, Pacific Grove, CA, November 9 - 12, 2003.
7. Wei Sun and Moeness Amin, “A Self-Coherence Based GPS Anti-Jamming Receiver,” The 2003 IEEE Workshop on Statistical Signal Processing, pp. 53 - 56, St. Louis, MO, September 28 - October 1, 2003.

8. Jun Yang, Wei Sun and Moeness Amin, “A Training Based Transmit Diversity Technique for Frequency Selective Fading Channels,” The 2003 IEEE Workshop on Statistical Signal Processing, pp 57 - 60, St. Louis, MO, September 28 - October 1, 2003.
9. Wei Sun, Hongbin Li, and Moeness Amin, “MMSE Detection for Space-Time Coded MC-CDMA,” Proceedings of the IEEE 2003 International Conference on Communications, pp. 3452 - 3456, Anchorage, AK, May 11 - 15, 2003.
10. Jun Yang, Wei Sun, and Moeness Amin, “Time-Reversed Space-Time Block Coding with Multipath Gains for Channels with Intersymbol Interference,” The 2003 IEEE Sarnoff Symposium, pp. 313 - 316, The College of New Jersey, March 11 - 12, 2003.
11. Y. Zhang, M. G. Amin, and A. R. Lindsey, "Improved blind separations of nonstationary sources based on spatial time-frequency distributions," Fourth International Symposium on Independent Component Analysis and Blind Signal Processing, Nara, Japan, April 2003.
12. Wei Sun, Hongbin Li, and Moeness Amin, “A Multiuser Receiver for Multicarrier CDMA Systems with Transmit Diversity,” The 2nd IEEE International Symposium on Signal Processing and Information Technology, pp. 719 - 723, Marrakech, Morocco, December 18 - 21, 2002.
13. Y. Zhang, M. G. Amin, A. Lindsey, and K. Yang, "Downlink CDMA systems with space-time codes and interference cancellation," IEEE Signal Processing Workshop on Signal Processing Advances in Wireless
14. Communications, Taoyuan, Taiwan, March 2001.
15. Y. Zhang, K. Yang, and M. G. Amin, "Convergence performance of subband arrays for spatio-temporal equalization," IEEE Workshop on Statistical Signal Processing, Singapore, Aug. 2001.
16. M. G. Amin, W. Mu, and Y. Zhang, "Spatial and time-frequency signature estimation of nonstationary sources," IEEE Workshop on Statistical Signal Processing, Singapore, Aug. 2001.
17. M. G. Amin, W. Mu, and Y. Zhang, "Improved time-frequency synthesis using array manifolds," IEEE International Symposium on Signal Processing and Its Applications, Kuala-Lampur, Malaysia, Aug. 2001.

18. Y. Zhang, M. G. Amin, and A. R. Lindsey, "Anti-jamming GPS receivers based on bilinear signal distributions," Military Communications Conference, Vienna, VA, Oct. 2001.